2023 Spring Meeting

March 10-11, 2023

Royal Sonesta New Orleans
New Orleans, Louisiana

Society for Pediatric Pathologists

Abstracts of the 2023 Spring Meeting

March 10-11, 2023

Hybrid Meeting

Platform I: Molecular Testing

1

Implementation of a Molecular Anatomic Pathology (MAP) service with Refinement Over Time Leads to Decreased DNA Failure Rates for Somatic NGS Testing

B Lockhart [1], P Kreiger [2], M Li [2], L Surrey [2]; [1] The Children's Hospital of Philadelphia, [2] The Children's Hospital of Philadelphia

Background: Molecular testing is an essential tool for the diagnostic, prognostic, and therapeutic work-up of many CNS and solid tumors. Pre-analytic testing parameters affect the performance and analysis of somatic genetic tests, with anatomic pathologists (AP) playing a critical role in tissue assessment to ensure high-quality molecular testing and compliance with laboratory accreditation rules. Herein we describe the creation of a “Molecular Anatomic Pathology” (MAP) service designed to facilitate the selection of high quality tissue for somatic solid tumor (ST) and fusion panels (FP) by NGS.

Methods: The MAP service was created in 2018 along with a new test, Molecular Adequacy Assessment (MAA), which documents in the electronic medical record tissue adequacy, sample available (frozen, formalin fixed, decalcified), and viable tumor percentage. This test was designed for retrospective use after case signout utilizing retrieval of archival tissue billing code 88363. Periodic review of real-time failure data led to ongoing pathologist re-education sessions and workflow adjustments to address tissue necrosis, thermal artifact, formalin fixation time, and decalcification. With the transition to Epic Beaker (mid-2021) and the increase in molecular testing requests, the MAP service was further streamlined by requiring pathologists to prospectively document best molecular tissue, tumor percentage, need for macrodissection, and other parameters in a non-reportable Quality Assurance (QA) field in lieu of an MAA (initiated July 2022). Additionally, an Ancillary Testing Coordinator (ATC) was appointed to further support the MAP service and decrease pathologist hands-on time. To evaluate the efficacy of adequacy assessment over time, we conducted a retrospective analysis of all ST and FP failures for insufficient quantity/quality of nucleic acid for in house specimens from 1/2016 through 11/2022. Samples obtained from consult and research samples were excluded. Feedback from pathologists was anecdotally assessed over time by the MAP service director.

Results: During the 7 year review, there were a total of 2,066 STs (mean per year 295, range 150-339) and 1,841 FPs (mean per year: 263, range 155-323) with overall volumes peaking in 2019. The average nucleic acid failure rate over 7 years was 7.2% for DNA (ST) and 5.7% for RNA (FP), with 2018 being a notable outlier for a higher than average yearly failure rate (see Table). Education/workflow interventions since 2018 resulted in progressively decreasing ST failure rates down to an average of 1.7% for 2022 while the rates of FP were largely unaffected. The average number of MAA reports per month prior to QA field implementation matches the average rate of QA field completion post-implementation (12/month pre and post). Feedback on the ease of MAP service work over time anecdotally improved with fewer complaints and increased satisfaction, particularly since implementation of the QA field and ATC.

Conclusion: The creation of a MAP service line in AP with refinement over time has resulted in a decreasing failure rate for DNA-based molecular testing since 2018. Pathologist current QA

field completion rate is equal to the prior rate of MAA reports with improved pathologist satisfaction.

	Nucleic Acid Failure Rate, % (n)	
	ST	FP
2016	5.3% (150)	3.9% (155)
2017	6.4 % (326)	5.7% (300)
2018	16.3% (312)	14.2% (287)
2019	8.6% (339)	4.3% (323)
2020	7.7% (286)	5.7% (314)
2021	4.1% (366)	2.1% (193)
2022	1.7% (287)	4.1% (269)

Platform I: Molecular Testing

2

Molecular testing on thyroid FNA samples provides superior pre-surgical risk assessment in pediatric thyroid nodules

H Ren [1], A Aekka [2], M Raval [2], S Finkelstein [3], J Levine [3], J Josefson [2], N Arva [2]; [1] Ann & Robert H. Lurie Children's Hospital of Chicago, [2] Ann & Robert H. Lurie Children's Hospital of Chicago, [3] Interpace Biosciences

Background: Fine-needle aspiration (FNA) is a valuable diagnostic tool for the preoperative evaluation of thyroid lesions; however, it has limitations, including intermediate results. Molecular testing has emerged as a reliable ancillary tool to improve preoperative risk stratification in adults but only few studies are done in children, and most on resection specimens. We investigated if molecular testing on FNA smears provides better pre-surgical risk assessment in pediatric thyroid nodules, which have a higher risk of malignancy.

Methods: We performed retrospective molecular analysis (ThyGeNEXT and ThyraMIR platforms, Interpace Biosciences, Inc.) on 27 FNA cases (8 Bethesda (B)II, 2 BIII, 3 BIV, 5 BV, 9 BVI) derived from pediatric thyroid lesions. ThyGeNEXT detects 38 fusions and mutations in 10 genes with findings reported as weak or strong-driver mutations; ThyraMIR evaluates 11 miRNAs and results are reported as negative or low/moderate/high positive. One single Diff-Quik-stained smear slide was used for analysis in each case. All cases yielded results. 25 patients had clinical or surgical follow-up. Sensitivity and specificity were calculated for the molecular assays; correlation between molecular results and histopathologic features of the resected lesions were assessed.

Results: Strong driver mutations (BRAFV600E or RET-PTC1 fusion) or high positive ThyraMIR had a specificity and sensitivity of 81.82% and 100%, respectively, for detecting malignancy. Individually, ThyGeNEXT had a specificity of 100% and sensitivity of 71.4%, whereas the specificity and sensitivity of ThyraMIR for predicting a malignant lesion were 81.81% and 100%, respectively. ThyGeNEXT and ThyraMIR results correlated with each other ($p=0.001$). All malignancies ($n=14$) were papillary thyroid carcinoma (PTC) and had high positive ThyraMIR results, but 4 demonstrated either no mutation ($n=2$) or weak driver (NRAS) mutation ($n=2$) on ThyGeNEXT. Interestingly, 5 BII cases had weak driver (NRAS, GNAS, HRAS) mutations, 2 of which were also ThyraMIR high positive: one considered benign clinically and one diagnosed as follicular adenoma. The ThyGeNEXT type of mutation (strong vs. no/weak drivers) did not correlate with any histopathologic features (tumor histologic type, size, focality, marginal status, presence of LVI, ratio of positive lymph nodes).

Conclusion: High positive ThyraMIR in combination with strong driver mutations on ThyGENEXT panel is very accurate in predicting malignancy on thyroid FNA specimens in children. RAS-like mutations are weak drivers and can also be detected in benign lesions. Mutational type does not correlate with histopathologic features of the resected tumor.

Platform I: Molecular Testing

3

Pediatric soft tissue and bone tumours classification by DNA methylation profiling: A validation study of the DKFZ sarcoma classifier

A Glembocki [1], R Siddaway [2], M Ku [2], A Shlien [1], A Villani [1], D Malkin [1], G Somers [1], C Hawkins [1], R Chami [1]; The Hospital for Sick Children, University of Toronto, [2] The Hospital for Sick Children

Background: Diagnosis of pediatric bone and soft tissue neoplasms remains challenging because of the large number of subtypes, many of which lack diagnostic biomarkers. DNA methylation (DNAm) profiles have shown to be a reliable basis for the classification of brain tumours and, following this success, a DNAm-based sarcoma classification tool from the DKFZ in Heidelberg has been developed. Herein, we assess the performance of the DKFZ sarcoma classifier using DNAm profiles from various subtypes of pediatric bone and soft tissue tumours.

Methods: Forty-two tumours representing 16 subtypes diagnosed at our institute during the last five years were included. Tumor areas with the highest tumor cell content (≥ 70%) were selected for DNAm analysis using the Infinium MethylationEPIC protocol. Control tissues were included. The methylation classification generated by the classifier was compared to the original diagnosis as rendered by the pathologist, and sensitivity and specificity was calculated. Discordant cases were further reviewed.

Results: Three specimens failed due to quality control issues. On limiting the validation to the 39 cases with diagnoses for which the Classifier was trained, 72% of cases (28/39) received a prediction with calibrated score > 0.9, and the original diagnosis was concordant with the predicted methylation class in 96% of these cases. 13% of cases (5/39) were also assigned to a methylation class matching their respective original/histological diagnoses, but with scores ranging from 0.5 to 0.74. Four cases were wrongly classified, but with low confidence score. The remaining two cases were unclassified. The classifier performed best when diagnosing Ewing sarcomas (5/5 100% sensitivity), synovial sarcoma (3/3) and rhabdomyosarcomas (1/12, 83% sensitivity). Amongst the subtypes least classified correctly were malignant peripheral nerve sheath tumours (0/3) and nodular fasciitis (0/2). The classifier predictions did not result in revision of our original histological diagnosis. The single discrepant case (1/28) that received a methylation class of embryonal RMS, with a high confidence score (0.947), is a case of MPNST with rhabdomyoblastic differentiation. This case showed loss of H3K27me3 expression and genetic alterations of the NF1 and PRC2 pathways that supported the original diagnosis. Tumour purity may have played a role in prediction, and it did not appear to completely correlate with classifier accuracy, but further investigation is required.

Conclusion: Our preliminary results show that the DKFZ Classifier accurately classifies pediatric soft tissue and bone tumours in 32/39 cases (82%). With refinement and inclusion of more and new pediatric subtypes, it has the potential to be a valuable diagnostic tool in pediatric tumours.

Platform I: Molecular Testing

4

Divergent Paths on the Road to Kaposiform Hemangioendothelioma- The Genetic Land scape of 10 Cases

S Barclay[1], N Shillingford [2], S Mangray [3], W Yu [4], E Chan [4], M Brundler [4], K Kurek [5]; University of Calgary [1], Children's Hospital Los Angeles [2], Nationwide Children's Hospital [3], Alberta Children's Hospital [4], Alberta Children's Hospital | University of Calgary [5]

Background: Kaposiform hemangioendothelioma (KHE) is a locally aggressive vascular tumor typically presenting as a solitary mass in infants, and can be associated with a life-threatening consumptive coagulopathy, Kasabach-Merritt phenomenon (KMP). Most KHEs do not regress despite various treatment approaches. We previously documented genetic heterogeneity in KHE, and further interrogated 10 cases using more comprehensive analyses.

Methods: Clinical and pathological findings were reviewed for 10 cases of KHE. DNA and RNA were isolated from lesional areas of archival tissue and genomic analysis was performed in a stepwise fashion, screening for select variants and fusions using the Oncomine Childhood Cancer Research Assay (ThermoFisher), followed by the Agilent SureSelect Clinical Research Exome. Potential variants were manually screened to select those with high base quality scores and depth of coverage. Digital PCR (dPCR) was also used to test for very low-level mosaicism of published NRAS variants.

Results: Most cases presented at birth (4) or within the first 6 months of life (4) and involved the skin and subcutaneous tissues (7). Two cases were in older children and involved bone. Most were associated with thrombocytopenia, two with mild KMP. Pathology review demonstrated classic histologic features in all cases. We found at least one cancer-associated variant in all tumors. Two cases contained a low-level NRAS p.G12D hotspot variant. No other (N)RAS or GNA/GNAQ alterations were identified, but one tumor had an oncogenic SH3BP2 variant (p.R512C) and another a VUS in RASAL2 (p.H800R). One case showed dual PIK3CA p.E542K and IDH1 p.R132C variants, and another had PIK3CD p.R601Q. Other variants were found in DMGDH (p.Y695H & p.E689Q in cis), ACVR1 (p.W478L), PPM1D (p.Q127X), and EHBP1 (p.V201A). A KHE of the maxilla in a 10-year-old contained a GOPC::ROS1 fusion.

Conclusion: The genetic heterogeneity in KHE is unprecedented amongst vascular anomalies, and the etiologic and clinical significance is unclear. An analysis of the genes involved demonstrates that KHE can be associated with aberrant activation of several signalling pathways, including RAS-MAPK (NRAS, SH3BP2, RASAL2, ROS1, GNA14*), PI3K-AKT (PIK3CA, PIK3CD, DMGDH), and BMP-p38 MAPK (PPM1D, ACVR1, ROS1, RAD50*), as well as by unknown mechanisms (EHBP1) (*published cases). Additionally, our finding of a GOPC::ROS1 fusion and previously reported t(13;16)(q14;p13.3) translocation (fusion partners unknown), suggest that KHE can also be a fusion-driven tumor. Given that KHE looks homogenous but can be associated with divergent signalling pathways, comprehensive molecular testing is needed to recommend optimal targeted treatments tailored to individual tumors.

Platform II: Morbidity and Non-invasive Testing

1

Umbilical Cord Abnormalities and Placental Inflammation Associated with Neonatal Hypoxic-Ischemic Encephalopathy

C Kim [1], K Carreon [2], K James [3], T Boyd [4], R Drucilla [3]; [1] Texas Children's Hospital, [2] Boston Children's Hospital, [3] Massachusetts General Hospital, [4] Texas Children's Hospital

Background: Our aim was to interrogate placental pathology findings and combinations of findings that are associated with hypoxic ischemic encephalopathy (HIE) and determine if any patterns are associated with worse fetal/neonatal outcomes.

Methods: A retrospective study of archival material from 2002 to 2022 was conducted. 265 term neonates from two pediatric referral hospitals who were transferred to the NICU for induced hypothermia due to high clinical suspicion for HIE were identified. 122 placentas sent for pathology review with the sole indication of maternal Group B strep (GBS) positivity from 2000 and 2004 were identified as controls. All cases were reviewed by 4 perinatal pathologists. Clinical data were ascertained via review of the electronic medical record. Demographics, pregnancy factors, and placental pathology factors were compared between HIE cases and GBS controls using parametric and non-parametric tests, as appropriate. Further associations between placental pathology lesions and fetal outcomes were also described using parametric and non-parametric tests. A p-value < 0.05 was considered statistically significant, except where otherwise noted.

Results: HIE cases tended to occur in mothers who were nulliparous ($p< 0.001$) and of older age (30.9) compared with controls (27.8) ($p < 0.001$). HIE cases were more likely to have anatomic cord abnormalities ($p=0.003$), evidence of fetal inflammatory response (FIR) in the setting of amniotic fluid infection (AFI) ($p=0.004$), and fetal vascular malperfusion (FVM) ($p< 0.001$). HIE cases were more likely to have a combination of AFI and FVM ($p=0.03$). HIE cases were more likely to have high grade villitis of unknown etiology (VUE) ($p = 0.019$), a higher maternal inflammatory response (MIR) grade ($p=0.02$), and higher FIR stage compared to controls ($p=0.01$). Fetal outcome data was available in 141 of 173 HIE cases (81.5%). Among HIE cases, anatomic cord abnormalities were more common in those who had died of disease ($p=0.013$), as were subchorionic intervillous thrombi ($p=0.04$). A combination of FVM and MVM was also more commonly seen in those who died of disease ($p=0.01$).

Conclusion: Anatomic cord abnormalities are more common in HIE versus controls and more common in HIE cases where the neonate died of disease. FVM was more prevalent in HIE than controls, but there was no difference in severity. VUE was similar between groups, but HIE cases were more likely to have high grade VUE. Advanced AFI was more common in HIE. A combination of AFI + FVM was more commonly identified in HIE cases, perhaps due to the deleterious effect of inflammatory cytokine release in the setting of existing fetal hypoxia. Routine placental pathologic examination in HIE cases is supported by the data and may help identify neonates at risk for adverse neurological outcomes.

Table 1: Demographic factors, fetal outcomes, pathologic findings, isolated and combination lesions, and severity/stage between HIE cases and controls

	GBS Controls (N=122)	HIE Cases (N=173)	p-value
Maternal age (mean, SD)	27.8 (5.52)	30.9 (6.0)	<0.001
Gravidity (median, IQR)	2 (1, 3)	2 (1, 3)	0.013
Parity (median, IQR)	1 (0, 2)	0 (0, 1)	<0.001
Gestational age at delivery (mean, SD)	39.5 (1.1)	39.1 (2.1)	0.074
Delivery method			--
Cesarean	--	94 (54.3%)	
Vaginal	--	77 (44.5%)	
Unknown	122 (100%)	2 (1.1%)	
Brain MRI	--	137 (79%)	--
Fetal outcome		144 (81.5%)	--
Alive with normal development	--	77 (54.6%)	
Alive with sequelae	--	49 (34.8%)	
Died of disease	--	15 (10.4%)	
Lost to follow up	--	32 (22.2%)	
Placental weight (mean, SD)	472.9 (105.9)	476.1 (104.7)	0.80
Placental weight percentile			0.25
≤25th	72 (59.0%)	100 (57.8%)	
25-50th	12 (9.8%)	30 (17.3%)	
50th-75th	22 (18.0%)	24 (13.9%)	
≥75TH	16 (13.1%)	18 (10.4%)	
Unknown	0 (0.0%)	1 (0.6%)	
Anatomic cord abnormality	9 (7.4%)	34 (19.7%)	0.003
Meconium	31 (25.4%)	47 (27.2%)	0.69
Amniotic fluid infection (AFI) with fetal inflammatory response (FIR)	17 (13.9%)	48 (27.7%)	0.004
Amniotic fluid infection (AFI) with maternal inflammatory response (MIR)	30 (24.6%)	44 (25.4%)	0.82
Placental infarct	24 (19.7%)	20 (11.6%)	0.06
Maternal vascular malperfusion (MVM)	16 (13.1%)	17 (9.8%)	0.38
Subchorionic intervillous thrombus	21 (17.2%)	19 (11.0%)	0.14
Villitis of unknown etiology (VUE)	25 (20.5%)	24 (13.9%)	0.14
Chronic chorioamnionitis	6 (4.9%)	1 (0.6%)	0.017
Chronic deciduitis	6 (4.9%)	8 (4.6%)	0.93
Fetal vascular malperfusion (FVM)	11 (9.0%)	53 (30.6%)	<0.001
Villous edema	6 (4.9%)	10 (5.8%)	0.74
Isolated lesions			
FVM only	2 (1.6%)	8 (4.6%)	0.16
Amniotic fluid infection (AFI) only	4 (3.3%)	13 (7.5%)	0.12
VUE only	5 (4.1%)	5 (2.9%)	0.57
MVM only	0 (0%)	1 (0.6%)	0.40
Lesion combinations			
FVM+AFI	1 (0.8%)	10 (5.8%)	0.03
FVM+VUE	1 (0.8%)	7 (4.0%)	0.15
FVM+VUE+AFI	1 (0.8%)	3 (1.7%)	0.64
VUE +AFI	3 (2.5%)	1 (0.6%)	0.31
MVM+AFI	1 (0.8%)	1 (0.6%)	1.00
MVM+FVM	0 (0.0%)	3 (1.7%)	0.27
MVM+VUE+AFI	0 (0%)	0 (0%)	--
MVM+VUE	3 (2.5%)	1 (0.6%)	0.31
MVM+VUE+AFI+FVM	0 (0%)	0 (0%)	--

Grade, amongst those with grade recorded			
FVM	11	52	0.034
Mild/ungradable + low grade (LG)	9 (82%)	27 (52%)	
High grade (HG) + diffuse/severe	2 (18%)	25 (48%)	
Mild/LG vs. HG/diffuse			0.097
VUE	25	24	0.14
Mild/ungradable + low grade	22 (88%)	14 (58%)	
High grade + diffuse/severe	3 (12%)	10 (42%)	
Mild/LG vs. HG/diffuse			0.019*
FIR in AFI	17	32	0.30
1	14 (82%)	22(69%)	
2	3 (18%)	10 (31%)	
MIR in AFI	30	37	0.02
1	27 (90%)	24 (65%)	
2	3 (10%)	13 (35%)	
Stage, amongst those with stage recorded			
FIR	17	43	0.01
1	14 (82%)	21 (49%)	
2	1 (6%)	20 (47%)	
3	2 (12%)	2 (5%)	
MIR	30	38	0.02**
1	11 (37%)	18 (47%)	
2	19 (63%)	14 (37%)	
3	0 (0%)	6 (16%)	

**Global p value distribution of VUE is <0.001 **Not significant at an adjusted p value threshold of 0.017*

Platform II: Morbidity and Non-invasive Testing
2

Evolution in Infectious Causes of Death in Liveborn Children in a Major Tertiary Children's Hospital: A Retrospective Autopsy Review of over 1200 Cases.

K Weaver [1], M Ramineni [2], C Casiano [2], D Leino [2], A Bernieh [2], J Kasten [2]; [1] Cincinnati Children's Hospital Medical Center, [2] Cincinnati Children's Hospital Medical Center

Background: Infections have historically been a leading cause of death, particularly in children. Medical advances, including vaccines and antimicrobials, have significantly decreased infection-related deaths, but infections remain a cause of pediatric mortality, especially in premature infants. The types of infections implicated in childhood deaths have changed with these advances, for example, meningitis and meningococcal infections were leading causes in 1981 but not in the later period. The incidence and etiologies of infection-related deaths may be altered by major events that modify not only medical practices but also societal attitudes and activities. Examples of such events include the HIV/AIDS epidemic that began in the early 1980s and the more recent COVID-19 pandemic. In order to investigate changes in infection-related pediatric deaths over time, we analyzed and compared autopsy cases performed during 5-year span prior to both the HIV/AIDS epidemic and the COVID-19 pandemic in which infections contributed to death.

Methods: Review of all autopsy cases performed at our institution between 1/1/1975-1/1/1980 and between 1/1/2015-1/1/2020 was performed to identify cases in which infection directly contributed to death, comprising 1262 cases. Only liveborn children were considered, and neonatal sepsis from amniotic sac infections was excluded. Comparison of decedent characteristics and infectious etiologies between the two time periods was performed, identifying age, race, sex, gestational age (for decedents less than 3 months of age), and etiologic class of agent (bacterial, viral, fungal or parasitic). TORCH infections and vaccine-preventable illnesses were specifically assessed. Proportions were compared using 1 (assessing TORCH, vaccine-preventable, and prematurity deaths)- or 2-tailed (all others) z-tests, with significance calculated at the < 0.05 level.

Results: In the 1970s cohort, 300 infectious autopsy cases were identified in liveborn children; 73 were identified in the 2010s. Compared to the 2010s cohort, the 1970s decedents were more likely to be white (85% v 53%, p=0.012), comprise children aged 1-5 and 13+ (22% v 6.8% [p=0.003] and 16.4% v 8.3% [p=0.036]), and were less likely to be premature (66.7% v 80.4%, p=0.039). Vaccine-preventable illnesses (for example: measles) accounted for 36 deaths in the 1970s cohort but only 2 in the 2010s cohort (p=0.009). Thirteen children died of TORCH infections (CMV, toxoplasmosis and HSV) versus 5 in the 2010s (CMV and HSV), which did not reach statistical significance.

Conclusion: Pediatric mortality secondary to infections has decreased significantly compared to fifty years ago, especially in younger children and in relation to vaccine-preventable infections such as meningococcal disease. This drop is largely attributed to medical advances, including vaccines and antimicrobial medications. Additional contributing factors could include practices adopted post-HIV/AIDS, especially in the community. Further exploration of how such changes

in medical and social practice impacted mortality and comparing them to changes occurring in the intra/post-COVID-19 era, is helpful. Yet, with the increased survival of premature infants, they remain at risk of devastating consequences from infections.

Platform II: Morbidity and Non-invasive Testing

3

Cell free microbial DNA utilization at a Children's Hospital

R Craver [1], S Collier [2], M Anderson [3]; [1] LSU Departments of Pathology and Pediatrics, [2] Louisiana State University School of Medicine in New Orleans, [3] Tulane University Medical Center

Background: As cell free microbial DNA (cfDNA) is now commercially available, we investigated the utilization of this $2000 test by a Children's Hospital.

Methods: This was a retrospective chart review of patients hospitalized between August 2020 through July 2022. We identified all tests ordered upon approval by the Infectious Disease service. Positive and negative results were tabulated. Progress notes were reviewed to determine if the results contributed to therapeutic decisions (continuing or switching antimicrobial therapy, discontinuing antimicrobial therapy), allowing an assessment of the test efficiency. Discrepant results with conventional techniques (culture, PCR) were recorded.

Results: There were 80 tests on 59 children, 45 were positive for at least one microbial agent (56.3%) on 34 (57.6%) children, 34 (42.5%) were negative in 31(52.5%) children, with 1 unevaluatable (interfering substances). Of 45 positive results, 24/80 (30%) were contributory, 15/80 (18.8%) were diagnostic (previous workup negative, no other tests provided timely results), 6/80 (7.5%) were diagnostic but the diagnosis could have been made with other testing modalities, and 3/80 (3.8%) were diagnostic with minimal previous workup. 21/80 (26.3%) positives were non-contributory. Of the 35 negative/ unevaluatable tests, 9/80 (11.25%) were contributory, and 26/80 (32.5%) were non-contributory. Efficiency for all contributory tests (24 positive and 9 negative results) was 41.25%. For those 15 positive tests with no other means for diagnosis, plus the 9 contributory negative tests, efficiency was 30%. The total cost for 79 tests (the unevaluatable test was credited) was $158K, for 33 contributory tests (24 positives and 9 negatives), the cost was $4787/contributory test, for those contributory tests with no other means of diagnosis (15 positive and 9 negative), the cost was $6583/contributory test. Results between routine detection (culture, PCR) and cfDNA were similar in 44 (55%). cfDNA detected infectious agents not detected by conventional techniques in 22 (27.5%). cfDNA and conventional testing detected different microbial agents in 9 (11.25%). Conventional testing identified microbial agents in 4 (5%) children in which no agents were detected by cfDNA. 17/59 (28.8%) patients tested have died.

Conclusion: The efficiency of cfDNA is between 30-40% when infectious disease approval was required. The cost per contributory test was between $4787 and $6583. As conventional techniques may detect other microbial agents or agents not detected by cfDNA, cfDNA may complement, not replace, conventional testing. Further data on which clinical settings have a high likelihood of benefiting from cfDNA testing may improve testing efficiency.

Platform II: Morbidity and Non-invasive Testing

4

Utility of non-invasive testing (donor-derived cell-free DNA) and gene expression profiling in pediatric heart transplantation.

H Ren [1], N Arva [2]; [1] Ann & Robert H. Lurie Children's Hospital of Chicago, [2] Ann & Robert H. Lurie Children's Hospital of Chicago

Background: Endomyocardial biopsy (EMB) represents the gold standard for diagnosis of rejection in heart transplantation (HT). However, the procedure is invasive, has low sensitivity due to sampling and is subjected to high interobserver variability. Alternative tests such as non-invasive plasma donor-derived cell-free DNA (dd-cfDNA) and allograft tissue gene expression profiling (GEP) are now commercially available as adjuncts for patient follow-up. We investigated the utility of Allosure (dd-cfDNA) and Molecular Microscope Diagnostic System (MMDx) (GEP) in detecting rejection by comparing with standard tissue EMBs diagnosis in our HT pediatric cohort.

Methods: Consecutive records of EMBs from 2022 were retrieved along with available dd-cfDNA and GEP data. EMBs obtained within one month from transplant were excluded. A cut-off value of 0.2% was used for dd-cfDNA, and GEP results were divided into thresholds favoring acute cellular rejection (ACR) and/or antibody-mediated rejection (AMR). Sensitivity, specificity, PPV and NPV for dd-cfDNA and GEP were calculated by comparing with the gold standard tissue EMB diagnosis using current ISHLT grading system. Correlations between GEP and dd-cfDNA were also evaluated for both ACR and AMR.

Results: Records of 312 EMBs from 168 patients were retrieved, of which 187 EMBs (115 patients) had corresponding dd-cfDNA or GEP results available. dd-cfDNA had a sensitivity and specificity of 74% and 62% respectively in predicting any rejection and a specificity and sensitivity of 85% and 59% respectively in predicting ACR greater or equal to 2R or any AMR. The PPV and NPV of dd-cfDNA in predicting ACR greater or equal to 2R or any AMR were 30% and 95%, respectively. GEP had a sensitivity and specificity of 20% and 99% respectively for predicting ACR, and predicted AMR with a sensitivity and specificity of 54% and 88% respectively. Combining dd-cfDNA and MMDX, the sensitivity and specificity in predicting ACR were 74% and 52%, and the sensitivity and specificity in predicting AMR are 87% and 52%. The PPV and NPV of GEF in predicting ACR were 81% and 87%, respectively, while the PPV and NPV of GEF in predicting AMR were 46% and 91%, respectively. The correlation coefficient between dd-cfDNA and MMDX was r=0.22 for ACR and r=0.44 for AMR.

Conclusion: dd-cfDNA has a relatively high sensitivity for rejection, especially for detecting ACR greater than 2R or any AMR, but the specificity is poor. GEP has high specificity for both ACR and AMR but poor sensitivity. dd-cfDNA and MMDX results correlate poorly for both ACR and AMR. When dd-cfDNA and GEP are combined, the sensitivity improves for the detection of AMR but not ACR; as such, these tests should be used in combination to improve their diagnostic value. However, a significant number of rejection episodes are associated with negative dd-cfDNA and GEP and EMBs remain an essential component of heart transplant

follow-up.

Platform III GI, Liver, and PEComas

1

Microvascular diversity and alterations in normal, regenerative and lesional liver

J Lu B Forgo, L Heilbroner, S Tan; Stanford HealthCare

Background: Endothelial cells (ECs) of the liver are exquisitely adapted mediators of key processes in homeostasis, regeneration and disease. Although indistinct by routine histology, single cell RNA sequencing (scRNAseq) has unveiled transcripts differentiating EC subpopulations e.g. liver sinusoidal endothelial cells (LSECs), portal and central veins (PVs and CVs), demonstrating zonation akin to hepatocytes. Using RNAscope in situ hybridization (R-ISH), we validate markers of different liver ECs in normal liver and characterize microvascular alterations in regenerating and lesional liver.

Methods: Explants, resections or biopsies of normal liver (away from lesions); cirrhosis (CIRR); hyperplasia (regenerating liver next to massive hepatic necrosis (REGL), focal nodular hyperplasia (FNH), nodular regenerative hyperplasia (NRH)); neoplasia (hepatoblastoma (HPB), hepatocellular carcinoma (HCC)); and vascular lesions (congenital hemangioma (CH), hepatic hemangioma (HH)), were retrieved from our archive (> 3 examples each, including 1-3 pediatric). Genes for R-ISH were selected based on differential scRNAseq expression between liver and non-liver ECs, and amongst liver ECs: OIT3 – unique to LSECs; AQP1, PLVAP – in most ECs including PVs but not LSECs; WNT2 – enriched in CVs, may mediate regeneration. EC lineage marker CDH5 confirms EC identity.

Results: In normal liver, PLVAP, AQP1 and OIT3 show zonal expression, delineating PV and periportal (PP) ECs (PLVAP/AQP1- positive (pos); OIT3-negative (neg)) from LSECs (OIT3-pos; PLVAP/AQP1-neg) (Fig 1A). PV to LSEC zonation is largely maintained in CIRR (Fig 1B) and REGL (Fig 1C). Interestingly, it is lost in NRH, with zone 1 and 2 OIT3-pos LSECs significantly diminished, replaced by PP-like ECs (PLVAP-pos) (Fig 1D). WNT2 is sparse in CVs of normal liver (Fig 1E-G) but in REGL, CV WNT2 is notably increased (Fig 1H-J). WNT2 is also increased in FNH (Fig 1K-L), in ECs near the interface of “portal-like” fibrous septae with “lobule-like” periseptal hepatocytes (Fig 1M-O). ECs in “portal-like” (AQP1-pos) and “lobule-like” (OIT3-pos) areas are zonal (Fig 1P), but at their interface many “double pos” ECs (Fig 1Q-R) accompany WNT2 increase. WNT2 is unchanged in CIRR and NRH. In HPB and HCC, LSEC expression is lost, with OIT3-pos, CDH5-weak LSECs replaced by OIT3-neg, CDH5-strong ECs (Fig 1S-T, * = HPB). In vascular lesions, ECs in CHs are "double-pos" (OIT3- and AQP1-pos) (Fig 1U-X), whilst HH ECs are AQP1-pos only (Fig 1Y-BB).

Conclusion: We describe a spatial-transcriptional framework of diverse liver ECs whose changes reflect different pathologic processes and distinct mechanisms: Hyperplasia could occur via periportal proliferation (NRH) or angiocrine WNT signaling (REGL, FNH); LSEC loss in hepatic neoplasia is synchronous to loss of native hepatocytes; and, differential expression of LSEC-specific markers in different vascular lesions suggest distinct cellular origins.

Figure 1

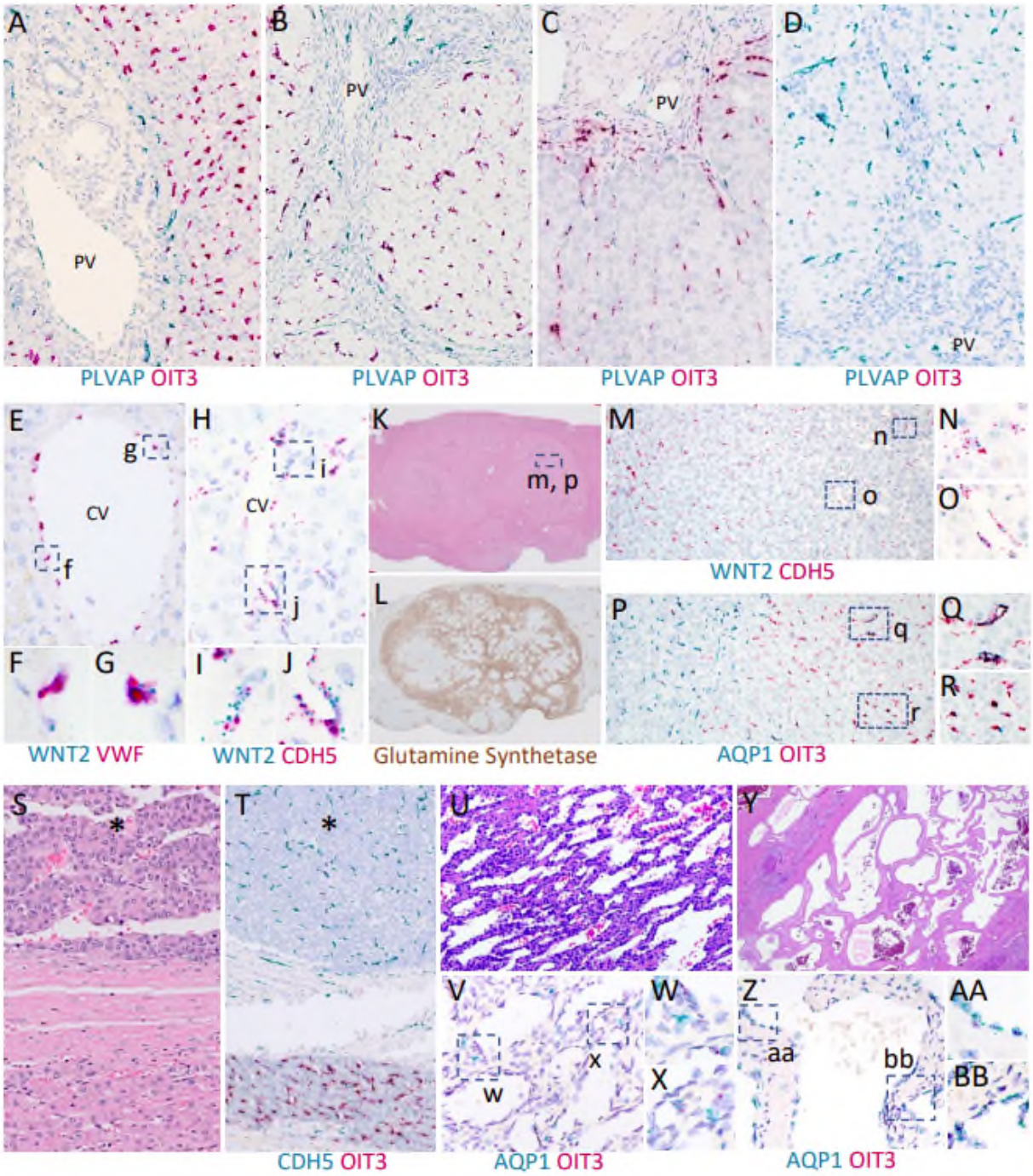
A
PV
B
PV
C
PV
D
PV
PLVAP OIT3
PLVAP OIT3
PLVAP OIT3
PLVAP OIT3
E
g
CV
f
H
i
CV
j
K
m, p
L
M
n
o
N
O
WNT2 CDH5
F
G
I
J
P
q
r
Q
R
WNT2 VWF
WNT2 CDH5
Glutamine Synthetase
AQP1 OIT3
S
*
T
*
U
Y
V
w
x
W
X
Z
aa
bb
AA
BB
CDH5 OIT3
AQP1 OIT3
AQP1 OIT3

Platform III: GI, Liver, and PEComas

2

Clinicopathologic features of a subset of pediatric hepatocellular neoplasms harboring novel large CTNNB1 deletions.

L Berklite [1], S Roy [2], S Ranganathan [2]; [1] Cincinnati Children's Hospital Medical Center, [2] Cincinnati Children's Hospital Medical Center

Background: Hepatoblastoma (HB) is the most common pediatric primary malignant liver tumor. Wnt pathway activation is critical in the pathogenesis of HB, driven most commonly by interstitial deletions and missense point mutations in exon 3 hotspot region of CTNNB1 gene. We present the clinicopathologic features of a series of hepatocellular tumors with novel large CTNNB1 deletions.

Methods: NGS testing was performed using a clinically validated comprehensive targeted NGS panel. Briefly, after isolation of DNA and RNA from FFPE specimens, NGS libraries were prepared using the IDT library preparation kit followed by hybrid capture probes for 531 and 184 cancer-related DNA and RNA genes. The raw data generated from the Illumina NextSeq 550 instrument was subjected to a custom DNA and RNA bioinformatics pipeline for identification of mutations in the CTNNB1 gene.

Results: A total of 8 patients were identified with tumors harboring large CTNNB1 deletions which ranged in size from 26-749 bp, all involving exon 3. Molecular and clinicopathologic features of all 8 cases are summarized in Table 1 (insert image).

Conclusion: We describe large deletions in CTNNB1 involving exon 3 and the flanking intronic regions in a subset of pediatric liver tumors which often were clinically aggressive and demonstrated either undifferentiated/primitive components or features of hepatocellular neoplasm, not otherwise specified including HCC-like areas, pleomorphic features or macrotrabecular growth.

Table 1. Clinicopathologic features of hepatocellular neoplasms with large *CTNNB1* deletions								
Case	Age (yrs)	Sex	Stage	Mets	*CTNNB1* deletion	Location	Deletion size (bp)	Histologic Features
1	2	F	IV	Y, lungs and brain	c.76_101del; p.Q26Nfs*15	exon-3	26	**Initial bx**: Epithelial HB (F, E, macro, pleo) **Brain mets:** E, macro
2	3	M	IV	Y, lungs and chest wall	c.14-116_241+30del; Splice site deletion	intron-2/exon-3/intron-3	374	**Initial bx**: Epithelial HB (CF, E, SCU) **Mets:** E
3	2	F	IV	Y, lungs		intron-2/exon-3/intron-3	286	**Initial bx:** Epithelial HB (E, CF, SCU, blastema); **Lung mets:** E, SCU **Post-therapy resection:** Mixed HB (E, pleo, HCC-like)
4	2	F	II	N	c.65_100del; p.V22_S33del	exon-3	36	**Initial bx**: Epithelial HB (macro, pleo, F, E, blastema, SCU, cholangio) **Post-therapy resection:** Mixed HB (CF, E, pleo, blastema, sq)
5	3	M	IV	Y, lungs	c.91_242-91del; Splice site deletion	exon-3	261	**Initial bx**: Mixed HB (WDF, CF, E, SCU, sq, pleo, macro) **Post-therapy resection:** Mixed HB (pleo, F, E) **Mets:** Pleo, features of HCN, NOS
6	17	M	UK	Y, lymph node	c.49_432del; p.R18_D145del	intron-2/exon-3/intron-3	584	**Initial bx**: Undifferentiated high grade neoplasm with strong SALL4 and Lin28 expression
7	5	M	UK	UK	c.103_223del; p.I35Lfs*5	intron-2/exon-3/intron-3	120	**Post-therapy resection:** HCN, NOS
8	10	M	II	N	c.14-110_452del; Splice site deletion	intron-2/exon-3/intron-3	749	**Post-therapy resection:** HB (CF, pleo, HCC-like, E)

F- fetal, E- embryonal, pleo-pleomorphic, CF- crowded fetal, HCC-hepatocellular carcinoma, HCN, NOS-hepatocellular neoplasm, not otherwise specified, sq- squamous, SCU- small cell undifferentiated, macro-macrotrabecular, cholangio- cholangioblastic, WDF- well-differentiated fetal, mets- metastasis, UK- unknown, N-No, Y-Yes

Platform III: GI, Liver, and PEComas

3

Pediatric Colonic Graft-Versus-Host Disease: Multi-Institutional Validation of a Novel Histologic Grading System

A Alkashash [1], B Wilkins [2], O Saeed [1], I Gonzalez [1]; [1] Indiana University School of Medicine, [2] Children's Hospital of Philadelphia

Background: Graft-versus-host disease (GVHD) is a major complication of stem cell transplantation (SCT) with colonic involvement being associated with non-relapse mortality. The cardinal histologic features are crypt apoptosis, crypt drop-out and ulceration. Multiple grading systems have been proposed, with the Lerner system being the most widely use; however, it lacks diagnostic criteria for grade 1 and does not account for the degree of apoptosis. A novel system has been proposed providing a clear diagnostic criterion (PMID: 35365769). In this study we evaluated for the first time both the Lerner and this novel system in a cohort of solely pediatric patients.

Methods: A retrospective search from two academic centers from 2010-21 (center 1) and from 2005-21 (center 2) was made for cases of colonic GVHD. Only cases with available slides were included and all cases were reviewed by the same pediatric pathologist.

Results: A total of 101 cases were included (57 from center 1 and 44 from center 2), 60 (59%) presenting in boys with a median age of 8.9 years. Acute leukemia was the indication for SCT in 50 cases, with the remainder performed for other neoplastic diseases, bone marrow failure, primary immunodeficiency, sickle cell anemia, and lysosomal storage disease. The median time from SCT to colonic biopsy was 2 months (interquartile range (IQR): 1 – 6) and only 4 cases (4%) presented < 21 days after SCT. All cases received an allogeneic SCT, with 76% and 24% being matched unrelated and matched related donors, respectively. All but 2 biopsies showed apoptosis with a median number per 10 continuous crypts of 7 (total range: 1 – 41), and 53 cases (54%) showed >6 apoptosis (Table 1). Only 19% of cases showed mucosal ulceration. In 48% no crypt drop-out was seen whereas in 17% it was multifocal and diffuse, respectively. The Lerner grade was 1 in 48%, 2 in 13%, 3 in 19% and 4 in 20% of the cases; and the novel grade was indeterminate in 35%, low in 25%, intermediate in 26% and high in 14% of the patients. 72 patients (71%) had extracolonic GVHD and most cases (91%) received treatment for GVHD with 58% of them achieving treatment response. 37 patients (37%) died during clinical follow-up. Neither the Lerner nor novel system correlated with treatment response or mortality.

Conclusion: Not surprisingly neither the Lerner nor the novel system correlated with treatment response or mortality as both were developed in cohorts from adult patients. A system specifically for pediatric patients is much needed to better stratify these patients.

Table 1. Histologic findings (N: 101)

Crypt apoptosis, n, %	
Yes	99, 98.0%
No	2, 2.0%[1]
Number of crypt apoptosis, median, range[2]	7, 1 – 41
Number of crypt apoptosis, n, % (n: 99)	
1 – 6	46, 46.5%
>6	53, 53.5%
Mucosal ulceration, n, %	
Yes	19, 18.8%
No	82, 81.2%
Crypt drop-out, n, %	
No	48, 47.5%
Focal	19, 18.8%
Multifocal	17, 16.8%
Diffuse	17, 16.8%
Crypt and mucosal damage, n, %	
No crypt drop-out or ulceration	50, 49.5%
Crypt drop-out without ulceration	32, 31.7%
Ulceration	19, 18.8%
Lerner grade, n, %	
1	48, 47.5%
2	13, 12.9%
3	20, 19.8%
4	20, 19.8%
Novel grade, n, %[3]	
Indeterminate	35, 34.7%
Low	25, 24.8%
Intermediate	27, 26.7%
High	14, 13.9%

[1]Both cases case with no crypts available; [2]Crypt apoptosis were counted in 10 continuous crypts; [3]Based on Farooq A, et al. Mod Pathol 2022; 35: 12-54-1261.
Percentages might not add to 100 due to rounding.

Platform III: GI, Liver, and PEComas

4

Clinicopathologic Features of Pediatric Perivascular Epithelioid Cell Tumors (PEComas)

P Hammer [1], A Toland [2], A Shenoy [3], A Esnakula [4], J Hicks [2], A Al-Ibraheemi [5], S Tan [1]; [1] Stanford University School of Medicine, [2] Texas Children's Hospital, [3] Nationwide Children's Hospital; The Ohio State University College of Medicine, [4] The Ohio State University College of Medicine, [5] Boston Children's Hospital

Background: Perivascular epithelioid cell tumors (PEComas) are uncommon mesenchymal tumors of uncertain histogenesis that express smooth muscle and melanocytic markers. They demonstrate a range of clinical behavior and are highly associated with tuberous sclerosis complex (TSC). Pediatric PEComas are rare, with less than 40 reported cases, and their clinicopathologic spectrum is not well-documented. Herein, we describe a multi-institutional series of pediatric PEComas.

Methods: PEComas (not otherwise specified, NOS), angiomyolipomas (AML), lymphangioleiomyomatosis (LAM), and clear-cell "sugar" tumors (CCST) were retrospectively identified from four institutions and authors' files. We included patients up to age 25. We also identified patients with TSC and documented associated neoplasms. Clinical history, tumor size, site, multiplicity, treatment course and clinical status were recorded. Histopathologic features were documented. Multiple co-occurring tumors at the same site and similar features were noted as "multiple" but counted as one.

Results: The clinical and histopathologic features are summarized in Table 1. Forty-nine PEComa-family tumors were identified occurring in 44 patients (median age 15 years, range 2-25), diagnosed over 32 years (1991-2022). They were more common in females (32/44), and occurred mostly in kidney (33/49), then liver (4/49). Twenty-three patients (23/44) had confirmed TSC, 2 had suspected TSC mosaicism, and 1 had Li-Fraumeni syndrome (LFS). The most common diagnoses were conventional (23/49) and epithelioid (16/49) AML. Amongst patients with AMLs, most (24/37) had TSC and were more likely to have multiple AMLs (12/24) than non-TSC patients (2/13). One, with TSC, developed malignant transformation of an AML to angiosarcoma (kidney). LAM (4/49) occurred in females only, and in the context of TSC (3/4). PEComas-NOS (4/49) occurred exclusively in non-TSC patients, one of whom had LFS. Two were malignant, and 1 indeterminate. Those in non-LFS patients (3) had SFPQ-TFE3 fusions and occurred in appendix, cecum and vagina. The LFS patient presented with concurrent TSC2-altered malignant PEComa of the uterus and TFE3-translocated renal cell carcinoma (RCC). Three additional patients (2 TSC) had concurrent RCCs (eosinophilic solid and cystic, type 1 papillary, and "chromophilic eosinophilic type"). No CCST were identified in this cohort. Of the 3 patients with malignant tumors, 2 died from disease.

Conclusion: We report the largest series of pediatric PEComas to date. Consistent with literature in all age groups, there was a strong association with TSC; AML was most common and LAM occurred exclusively in "older" females (late teenage/early adult). In our pediatric cohort, TSC was more prevalent among patients with AML than previously reported. Although generally

benign, we note a rare case of malignant angiosarcomatous transformation of AML in a TSC patient. The 4 PEComas-NOS were in non-TSC patients, often malignant, and showed frequent SFPQ-TFE3 fusions, suggesting a distinct clinicopathologic profile. Co-occurrence of TSC2-altered malignant PEComa and TFE3-translocated RCC in an LFS patient, as well as concurrent RCCs seen in 3 others, suggest intriguing association worth further investigation.

Table 1. Clinical and Histologic Features of Pediatric PEComas

Diagnosis	TSC*	Age (median, years)	Sex (male vs female)	Location	Single vs. multiple	Largest tumor size (median, cm)	Predominant histologic component	Cytologic atypia	Necrosis	Increased mitoses (>1/10 high-power fields)	Malignant
AML (n = 23)	Yes n = 13	15 (6 – 17)	F = 9 M = 4	Kidney = 12 Liver = 1	Single = 4 Multiple = 9	4.5 (0.8 - 7.5)	Spindled = 8 Fat = 2 Vessels = 1	0%	0%	0%	0%
							Slide unavailable = 2				
	No n = 9	17.5 (9 – 23)	F = 6 M = 3	Kidney = 7 Liver = 1 Cutaneous = 1	Single = 7 Multiple = 2	3.9 (0.5 - 4.4)	Spindled = 2 Fat = 4	0%	0%	0%	0%
							Slide unavailable = 3				
Epithelioid AML (n = 16)	Yes n = 11	12 (5 – 22)	F = 6 M = 3	Kidney = 9 Liver = 2	Single = 8 Multiple = 3	5.0 (0.5 - 10)	Epithelioid = 11	18% (2/11)	10% (1/11)	10% (1/11)	0% (indeterminate = 1)
	No n = 4	10.5 (6 – 22)	F = 2 M = 2	Kidney = 4	Single = 4	5.6 (2.5 - 19.6)	Epithelioid = 4	33% (1/3)	33% (1/3)	33% (1/3)	0% (indeterminate = 2)
							Slide unavailable = 1				
Angiosarcoma arising from AML (n = 1)	Yes	22	F	Kidney	Single	8.5	Spindled	100%	100%	100%	100%
PEComa, NOS (n = 4)	Yes n = 0	N/A	N/A	N/A	N/A	N/A	N/A	N/A	N/A	N/A	N/A
	No n = 4	14 (11 – 17)	F = 4	Uterus = 1 Appendix = 1 Liver (metastasis from cecum) = 1 Vagina = 1	Single = 4	4.2 (4 – 33)	Epithelioid = 4	50% (2/4)	50% (2/4)	75% (3/4)	50% (2/4) (indeterminate = 1)
LAM (n = 4)	Yes n = 3	20 (17 – 23)	F = 3	Lung = 3	Multiple = 3	0.1 (<0.1 - 0.2)	Spindled = 3	0%	0%	0%	0%
	No n = 1	25	F = 1	Lung	Multiple	0.2	Spindled	0%	0%	0%	0%
PECOsis (n = 1)	Yes	2	F	Periaortic	Multiple	1.7	Vessels	0%	0%	0%	0%

*Also includes patients with suspected somatic mosaicism in *TSC* (n = 2)

Posters

Note: Posters #1, #36, and #54 are not able to be presented.

2

Evaluation of CITED1 protein expression in pediatric round cell sarcomas and Wilms' tumours: a potential diagnostic immunohistochemical marker for tumours with BCOR genetic alterations

A Glembocki [1], G Garcia [2], B Ngan [1], G Somers [1], R Chami [1]; The Hospital for Sick Children, University of Toronto, [2] The Hospital for Sick Children

Background: CITED1 is the first member of the CITED family of cofactors that are involved in regulating a wide variety of CBP/p300-dependent transcriptional responses. Its overexpression has been observed in a variety of cancers including Wilms' tumor, hepatoblastoma, melanoma, and epithelial tumours. However, the immunohistochemical (IHC) diagnostic potential of this marker has not been tested for soft tissue tumours. Herein, we report semiquantitative CITED1 IHC expression across different subtypes of pediatric soft tissue tumours.

Methods: We immunostained representative sections and/or TMAs of tumours with BCOR genetic alterations (including tumours with BCOR ITD and tumours with BCOR-CCNB3 fusion; n=11), CIC-rearranged sarcomas (n=4), Ewing sarcoma (n=21), rhabdomyosarcomas/RMS (n=16), synovial sarcomas (n=5), unclassified round cell sarcomas with no genetic hallmarks (n=5), clear cell sarcoma of kidney with BCOR ITD (n=1), and Wilms tumours (n=14). The assay was conducted on the DAKO Omnis staining platform using anti-CITED1 antibody (clone 5H6, monoclonal mouse, Ready-to-Use, DAKO, Cat. No. GA701) and the Envision Flex detection kit (DAKO, Cat. No. GV800). Appropriate positive and negative controls were used. CITED1 positivity was defined as mild, moderate or strong nuclear immunoreactivity in at least 5% of cells.

Results: IHC for CITED1 was positive in all tumours with BCOR alterations including the CCSK; all cases showed extensive and moderate to strong staining. These tumours showed nuclear BCOR positivity. All Wilms tumours cases showed patchy to extensive nuclear staining for CITED1, mainly in the blastema and focally in the immature epithelial component. CITED1 was positive in five cases of embryonal RMS; one of which showed moderate nuclear staining in about 30% of cells and four showed weak to mild immunoreactivity in about 5% to 10% of cells. All other sarcomas, including five cases of alveolar RMS, were completely negative for CITED1.

Conclusion: Our results showed that CITED1 is a sensitive but not highly specific marker for Wilms tumours and tumours with BCOR genetic alterations. Nonetheless, CITED1 may be helpful to distinguish monophasic or biphasic Wilms tumours from some histologic mimics including CIC-rearranged sarcomas and synovial sarcomas. Further, the study reinforces that CITED1 is a useful immunohistochemical marker for BCOR-altered tumours, and the combination of CITED1 and BCOR is a powerful diagnostic tool that can differentiate this entity from other small round cell sarcomas.

3

Automated deep learning-based recognition of Wilms tumor histopathology

R de Krijger [1], T de Bel [2], A Mavinkurve-Groothuis [1], J Rutgers [1], L van Alst [2], M van den Heuvel-Eibrink [1], A van der Kamp [1], J van der Laak [2]; [1] Princess Maxima Center for pediatric oncology, [2] Radboud University Medical Center

Background: Histopathological assessment of Wilms tumors (WT) is crucial for risk group classification to guide postoperative stratification in chemotherapy pre-treated WT cases. However, due to the heterogeneous nature of the tumor, significant interobserver variation between pathologists in WT diagnosis has been shown, potentially leading to misclassification and suboptimal treatment. We investigated whether artificial intelligence (AI) can contribute to accurate and reproducible histopathological classification of WT, through recognition of individual histopathological tumor components.

Methods: We assessed the performance of a deep learning-based AI system in quantifying WT components in hematoxylin and eosin-stained slides by calculating the Sørensen-Dice-coefficient for 15 predefined renal tissue components, including six tumor-related components. We trained the AI system using multiclass annotations from 72 whole-slide images of patients diagnosed with WT. The agreement between pathologist and the DL-based system was calculated using Cohen's Kappa.

Results: The overall Dice-coefficient for all fifteen tissue components was 0.85 and for the six tumor-related components 0.79. Tumor segmentation worked best for necrosis (Dice-coefficient 0.98) and blastema (Dice-coefficient 0.82).

Conclusion: Reproducible histopathological classification of WT may be feasible using a digital pathology-based AI system in a national cohort of WT patients.

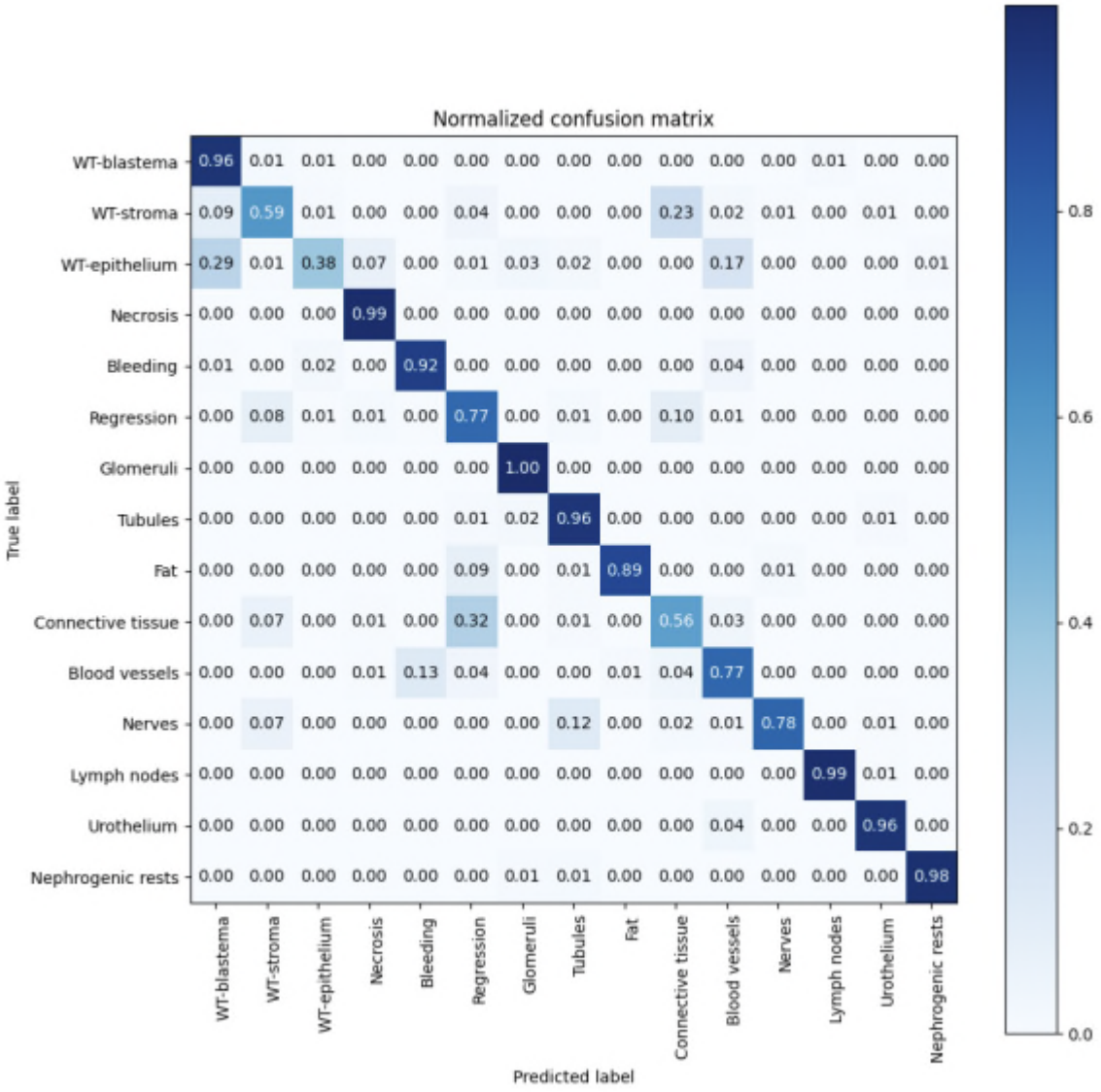
Normalized confusion matrix
True label
Predicted label
WT-blastema
WT-stroma
WT-epithelium
Necrosis
Bleeding
Regression
Glomeruli
Tubules
Fat
Connective tissue
Blood vessels
Nerves
Lymph nodes
Urothelium
Nephrogenic rests
0.0
0.2
0.4
0.6
0.8

4

Comprehensive molecular characterization of pediatric CIC-rearranged sarcomas: opportunities and pitfalls

[1], P Stow [2], Z Shi [2], J Neary [2], D Wheeler [2], L Furtado [2]; [1] , [2] St. Jude Children's Research Hospital

Background: CIC-rearranged sarcomas (CIC-RS) are very rare soft tissue and brain sarcomas with a dismal prognosis. Detection of the defining CIC rearrangement is critical for accurate diagnosis; however, each of the readily available molecular detection methods can mistakenly miss a CIC alteration.

Methods: Pathology archives through December 2022 were searched for cases that were positive, equivocal, or suggestive for CIC rearrangement by the following modalities: 1) FISH positive or equivocal for CIC rearrangement; 2) molecular (whole transcriptome [RNAseq] and/or DNA methylation array analysis [MA]) testing containing a CIC rearrangement or with a classification of CIC-RS; or 3) pathology report including CIC-RS in the differential diagnosis. Definitive non-CIC-RS diagnoses were excluded. Histologic findings were reviewed, and all available molecular results were tabulated. For cases with available material and incomplete molecular testing, FISH, RNAseq, and/or MA were performed as appropriate.

Results: 56 tumors from 46 patients were identified, including brain (18 patients, 23 tumors), solid tumor (27 patients, 31 tumors), and hematologic (1 patient, 2 samples). Age at diagnosis was 3 weeks to 41 years (mean 10.3 years, median 9 years). Histologic diagnoses were round cell sarcoma (25), high-grade neuroepithelial tumor (5), high-grade sarcoma (5), malignant tumor (5), embryonal tumor (4), myeloid sarcoma (1), and primitive neuroectodermal tumor (1). 43 tumors (31 positive, 4 equivocal, 8 negative) had CIC FISH performed, 33 (15 CIC::DUX4, 4 CIC::NUTM1, 3 CIC::LEUTX, 2 CIC::NUTM2A/B, 1 ATXN1::NUTM1, 1 ATXN1::NUTM2, 1 CIC::DUX4 proximity, 1 novel DOCK1::DUX4, 1 ZNF532::NUTM1, 4 negative) had RNAseq, and 34 (28 CIC-RS [EFT_CIC], 6 unclassifiable) had MA. Tumors from 26 patients had both FISH and RNAseq, 34 had both FISH and MA, 25 had both RNAseq and MA, and 25 with all three methods. For CIC::DUX4 and CIC::NUTM1 fusions (n=19), FISH and RNAseq agreed in 10/15 (67%) tested tumors (equivocal in 2, negative in 3). All 15 tested cases classified as EFT_CIC by MA. For tumors with unusual CIC partners or CIC-related rearrangements, FISH and RNAseq agreed in 9/12 (75%); discordant results were 2 negative FISH results (1 CIC::NUTM2, 1 CIC::LEUTX by RNAseq) and 1 equivocal FISH result (DOCK1::DUX4 by RNAseq). Overall, MA results agreed with FISH and/or RNAseq in 26/31 (84%) cases; all 3 CIC::LEUTX tumors and 2 FISH-positive, RNAseq-negative tumors were unclassifiable by MA. Both ATXN1-fused tumors classified as EFT_CIC by MA. < Insert table here>

Conclusion: This large pediatric-focused study assessed the technical performance of different molecular methods for CIC rearrangement detection. CIC FISH and RNAseq both miss >20% of CIC-RS. MA can accurately detect CIC-RS. ATXN1::NUTM1/2 tumors are similar to CIC-RS by MA, but are missed by CIC FISH. Despite the presence of a CIC rearrangement, CIC::LEUTX tumors may be biologically distinct. Multimodal molecular testing is needed for accurate diagnosis of this rare tumor type.

FISH (43 tested)	**RNAseq** (33 tested)	**MA** (34 tested)
Positive (31)	*CIC::DUX4* (9)	EFT_CIC (8) Not performed (1)
	CIC::DUX4 proximity (1)	EFT_CIC (1)
	CIC::LEUTX (2)	Unclassifiable (2)
	CIC::NUTM1 (2)	EFT_CIC (2)
	CIC::NUTM2A (1)	Not performed (1)
	Negative (4)	EFT_CIC (2) Unclassifiable (1) Not performed (1)
	Not performed (12)	EFT_CIC (7) Unclassifiable (1) Not performed (4)
Equivocal (4)	*CIC::DUX4* (2)	EFT_CIC (2)
	DOCK1::DUX4 (1)	Not performed (1)
	Not performed (1)	EFT_CIC (1)
Negative (8)	*CIC::DUX4* (3)	EFT_CIC (3)
	CIC::LEUTX (1)	Unclassifiable (1)
	CIC::NUTM2B (1)	Not performed (1)
	ATXN1::NUTM1 (1)	EFT_CIC (1)
	ATXN1::NUTM2 (1)	EFT_CIC (1)
	ZNF532::NUTM1 (1)	Unclassifiable (1)
Not performed (3)	*CIC::NUTM1* (2)	Not performed (2)
	CIC::DUX4 (1)	Not performed (1)

5

Histiocytic Neoplasms with BRAF Rearrangements and Loss of CDKN2A: A Distinct Entity with Uncertain Malignant Potential?

C Casiano [1], R Alaggio [2], L Berklite [3], A Breaux [3], A Cardoni [2], G Gheorghe [4], S Koo [4], A Kumar [3], R Lorsbach [3], S Roy [3], P Russo [5], B Sisk [6], L Surrey [5], S Szabo [3], N Wadhwani [7], J Weinstein [7], J Picarsic [3]; [1] Cincinnati Children's Hospital Medical Center, Cincinnati, OH, USA, [2] Ospedale Pediatrico Bambino Gesu, Rome, Italy, [3] Cincinnati Children's Hospital Medical Center, Cincinnati, OH, USA, [4] St. Jude Children's Research Hospital, Memphis, TN, USA, [5] Children's Hospital of Philadelphia, Philadelphia, PA, USA, [6] Washington University School of Medicine, St. Louis, MO, USA, [7] Lurie Children's Hospital, Chicago, IL, USA

Background: Gene alterations in the mitogen-activated protein kinase-extracellular signal-regulated kinase (MAPK-ERK) pathway, particularly BRAF mutations, are well recognized in several histiocytic neoplasms, including Langerhans cell histiocytosis (LCH); however, rearrangements of the BRAF gene are infrequently reported, particularly in non-LCH histiocytic neoplasms. Little is known about their association with loss of cell cycle control at the CDNK2a/p16 locus. We present 7 cases with BRAF rearrangement and loss of cell cycle control (CDKN2a/p16) with a spectrum clinicopathologic features.

Methods: Cases that had a predominantly non-LCH immunophenotype with loss of p16 immunostaining and harboring BRAF rearrangements were collected per institutional and/or IRB protocol/regulation. One case was previously published.

Results: Seven cases were identified, including 3 female and 4 male patients, ranging in age from 6 months to 22 years. Four patients had reported histologic or radiographic evidence of multifocal disease. The cases reviewed involved multiple sites including the skin, soft tissue, bone, inguinal region, lungs, and brain. All cases had epithelioid morphology with a range from low-grade to high-grade nuclear atypia. All 7 cases were positive for at least two macrophage markers (CD163, CD68, and/or CD14) and showed strong expression of p-ERK and, when performed, cyclin D1 (n=6). The mutant specific BRAF VE1 stain was negative in all cases. The Ki-67 proliferative index was quite variable (10-70%) and did not show concordance with the degree of nuclear atypia. All cases had CDKN2a loss with confirmed loss of p16 staining in lesional cells, including one that also harbored a presumed germline deletion of CDNK2a. The BRAF fusion partners identified were BICD2, PICALM, PLEK, SLC44A1, MTAP, MS4A6A, and NRF1. Clinical behavior ranged from indolent to aggressive with systemic disease presentation.

Conclusion: Little is known about the clinical, morphologic, and integrated genomic findings in non-LCH neoplasms with BRAF rearrangements. It is possible that the additional loss of cell cycle control at the CDNK2a/p16 locus may further contribute to the atypical morphology and/or clinical behavior in these cases. Further investigation is needed to explore if this group may represent a new distinct entity of histiocytic neoplasms with uncertain malignant potential (HUMPs).

6

Pediatric Central Nervous System Histiocytic Tumors: A single-institution study

F Alnoor [1], O Anelo [2], J Chiang [3], G Gheorghe [3]; [1] University of Utah Health/ARUP Laboratories, [2] The University of Tennessee Health Science Center, [3] St. Jude Children Research Hospital

Background: Histiocytic disorders comprise a group of heterogeneous tumors and manifest as isolated or systemic diseases with a wide age distribution. Central nervous system (CNS) involvement is uncommon and may be underreported. The clinical and imaging characteristics of CNS histiocytic lesions overlap with those of primary brain tumors. Accurate classification is challenging, particularly in small brain biopsies, due to a lack of defined morphologic and molecular markers.

Methods: The pathology records were searched for CNS histiocytic lesions in the past twenty years. The clinical course, radiology, and pathology were reviewed.

Results: Our retrospective review identified ten cases of histiocytic lesions, including histiocytic sarcoma (HS); n=3, Langerhans cell histiocytosis (LCH); n=3, Rosai-Dorfman Disease (RDD); n=2, and a single case of each juvenile xanthogranuloma (JXG), and Erdheim-Chester disease (EDD). Patients' ages range from 8 months to 16 years (median age: 10 years) with a 0.8:1 male-to-female ratio. By imaging, 40% (n=4) were dura-based and 60% (n=6) involved brain parenchyma. 80% of cases (n=8) demonstrated unifocal lesions (all cases of HS, LCH, JXG, CRH, and one case of RDD). Four patients (JXG, ECD, LCH, and RD) had additional clinical follow-up data. Of these four, two patients (RD and ECD) had systemic diseases. BRAF V600E mutation by immunohistochemistry (IHC) was identified in one HS and one ECD (confirmed by next-generation sequencing). FISH demonstrated BRAF rearrangement in one HS case negative for BRAFV600E.CDKN2A deletion was identified in two cases of HS. Following therapy, radiological evidence of stable disease was reported in ECD and one case of RD, while two patients with JXG or LCH showed no residual disease. (see table 1)

Conclusion: We are reporting ten cases of histiocytic lesions involving the CNS; 4 of them are dura-based. The majority (8/10) had unifocal lesions. Four patients with available clinical follow-up had either stable disease course or no evidence of disease following therapy. Ancillary studies showed BRAF V600E mutation in one ECD and one HS case, and BRAF rearrangement in one HS case, along with CDKN2A deletion in two cases of HS. Since untreated CNS involvement may have an adverse outcome, timely recognition is paramount. Workup to include imaging, immunohistochemistry, and molecular studies is necessary to avoid misdiagnosis of primary brain tumors or other hematopoietic neoplasms.

Table 1: Summary of all cases of pediatric central nervous system histiocytic lesions

Case number	Age at diagnosis	Sex	Diagnosis	Clinical presentation	Imaging findings / CNS involvement		Other sites involvement	Pertinent ancillary findings	Treatment and outcome
1	9 years	M	ECD	Poor coordination and abnormal gait	Multifocal enhancing masses in seller/suprasellar region, ventricles, and right temporal lobe. Abnormal signals in the cerebellum, pons, and basal ganglia. No definite skull lesions.	Multifocal	PET Avid signals uptake in the right maxillary sinus and long bones.	Immunohistochemistry (IHC): Weak positive for *BRAF* V600E Targeted NGS: *BRAF* NM004333:c.1799T>A, p.Val600Glu	Targeted therapy with dabrafenib. Radiological evidence of stable disease.
2	8 years	F	HS	Headache and intermittent projectile vomiting for 3 months	4.8 cm heterogeneous and contrast-enhancing cortical-based cystic and solid mass with internal small foci of calcification at the right temporal area.	Supratentorial	NA	IHC: Positive for *BRAF* V600E FISH: *CDKN2A* deletion	NA
3	6 years	M	HS	Seizures	Extra axial Left posterior parietal dural based tumor.	Extra axial/ Dura	NA	NA	NA
4	8 months	F	HS	NA	Midline cerebellar mass.	Infratentorial	NA	IHC: Negative for *BRAF* V600E FISH: *BRAF* gene rearrangement and homozygous deletion of *CDKN2A*	NA
5	14 years	M	JXG	Seizures	Dural based lesion in the right temporal lobe.	Extra axial/ Dura	PET scan negative for systemic disease.	NA	No radiological evidence of disease 6 years post-resection.
6	11 years	F	LCH	Diabetic insipidus	Absent normal bright signals of the neurohypophysis and a thickened, enhancing pituitary stalk.	Supratentorial	PET scan negative for systemic disease.	IHC: Negative for *BRAF* V600E	6 courses of cladribine and maintenance therapy with 6-MP and MTX. No radiological evidence of disease 12 months post-treatment.
7	14 years	F	LCH	Weight loss increased thirst and urination at night. Growth hormone deficiency	Hypothalamic optic chiasmatic enhancing mass measures 1.2 cm x 1.1 cm x 1.1 cm.	Supratentorial	NA	IHC: Negative for *BRAF* V600E	NA
8	3 years	F	LCH	Diabetic insipidus	Thickened pituitary stalk.	Supratentorial	NA	NA	NA
9	16 years	F	RD	Papilledema and headache for 2 years	Foci of dural nodularity on the anterior falx. Infiltration around the optic nerve of the left eye immediately behind the globe.	Supratentorial	Pathological evidence of left orbital involvement.	NA	Radiological evidence of stable disease 8 years post-diagnosis.
10	15 years	M	RD	Seizures	Dural based lesion in the right posterior temporal lobe.	Extra axial/ Dura	NA	NA	NA

M, Male; F, Female; CNS, central nervous system; IHC, Immunohistochemistry; NGS, Next-generation sequencing; ECD, Erdheim-Chester disease; HS, Histiocytic sarcoma; JXG; Juvenile xanthogranuloma; LCH, Langerhans cell histiocytosis; RD, Rosai-Dorfman disease; CSH, crystals storing histiocytosis; FISH, Fluorescent in situ hybridization; MTX, methotrexate; NA, not available.

7

ALK-positive histiocytic proliferation associated with pneumothorax

S Sirotnikov [1], J Velazquez-Vega [2], H Yin [2]; [1] Children's Healthcare of Atlanta, [2] Children's Healthcare of Atlanta

Background: ALK-positive histiocytosis is a rare histiocytic neoplasm, initially described in 2008, with the largest case series to date describing 39 cases. Various clinical subtypes have been recognized (groups 1A, 1B and 2). Group 1A and 1B are both multisystem diseases with 1A showing involvement of liver, spleen and bone marrow while 1B tends to involve the nervous system but may also involve the lungs, bone, liver, skin and lymph nodes. Group 2 is characterized by single system disease with reported sites including nervous system and skin/soft tissue. Histologically, they can range from classic xanthogranuloma features with foamy histiocytes and Touton giant cells to a more monomorphic cellular appearance with variable epithelioid or spindled morphology. Immunophenotypically, ALK is characteristically positive with a cytoplasmic pattern but may be focal or weak. Expression of at least 2 histiocytic markers (CD163, CD68, CD14, CD4) is required for the diagnosis. Additional expression of S100, cyclin D1 or factor XIIIa may be seen as well. These tumors harbor ALK gene translocation, with KIF5B being the most common partner, however, fusion with uncommon partner genes has been reported.

Methods: We describe one case of an ALK-positive histiocytic proliferation. The workup included assessing hematoxylin & eosin (H&E)-stained slides, immunohistochemical stains and fluorescent in-situ hybridization (FISH).

Results: An 11-year-old female initially presented with acute onset chest pain and increased respiratory rate. Chest x-ray showed a bleb/cyst in the left lower lobe of the lung measuring 11 x 12 x 11 mm, consistent with a spontaneous pneumothorax. Brain magnetic resonance imaging (MRI) and positron emission tomography/computed tomography (PET-CT) were negative. The treatment plan opted for continued surveillance. To date, 5 months after the initial diagnosis, imaging has shown no evidence of disease. H&E-stained slides showed a ruptured cyst in the subpleural surface lined by epithelioid histiocytes with giant cells and cholesterol clefts. The epithelioid cells were positive for ALK-1, CD163 (focal), CD68 (focal), FXIIIa, CD1a (focal), S100 (focal), and CD45. They were negative for CD30, EMA, WT1, D2-40, calretinin, AE1/AE3 and TTF-1. Fluorescence in situ hybridization (FISH) was positive for rearrangement of the ALK(2p23) locus.

Conclusion: ALK-positive histiocytosis is a recently described entity in the WHO classification. Isolated lesions within the lung have not previously been described. Due to their rarity, long term follow-up is needed to better understand their behavior.

8

ALK-rearranged Epithelioid Mesenchymal Neoplasm: Expanding the Spectrum of Tyrosine Kinase Altered Mesenchymal Tumors

C Gestrich [1], J Davis [2], L Biederman [3], I John [1], R Alaggio [4], M Arnold [5], A Shenoy [3], A Tchakarov [6], A Al-Ibraheemi [7]; [1] University of Pittsburgh Medical Center, [2] Oregon Health and Science University, [3] Nationwide Children's Hospital, [4] Bambino Gesu Children's Hospital, [5] Children's Hospital Colorado, [6] University of Texas Health Science Center McGovern Medical School, [7] Boston Children's Hospital

Background: The anaplastic lymphoma kinase (ALK) gene encodes a receptor tyrosine kinase and fusions involving this gene have been reported in a variety of mesenchymal neoplasms. ALK-altered tumors with epithelioid morphology have been described in epithelioid inflammatory myofibroblastic sarcoma, epithelioid fibrous histiocytoma, and recently reported in three mesenchymal tumors occurring in adult patients. Herein, we are describing clinicopathologic features of 7 mesenchymal tumors with epithelioid morphology occurring predominately in the pediatric population.

Methods: Clinical, histopathologic, and genomic data was collected from six hospitals. Next generation sequencing was performed on formalin fixed paraffin embedded samples.

Results: We identified 7 tumors occurring in 4 females and 3 males, with an age ranging from 1 month to 28 years (median: 17 years). Five tumors were superficial and solitary, while one presented with multiple peritoneal and omental nodules and one presented as a large mediastinal mass. The sizes ranged from < 0.5 to 14.0 cm. Morphologically, all tumors were comprised of epithelioid cells arranged in sheets, anastomosing cords, or small clusters embedded in a myxohyaline stroma. The cells had slightly variably-sized ovoid nuclei with moderately-prominent nucleoli and abundant eosinophilic cytoplasm. Other morphologic features were: rhabdoid cytology (n=3), focal spindling (n=3), and round cell cytology (n=1). Mitotic figures were sparse in 4 cases and did not demonstrate necrosis. The remaining three tumors (2 deep, 1 superficial) had more than 10 mitoses per 10hpf as well as foci of necrosis. CD34 was positive in 2 cases and S100 was patchy/focally positive in 2 cases. ALK fusions were identified in all cases (table). One tumor recurred locally 2 years after initial resection, 1 patient had widely metastatic disease (mediastinal tumor). At time of last follow up (n=6): 4 patients were alive without evidence of disease, 1 died due to complications of therapy (peritoneal tumor), one was alive with disease.

Conclusion: Our findings expand the spectrum of ALK-rearranged mesenchymal tumors. Our cases predominately occurred in older children and mainly exhibited epithelioid to round cell morphology, as opposed to spindle cell morphology and did not have characteristic features/fusions associated with epithelioid myofibroblastic sarcoma. Tumors in a deep location with high grade features follow a more aggressive clinical course.

Case #	Age (years)/Sex	Location	Size (cm)	Recurrence/progression	Metastasis	Treatment	F/U	Fusion
1	16/F	Finger	1.5	Yes	No	Resection	ANED	*HMBOX1::ALK*
2	28/F	Foot (fascia)	<0.5	No	No	Resection	NA	*VCL::ALK*
3	18/F	Peritoneum/omentum	Up to 4.5 (multiple)	Yes	No	Chemotherapy, Alectinib	Died*	*PRRC2B::ALK*
4	11/F	Arm	2.2	No	No	Excisional biopsy	ANED	*MYH10::ALK*
5	17/M	Shoulder	8.5	No	No	Resection	ANED	*STRN::ALK*
6	1 month/M	Arm	4.5	No	NA	Resection	ANED	*EML4::ALK*
7	17/M	Mediastinum	14.0	Yes	Yes	Resection, radiation, chemotherapy	AWD	*EML4::ALK*

F: female, M: male, ANED: alive with no evidence of disease, AWD: alive with disease, *Died from complications of therapy

9

Sarcoma with BCOR genetic alterations: clinical and pathologic features of 10 pediatric cases

A Gilani [1], M Qureshi [2], N Uddin [3]; [1] University of Colorado, Childrens Hospital Colorado, The Aga Khan University Hospital- Karachi, [2] The Aga Khan Univerity Hospital, [3] The Aga Khan University Hospital

Background: Sarcomas with BCOR genetic alterations a rare group of round cell sarcomas that show variable clinical presentations but overlap regarding morphology, immunoprofile, and gene expression, suggesting a shared pathogenesis. These tumors can show both BCOR-related gene fusions, most frequently BCOR-CCNB3 or BCOR internal tandem duplication (BCOR-ITD). We present a series of pediatric BCOR-rearranged sarcomas from our practice to emphasize the clinical and histologic spectrum of this entity and to help distinguish this tumor from other morphologically similar entities.

Methods: Electronic records of the pathology department were searched for confirmed or suspected cases of BCOR-altered sarcomas from 2016-2022 (both inclusive). 10 cases were identified. BCOR immunohistochemistry was performed on cases without prior use of this stain.

Results: Out of a total of 10 cases, 4 presented under the age of 5 yrs. As reported previously, a male preponderance was seen (8M; 2F). 2 cases presented in the head and neck, 1 in hand, 1 in foot, 3 in the spine or adjacent skeleton, 2 in the leg or thigh, and 1 in the abdomen. 5 cases were confirmed on NGS studies, 3 with BCOR-CCNB3 fusion, 1 BCOR::MAML3 and 1 BCOR ITD. BCOR IHC was the most helpful stain as all molecularly confirmed cases showed strong BCOR immunopositivity. Most common morphologic features reported were small round to oval cells in myxoid background. Epithelial-like glandular appearance was seen in 2 cases. Interestingly, a FISH based BCOR rearrangement assay was negative in a case with BCOR-ITD that was later confirmed on NGS.

Conclusion: BCOR-altered sarcomas need to be part of the differential diagnosis in the pediatric age group, in particular cases with round cell or myxoid histology. BCOR IHC followed by NGS-based RNA sequencing can help in the diagnosis.

10

Nasal Chondromesenchymal Hamartoma; A clinicopathological study of 5 cases

A Gilani [1], N Uddin [2]; [1] University of Colorado, Childrens Hospital Colorado, The Aga Khan University Hospital- Karachi, [2] The Aga Khan University Hospital

Background: Nasal Chondromesenchymal Hamartoma (NCMH) is a rare benign mesenchymal tumor of sinonasal tract. It is histologically characterized by lobules of cartilage and a variably myxoid spindle cell stroma underneath respiratory lining. In a systematic review, 62 cases of NCMH have been published.

Methods: Cases diagnosed as NCMH were searched electronically (2015-2022). Demographic data was obtained from surgical reports. H&E slides were reviewed, and follow-up was obtained.

Results: A total of 5 cases were diagnosed during the study period. Age ranged from 3.5 years to 12 years (mean 7.7 years). Three were females and 2 were males. Clinical symptoms included nasal obstruction, epistaxis and proptosis. Tumor was located in nasal cavity in 3 cases and paranasal sinuses and fronto-ethmoid sinuses in one case each. Tumor size in aggregate ranged from 3.5 to 5 cm (mean 4.5 cm). Histologically a lobulated growth pattern was seen in all cases composed of immature and mature cartilage along with spindle to stellate cells present in a myxoid stroma. Host bone entrapment was noted in 2 cases. Overlying respiratory epithelium was noted in all cases. Scattered osteoclast type giant cells were noted in one case. S100 was positive in all cases. Follow up was available in 4 patients. Recurrence was seen in patients, 3 and 4 years after surgery respectively. The other two patients are free of disease 2 months and 17 months after surgery respectively. Although germline DICER1 testing was recommended, to-date it has not been performed in any case

Conclusion: We report clinicopathological features of 5 cases of rare nasal chondromesenchymal hamartoma. A slight female predominance was seen in our series and a slight older age (7.7 years vs 5.1 years) as compared to the recent literature. Nasal cavity was a common site in contrast to paranasal sinuses.

11

Atypical and Malignant Peripheral Nerve Sheath Tumors in Children: An institutional experience

L Biederman [1], S Chen [2], A Rubrecht [2], A Shenoy [2]; [1] Nationwide Children's Hospital, [2] Nationwide Children's Hospital

Background: Atypical neurofibromas and malignant peripheral nerve sheath tumors (MPNST) are uncommon pediatric tumors with a wide range of histologic findings, clinical presentations, and prognoses. Consensus criteria have been proposed to categorize and prognosticate these tumors in patients with germline neurofibromatosis type 1 (NF1) mutations. We present a pediatric series of atypical and malignant peripheral nerve sheath tumors in patients with and without NF1 mutations.

Methods: Institutional pathology records were queried for atypical neurofibromas and MPNSTs between 1/2010 to 12/2022. Archived slides and reports were reviewed by two pathologists for confirmation of diagnosis, and classification of cases was performed based on consensus criteria. Clinical records were reviewed for demographic data, genomic data, and follow-up information.

Results: We identified a total of 11 tumors in 10 patients (age range 12 -24 years; median: 17.5 years; 6 males, 4 females). Five high grade MPNSTs were identified in 5 patients. These occurred in 3 patients with NF1, 1 patient with schwannomatosis and a germline SMARCB1 mutation, and 1 patient with a history of radiation in the area of the MPNST. All cases had high cellularity and a high mitotic rate (>10/10 HPF), and all but one biopsy demonstrated necrosis. Two low grade MPNSTs were identified, one in a patient with NF1 and one with negative NF1 testing. Both had increased mitotic rates, high cellularity, effaced architecture, and no necrosis. Three atypical neurofibromatous neoplasms of uncertain biologic potential (ANNUBP) were identified which met two of three criteria, including atypia, loss of architecture, cellularity, and/or mitotic activity. Finally, in the patient with the SMARCB1 germline mutation discussed above, a second schwannian tumor with atypical features was identified. S-100 staining was reviewed in 9 tumors and was highly variable in percentage of tumor cells staining. H3K27me3 immunohistochemical stain was not uniformly performed on all cases. All patients with ANNUBP and low grade MPNST are alive at last follow up (range: < 1-9 years), while 4/5 patients with high grade MPNST were deceased. The patient with post radiation high grade MPNST is alive at last follow up with no disease.

Conclusion: Our findings build upon the accepted consensus criteria established for atypical neurofibromatous tumors in patient with NF1 expanding the application of criteria to include atypical tumors in patients without NF1. Forty percent of the cases examined were in patients either with no clinical stigmata of NF1 or negative testing. High-grade MPNSTs in our series only occurred with a predisposing factor. Low-grade and atypical nerve sheath tumors had a uniformly good outcome.

12

Pitfalls of H3K27me3 and SATB2 Immunohistochemistry in Osteosarcoma

A Rubrecht [1], A Shenoy [2], S Chen [2]; [1] Nationwide Children's Hospital, [2] Nationwide Children's Hospital

Background: Loss of expression of H3K27me3 is well documented in malignant peripheral nerve sheath tumors, however expression in osteosarcomas (OS) has not been elucidated. SATB2 expression is a well-established marker of osteogenic differentiation, may be useful in OS with minimal osteoid production. We explored the expression pattern of H3K27me3 and SATB2 in OS biopsies and subsequent resections.

Methods: An institutional search (January 2018-2022) identified 20 cases of primary OS biopsy and subsequent resection. Histologic subtypes and the presence or absence of decalcification was recorded. Patient demographics and clinical data were extracted from the electronic medical chart. A representative formalin-fixed paraffin embedded block was selected and H&E, H3K27me3 and SATB2 immunohistochemistry was performed and reviewed for extent of expression (< 10%, 10-50%, 51-75%, >75%) and intensity (weak, moderate, strong) of nuclear staining. Statistical analysis was performed using a paired t-test.

Results: Twenty patient cases (9M; 11F; age range: 6-18 years) were examined. Histologic subtypes included osteoblastic, chondroblastic, telangiectatic, osteoblastoma-like, fibroblastic and epithelioid. A spindled component was identified at least focally in 25% (5/20) cases. Two (10%) biopsies demonstrated areas of crush artifact. Sites of origin included femur (9), tibia (7), occipital bone (1), humerus (1), vertebral body (1), fibula (1). Half of the biopsies were decalcified. Definitive SATB2 positivity (>75% staining with 3+ intensity) was identified in 30% (6/20) biopsies (50% decalcified) and 10% of resections. Definitive H3K27me3 staining (>50% of cells with ≥2+ intensity) was noted in 75% of biopsies and 50% of resections. Notably, loss of H3K27me3 staining was noted in areas of spindling or crush artifact.

Conclusion: Loss of staining in areas of spindling without osteoid and in areas of crush artifact highlights an important pitfall of H3K27me3 in OS that could be challenging on small biopsies. Decalcification appears to impact SATB2 expression between biopsy and resection (p=0.04), as observed on paired samples. However, there was no difference in H3K27me3 expression despite decalcification (p=0.11).

13

Altered p53 expression and molecular analysis in Osteosarcoma

A Rubrecht [1], S Chen [2], C Cottrell [2], K Schieffer [2], A Shenoy [2]; [1] Nationwide Children's Hospital, [2] Nationwide Children's Hospital

Background: Molecular alteration of TP53 is a known finding in osteosarcoma (OS). We aimed to determine the expression of p53 in OS on paired biopsy and subsequent resections and compare expression profile to mutation status.

Methods: A retrospective search from January 1st 2018 to January 2022 identified 20 cases of primary biopsy and subsequent resection, from which a representative formalin-fixed paraffin embedded block was selected. p53 immunohistochemistry was performed and stains were reviewed for extent of expression as follows: < 5%, 5-50%, >50% and intensity (weak, moderate, strong) of nuclear staining. Decalcification status of biopsy tissue was noted. Available molecular results were recorded. Patient demographics and clinical data were extracted from the electronic medical chart.

Results: Twenty patient cases (9M, 11F; age range: 6-18y, median: 13y) were examined. Sites involved included the femur (9), tibia (7), occipital bone (1), humerus (1), vertebral body (1) and fibula (1). Histologic subtypes included osteoblastic, chondroblastic, telangiectatic, fibroblastic, osteoblastoma-like and epithelioid. Molecular data was available for nine patients with 22% (2/9) having germline p53 alterations. Additionally, one patient carried a diagnosis of Li-Fraumeni syndrome without available molecular studies. Both patients with germline p53 mutations, as well as the Li-Fraumeni patient had increased p53 expression (75-95%) on biopsy, which was retained in only one case at resection. Somatic mutations were detected in six patients (67%). Of these patients half had < 5% and half had between 5-50% p53 expression. The remaining patient with no detectable p53 mutation had moderate (25%) p53 expression by IHC. Half of all biopsies (decalcified and non-decalcified) showed < 5% p53 expression. 10% and 40% decalcified biopsies showed >50% and 5-50% p53 expression, compared to 20% and 30% non-decalcified biopsies. Resections demonstrated < 5%, 5-50% and >50% p53 expression in 70%, 25% and 5% of cases respectively. In 40% of non-decalcified biopsies, p53 expression decreased by one tier at resection.

Conclusion: Our findings indicate that p53 immunohistochemical expression is higher in patients with germline alterations despite decalcification and lower expression suggests somatic alteration without germline involvement. In addition, decalcification affects p53 expression from biopsy to resection, though not statistically significant (decal: p=0.45 vs non-decal p=0.055).

14

Ectopic Thymus, a Rare Embryologic Anomaly

A Rubrecht [1], S Kahwash [2], P Walz [2], L Zhang [3], S Chen [2]; [1] Nationwide Children's Hospital, [2] Nationwide Children's Hospital, [3] The Ohio State University

Background: Thymic tissue is anatomically located in the anterior mediastinum. However, ectopic thymus may be located along its course of embryologic development in the head and neck. We describe thymic ectopia in an unusual location – the middle ear.

Methods: A 19–month-old male presented to otolaryngology for evaluation of recurrent ear infections. On physical exam, a mucoid effusion of the right tympanic membrane was noted and the left tympanic membrane was unremarkable. Bilateral tympanostomy tube placement was recommended. At the time of surgery a small mass was noted in the inferior mesotympanum of the left ear.

Results: A biopsy of the left ear mass was performed submitted to pathology. Grossly, the lesion consisted of multiple tan-pink to red focally fibrotic soft tissue fragments, measuring up to 0.3 cm in greatest dimension. Histologic sections demonstrated a lymphoid lesion comprised of small lymphocytes and well-formed Hassall's corpuscles (Figure 1 A&B). Immunohistochemical stains CD3 (Figure 1C) and Tdt (Figure 1E) highlighted the majority of small lymphocytes with scattered positive CD20 cells (Figure 1D). < insert image>

Conclusion: The histopathologic features, as well as the staining pattern supports the diagnosis of an ectopic thymus. The thymus is embryologically derived from the third pharyngeal pouch and has rarely been described in the middle ear, with one case report having associated otic malformation and another without. This case highlights a rare congenital/developmental anomaly that otolaryngologists and pathologists should include in the differential diagnosis of middle ear masses in young children.

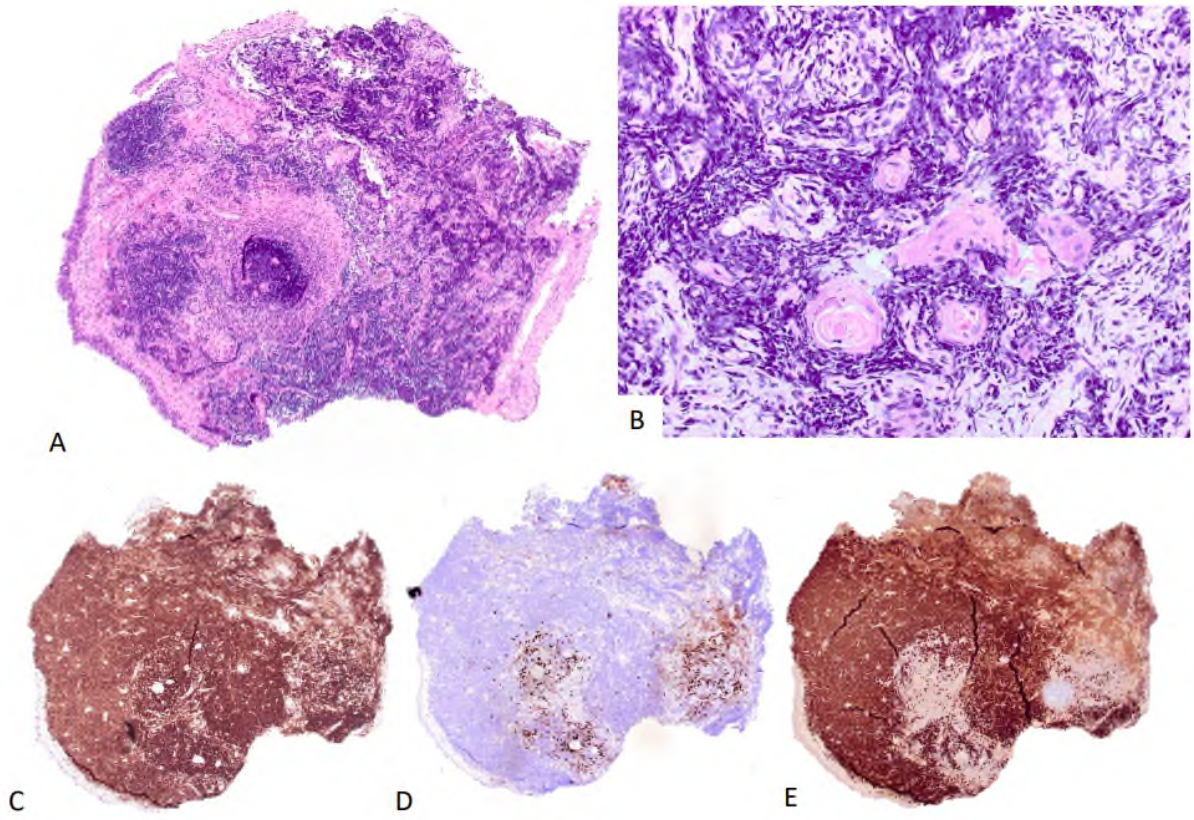
A
B
C
D
E

15

Lost in Translocation—A Case Report of a CIC-DUX4 Sarcoma with Novel Loss of H3K27me3 Expression

A Andrews [1], J Saunders [2]; [1] Division of Anatomical Pathology, British Columbia Children's Hospital and Women's Hospital and Health Center, [2] Division of Anatomical Pathology, British Columbia Children's Hospital and Women's Hospital and Health Center

Background: Molecular classification is increasingly important in the day-to-day practice of pathology. Immunohistochemical surrogates for molecular alterations streamline this process, but lack of specificity in these markers can lead to diagnostic conundrums. Loss of immunohistochemical staining for trimethylation of lysine 27 of histone H3 (H3K27me3) is a sensitive marker for Malignant Peripheral Nerve Sheath Tumour (MPNST) when the morphologic differential diagnosis includes spindle cell lesions of soft tissue. However, there are increasing reports of other sarcomas with loss of H3K27me3 expression, which can make definitive classification difficult in cases where MPNST is a diagnostic consideration. The rarely reported CIC-DUX4 sarcoma, which occurs in the somatic soft tissue of young adults, is classically considered a small round cell sarcoma; however, has recently been described to have a wider morphologic spectrum, which can include round, epithelioid and spindle cells. We herein describe a rare case of a young male, without clinical evidence of Neurofibromatosis-1, who presented with an aggressive spindled and round cell sarcoma of the thigh, ultimately diagnosed as a CIC-DUX4 sarcoma, whose concurrent loss of H3K27me3 represented a significant diagnostic pitfall during pathologic evaluation.

Methods: The patient underwent open biopsy, which was evaluated with H&E and an immunohistochemical staining panel consisting of H3K27me3 (Cell Signaling Technology; C36B11), BCOR, NTRK, AE1/AE3, high molecular weight cytokeratin, EMA, S100, CD34, desmin, myogenin, TLE-1, CD99, and NKX2.2. Nanostring pan-sarcoma panel was performed (BC Cancer Agency, Vancouver, Canada). The case was reviewed at sarcoma multidisciplinary conference and the immunohistochemical and morphologic differential diagnosis included an MPNST versus a high grade spindle and round cell sarcoma. Given the lack of supporting clinical and radiologic evidence for MPNST, further genetic work-up was performed via Trusight RNA-Sequencing (Mt. Sinai, Toronto, Canada).

Results: The biopsy showed a high-grade sarcoma composed of sheet-like growth of predominantly short spindled cells with areas of smaller, round to polygonal cells and abundant geographic necrosis. Mitoses were brisk but not atypical. Immunohistochemical evaluation was uninformative with the exception of complete nuclear loss of H3K27me3 (Cell Signaling Technology; C36B11) in the lesional cells. Nanostring pansarcoma fusion assay did not reveal any identifiable translocation despite covering the most common break points for the CIC-DUX4 gene fusion. Radiologic findings showed no direct relationship between the mass and any large nerves. Follow-up Trusight RNA sequencing demonstrated a CIC-DUX4 gene fusion. The resection specimen showed similar morphology and loss of H3K27me3 staining.

Conclusion: We report a novel case of a CIC-DUX4 sarcoma with predominant spindled morphology and complete nuclear loss of H3K27me3 on immunohistochemical work-up, a

finding not previously reported. The present case demonstrates a few of the challenges in diagnosis of CIC-DUX4 sarcoma, which can show a wide morphologic spectrum, and adds to the growing list of high grade sarcomas which can show loss of H3K27me3.

16

Rare Aggressive Osteoblastoma of the Calvaria with Dural Nodules Treated with Denosumab After Primary Resection and Local Recurrence

A Andrews [1], J Saunders [2]; [1] Division of Anatomical Pathology, British Columbia Children's Hospital and Women's Hospital and Health Center, [2] Division of Anatomical Pathology, British Columbia Children's Hospital and Women's Hospital and Health Center

Background: Osteoblastoma is a rare benign bone-forming tumour, accounting for 1-2% of primary bone malignancies, which is most commonly reported in the paediatric age group and demonstrates a predilection for the axial skeleton, although has rarely been reported in the cranial vault. Although the World Health Organization has yet to subclassify osteoblastoma, two distinct clinicopathologic variants have been described, a conventional and aggressive subtype, defined by subtle histologic differences but distinct clinical behaviour. Since denosumab was approved for treatment of giant cell tumors in 2013 numerous case reports have shown that osteoblastomas can respond to denosumab. We herein describe a unique case of a young female with aggressive calvarial osteoblastoma with dural nodules successfully treated with denosumab after primary resection and local recurrence.

Methods: An 11-year-old female presented with a progressive, painless mass of the occiput with a 5 month history of slow but increasing growth. Computer tomography (CT) and magnetic resonance imaging (MRI) of the brain showed a highly vascular, expansile mass centred within the posterior occipital skull bone, measuring 6.4 x 4.5 x 4.1 cm. Positron emission tomography (PET) scan showed moderate avidity with no other sties of apparent disease. CT-guided biopsy was performed, although the histology was challenging to interpret the diagnosis of osteoblastoma was favoured. Pre-operative endovascular embolization of intra and extra-cranial feeding blood vessels, occipital craniotomy and complete tumour bed resection with grossly clean margins was performed. The final pathology confirmed an osteoblastoma with epithelioid features and secondary aneurysmal bone cyst components. Although circumferential boney margins were narrowly clear, the inner table of skull showed extensive bony erosion.

Results: Cranioplasty and repair of the skull was delayed at primary resection given the high likelihood of recurrence. Surveillance MRI at approximately 18 months follow-up showed interval growth of multiple enhancing dural nodules at the resection site as well as local recurrence at the skull defect margin. After multidisciplinary review, given the morbidity of additional surgical resection, the decision to start denosumab 120 mg weekly for 4 weeks and monthly thereafter for a 12 month treatment duration was made. Surveillance MRI at the mid point of denosumab therapy demonstrated interval regression and increased ossification of the dural nodules and occipital bone recurrence.

Conclusion: We report a rare case of an aggressive osteoblastoma with secondary aneurysmal bone cyst involving the calvaria with dural nodules at local recurrence, a finding reported only once in the adult literature and never in the paediatric age group. In addition, the present case report demonstrates a pediatric osteoblastoma successfully treated with denosumab after local recurrence, offering further support that this therapy can induce tumor regression in a variety of bony lesions beyond giant cell tumor of bone.

17

Primary intraosseous Spindle Cell Rhabdomyosarcoma: A Case Report in an Unusual Location.

A Heider J Plotzke, R Rabah, D Robinson, R Mody, A Heider; University of Michigan

Background: Spindle cell/sclerosing rhabdomyosarcoma is a defined subtype of rhabdomyosarcomas according to the most recent World Health Organization (WHO) Classification of Soft Tissue and Bone Tumours. Recently, a novel category of intraosseous spindle-cell rhabdomyosarcomas with EWSR1- or FUS-TFCP2 fusions has been described. We report a case of intraosseous spindle cell rhabdomyosarcoma (ISCRMS) with EWSR1-TFCP2 fusion presenting in the femur mimicking osteosarcoma in this unusual primary location.

Methods: An 18-year-old male with presented with relapsed widely metastatic bone sarcoma, responding poorly to chemotherapy, which was initially presented in the distal femur. Sections showed a high-grade malignant neoplasm with sheets of epithelioid and spindled cells without obvious rhabdomyoblastic differentiation. The cells demonstrated significant nuclear pleomorphism, prominent nucleoli, moderately abundant cytoplasm, and brisk mitotic activity with areas of tumor necrosis. There was focal osteoid formation, including in areas away from bony involvement, such as in lymph node metastases. Given the patient's aggressive clinical course and search for targeted therapy, Peds-MiOncoSeq was performed, and retrospective immunostaining analysis was conducted.

Results: Sequencing analysis identified t(12;22) EWSR1-TFCP2 with high expression of MYOD1. Immunohistochemically, the tumor co-expressed both skeletal muscle and epithelial markers. The tumor cells were diffusely positive for pancytokeratin, MyoD1, and ALK by immunohistochemistry (Figure 1). Desmin and SATB2 were focally positive. Myogenin was negative, and INI-1 expression was retained. Figure 1. Epithelioid and spindled morphology, H&E 100x (A). Epithelioid morphology with conspicuous mitotic activity, H&E 400x (B). Lymph node metastasis with osteoid formation, H&E 100x (C). MyoD1, 100x (D). Desmin, 100x (E). Myogenin, 100x (F). ALK, 100x (G). Pancytokeratin, 100x (H). SATB2, 100x (I).

Conclusion: Fewer than 50 cases of ISCRMS with EWSR1- or FUS-TFCP2 fusions have been reported in the literature to date. This malignancy most commonly involves craniofacial and pelvic bones. Rarely, the tumors can originate in long bones, as in this case. In the current case, osteosarcoma was the primary diagnostic consideration based on the distal long bone location, patient age, and evidence of osteoid formation. The distinction between the two entities may be nearly impossible on morphologic grounds alone. In summary, we present a case of ISCRMS harboring a EWSR1-TFCP2 gene fusion, mimicking primary bone osteosarcoma. To our knowledge, this is the 47th case presented in the literature describing a rarely seen primary location within the femur, which can cause a diagnostic pitfall without the molecular sequencing or extensive immune profiling data.

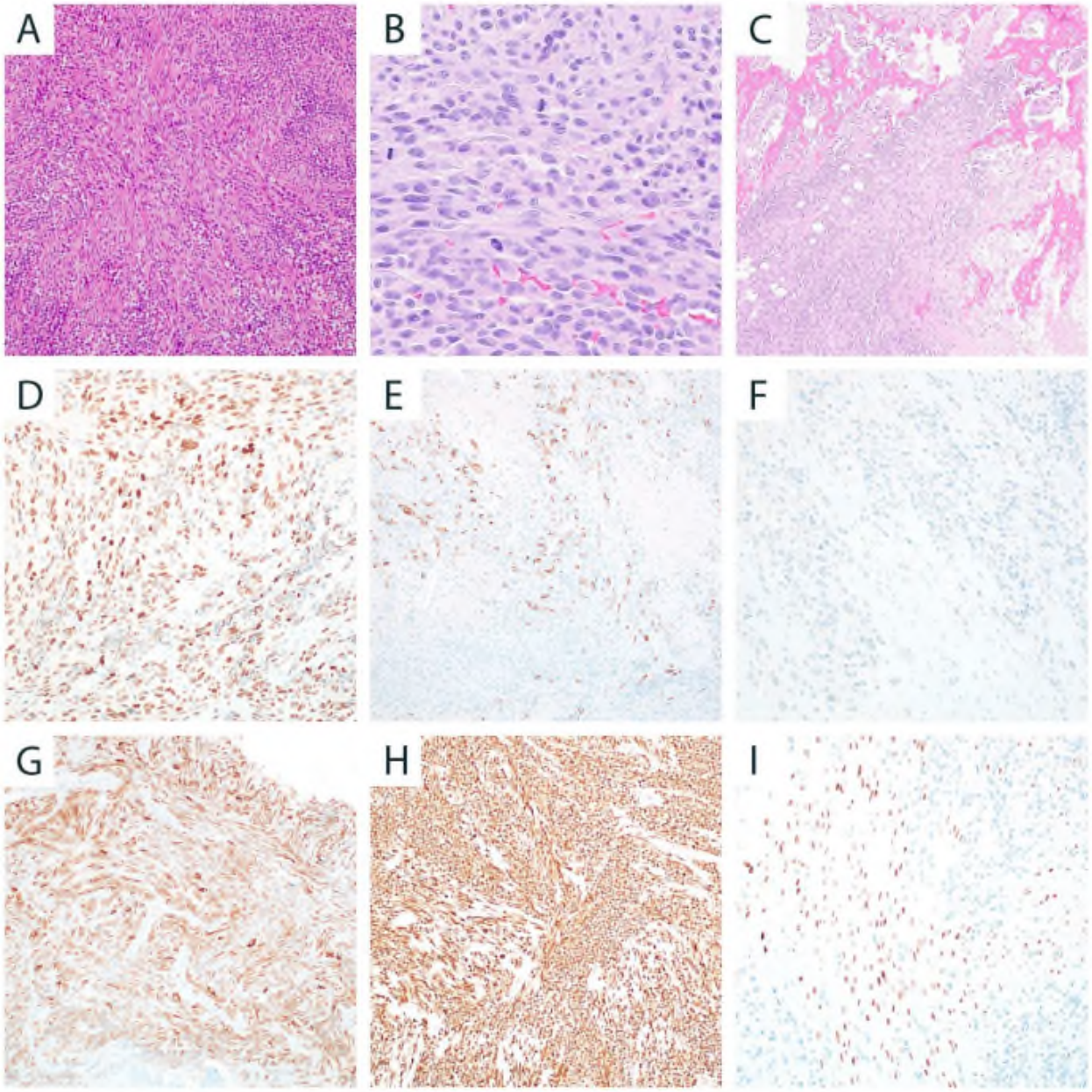
A
B
C
D
E
F
G
H
I

18

Blastic Plasmacytoid Dendritic Cell Neoplasm: A Rare Entity in Children with Distinctive Clinicopathologic Features

H Ren [1], R Werk [2], J Kabat [2], J Rossoff [2], E Morgan [2], A Richardson [2], S Gong [2]; [1] Ann & Robert H. Lurie Children's Hospital of Chicago, [2] Ann & Robert H. Lurie Children's Hospital of Chicago

Background: Blastic plasmacytoid dendritic cell neoplasm (BPDCN) is a rare, aggressive hematologic malignancy, even rarer in children. Pediatric BPDCN appears to be less aggressive than adult cases although the number of cases reported so far is extremely small. Diagnosing BPDCN can be very challenging. Clinical diagnosis is challenging due to a non-specific presentation, and pathologically, BPDCN may be misdiagnosed as acute myeloid leukemia/myeloid sarcoma (AML/MS) or the new emerging entity BPDCN-like AML (pDC-AML). Patients with pDC-AML usually demonstrate pDCs positive for CD34 and CD123 but negative for TCL-1 and CD56. They are also more likely to show skin involvement, and strongly associated with somatic mutations in RUNX1. Furthermore, little is known about the genomic landscape of pediatric BPDCN. Here we describe a series of typical and atypical pediatric BPDCN cases with molecular correlation using next-generation sequencing (NGS).

Methods: Pediatric patients with BPDCN were identified after searching our archives. We reviewed clinical, histologic, immunohistochemical, flow cytometry, and molecular data. NGS on RNA and DNA extracted from either bone marrow or tissue was performed.

Results: Three patients aged 9-17, with 2 males and 1 female. One patient had only skin and nodal involvement initially while two had a leukemic presentation in addition to skin and/or nodal involvement. All three patients showed typical histopathologic features of BPDCN, with similar immunophenotypes by flow cytometry and/or immunohistochemistry. While all three cases were positive for CD4, CD56, and CD123 , only two cases were positive for TCL1. The case that did not show skin involvement was negative for TCL1, making it atypical both clinically and pathologically. However, the blasts were positive for plasmacytoid dendritic cell-specific transcription factor TCF4, confirming the diagnosis. Two patients with NGS data available revealed TET2 and RAS signaling pathway mutations, but not RUNX1 mutations reported in pDC-AML.

Conclusion: Our results demonstrated the complexity of diagnosing BPDCN in children. For rare TCL1 negative cases, TCF4 IHC stain may be needed. Furthermore, in contrast to pDC-AML with strong association with RUNX1 mutations, BPDCN shows predominantly TET2 and RAS signaling pathway mutations. Importantly, the consensus for initial BPDCN therapy is lymphoid-directed (following upfront acute lymphoblastic leukemia regimens) versus pDC-AML for which myeloid-directed therapy is recommended.

19

Homozygous INI-1 loss in poorly differentiated Sertoli-Leydig tumor: case report of a rare pediatric ovarian tumor with institutional review

H Ren [1], J Reichek [2], M Raval [2], A Gupta [2]; [1] Ann & Robert H. Lurie Children's Hospital of Chicago, [2] Ann & Robert H. Lurie Children's Hospital of Chicago

Background: Sertoli-Leydig cell tumor (SLCT) represents 1-2% of all pediatric ovarian neoplasms. In the pediatric population, SLCT has been associated with DICER1 mutation/syndrome. We present a primer case of poorly differentiated SLCT with homozygous INI-1 loss by immunohistochemistry and next-generation sequencing. INI-1 loss in ovarian neoplasms has been reported in rare cases of small cell carcinoma of the ovary, hypercalcemic type (SCCOHT). Herein, we describe the clinicopathological feature of our current case, and examine the INI-1 status in the SLCT, diagnosed at our institution since 2000.

Methods: Archival records of the SLCT are retrieved, and representative sections are reviewed to confirm the diagnosis. Next-generation sequencing (NGS) results are reviewed when available.

Results: Previously healthy 12-year-old presented with abdominal pain and fever for 7 days. CT abdomen demonstrated a 10.6 cm heterogeneous mass with cystic components within the pelvis. Pertinent lab findings were elevated estrogen levels, normal AFP, normal BHCG, normal CA-125, normal FSH, normal calcium levels, mild normocytic anemia, and elevated LH. Surgery showed a ruptured large ovarian mass and 3 liters of ascites (A). Pathology revealed sheets of small round cells with hyperchromatic nuclei and scant cytoplasm (B). The cells are occasionally arranged in rosettes/pseudo-rosettes with foci of heterologous cartilage (C, D). There are small clusters of large eosinophilic cells with small round nuclei consistent with Leydig cells. Mitotic activity is brisk, and there are large areas of hemorrhage and necrosis. Immunostains demonstrate foci of positivity for calretinin, inhibin, WT1, and FOXL2. SMARCA4/BRG1 is retained, but SMARB1/INI-1 is lost. By next-generation sequencing, homozygous loss of INI-1 is confirmed. Due to the presence of Leydig cells, immunohistochemistry results, lab results, and heterologous differentiation, the findings are most consistent with a poorly differentiated SLCT with INI-1 loss. In addition, our archives identified three cases of moderately differentiated SLCT. All three cases demonstrated pathogenic DICER1 mutation by NGS, with no mutation identified in SMARCA4 or SMARCB1.

Conclusion: Although our case of poorly differentiated SLCT has many morphological features overlapping SCCOHT along with only a handful of cases in the literature of INI-1 loss in the latter, the combination of the presence of Leydig cell component, heterologous cartilage, lack of elevated calcium, and positivity for sex-cord stromal cells via immunochemistry confirms SLCT. INI-1 evaluation has not been previously studied in detail in poorly differentiated SLCT thus larger studies are warranted as treatment options may differ.

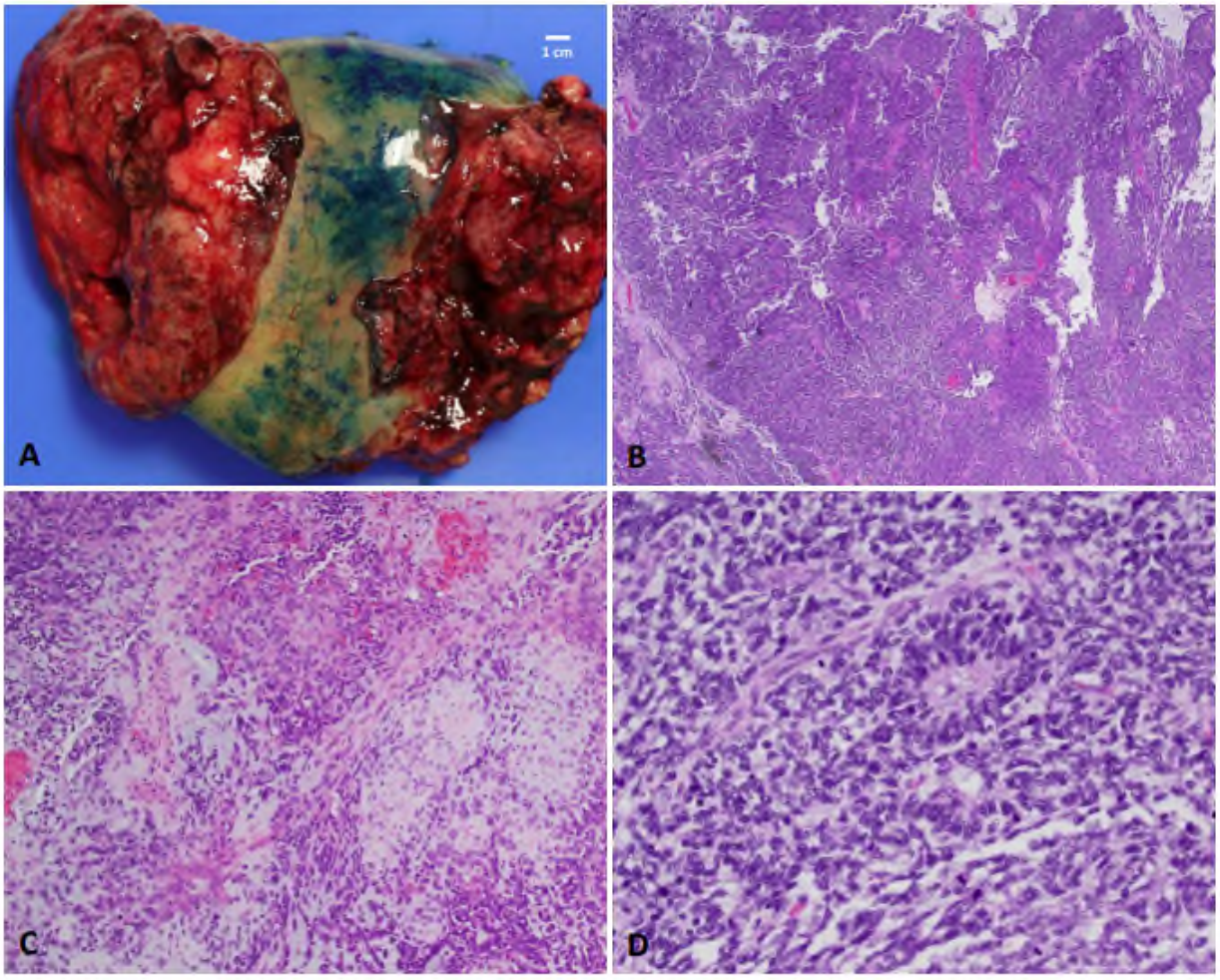
1 cm
A
B
C
D

20

DICER1 mutation in pediatric Sertoli-Leydig cell tumors (SLCT)

C GUARDADO SALAZAR [1], W Chour [2], R Schmidt [2], Y Bo [2], W Larry [2], B Pawel [2], Z Shengmei [2], N Shillingford [2], M Warren [2], P Zamiara [2]; [1] Los Angeles children's hospital, University of Southern California, [2] Los Angeles Children's Hospital, University of Southern California

Background: Sertoli-Leydig cell tumors (SLCTs) are rare sex-cord stromal tumors, accounting for < 0.5% of all ovarian neoplasms. In pediatric patients, these tumors have a broad spectrum of morphology overlapping those of other tumors within the differential diagnosis. The presence of heterologous elements further complicates the final diagnosis and may also affect treatment decisions. Traditionally, the immunohistochemical stains used to diagnose SLCTs include Inhibin and Calretinin, and rarely AFP. More recently, the identification of DICER1 mutation as a potential marker of SLCT may augment existing methods of characterization. In DICER1 syndrome, the DICER1 mutant allele is inherited in an autosomal-dominant fashion and is associated with a variety of benign and malignant neoplasms. The most common malignant sex cord-stromal tumor associated with DICER1 syndrome is SLCT tumor of the ovary, which has pathologic features distinct from their adult counterparts.

Methods: To evaluate the clinicopathologic features, molecular findings and outcome of pediatric ovarian Sertoli-Leydig cell tumors (SLCTs), 13 patients with the diagnosis of ovarian SLCT between 1990 and 2022 were reviewed retrospectively. Seven cases went through molecular studies and five of these seven also had germline testing. Tumors were classified according to World Health Organization (WHO) and staged according to International Federation of Gynecological Oncology (FIGO).

Results: All 13 cases had a tumor confined to ovarian tissue and were completely resected. All cases showed histopathologic features such as hollow or solid tubules of cuboidal to columnar Sertoli cells, intervening stroma containing nests, and single Leydig cells across to moderately differentiated tumor tissue, diagnosed as intermediate to poorly differentiated SLCT. All samples with available for molecular assessment (n = 7) had DICER1 mutation (100%). Three of five cases had germline mutation. The patients underwent chemotherapy and only one case with somatic mutation without germline mutation had evidence of metastasis (lung). Chemotherapy-related complications were infrequent/not reported, and all patients remain in remission.

Conclusion: DICER1 mutation was in 100% and germline mutation in 60% of pediatric SLCT cases in our cohort, demonstrating DICER1's potential usage as a reliable diagnostic marker for SLCT. DICER1 mutation including germline mutation does not have a prognostic value in pediatric SLCT. Our next steps are to expand the size of the study, to assess whether DICER1 mutation may be sub-stratified within SLCT cases, and to identify clinical/pathologic features which might correlate with DICER1 status.

21

Activated CD8 T-cell hepatitis in children: a single institution experience

C GUARDADO SALAZAR [1], Y Bo [2], W Larry [2], B Pawel [2], N Shillingford [2], M Warren [2], P Zamiara [2], S Zhou [2]; [1] Los Angeles children's hospital, University of Southern California, [2] Los Angeles Children's Hospital, University of Southern California

Background: Pediatric acute liver failure is a rare and serious life-threatening situation, principally for the 30 to 50% of children in whom the etiology of their liver failure is unclear or indeterminate. Treating these patients is challenging, requiring constant assessment over time with regular evaluation for possible liver transplantation. Children with pediatric acute liver failure of undetermined etiology have lower spontaneous survival and higher rates of transplantation and death than other diagnostic groups. Emerging evidence suggests that a subgroup of patients with indeterminate pediatric acute liver failure have clinical, laboratory, and liver biopsy features of immune dysregulation with a dense infiltration of CD8 T cells.

Methods: In 2022, we received percutaneous liver biopsies from three children with acute hepatic dysfunction that showed an increased number of lymphocytes including CD8 T cells. For each case, routine H&E stains with levels, special stains and immunostains were performed. The first biopsy was from an 18-month-old male who presented with COVID infection, pancytopenia, elevated transaminases, and synthetic liver dysfunction (elevated INR). The second was from a 9-year-old female with a history of elevated liver enzymes with no clear cause. The third case was from a 2-year-old male with elevated liver enzymes, coagulopathy, and cholestasis.

Results: The three cases showed similar histopathologic findings; an acute liver injury pattern with lobular architectural disarray, giant cell formation, reactive changes, single cell necrosis, cholestasis and marked mixed lymphocytic infiltrates. The infiltrates were predominantly composed of CD8-positive T-lymphocytes with scattered neutrophils, eosinophils and rare plasma cells. Portal areas were mildly expanded with mild bile ductular proliferation and mild to moderate lymphocytic infiltrates. Immunostains for CD8 demonstrated that the infiltrates were predominantly composed of CD8-positive T-lymphocytes. All three patients received steroids and responded to treatment evidenced by normalization of liver enzymes and function.

Conclusion: Dense hepatic CD8 T-cell infiltration is a major finding inactivated CD8 T-cell hepatitis. However, the percentage distribution of lymphocyte subtypes in the setting of hepatitis is not well established, and CD8 T-cell infiltration has also been described in cases of drug-induced hypersensitivity reactions, viral hepatitis, hemophagocytic lymphohistiocytosis, and macrophage activation syndrome, as well as autoimmune hepatitis. Further investigation is needed to better understand the diagnostic criteria in this disease.

22

Beckwith-Wiedemann syndrome patient with absence of the corpus callosum, cortical neuronal heterotopias, and multifocal atypical chondromatous lesions.
S Collier R Craver; CHNOLA

Background: Beckwith-Wiedemann syndrome (BWS) is an overgrowth disorder that results from genomic imprinting and is characterized by phenotypic variability and molecular heterogeneity. Many of the clinical features are well established, but there may still be emerging novel associations. We encountered a child with clinical and molecular features of BWS with the novel findings of cardiomyocyte disarray, multifocal skeletal chondromatous lesions, and cerebral cortical heterotopias.

Methods: A 33 week gestational age female presented with placental mesenchymal dysplasia, omphalocele, and intractable hypoglycemia. Detection of hypermethylation of H19 (IC1) and hypomethylation of LIT1 (IC2) confirmed Beckwith-Wiedemann syndrome. Additional findings included right hemihypertrophy, multiple cystic hepatic mesenchymal hamartomas and coexistent hepatic hemangioendotheliomas, cystic pancreatic lesions and nesidioblastosis, cardiac hypertrophy with myocyte disarray, right mid-tibial and 5th right rib atypical chondromatous lesions, and absent corpus callosum and numerous right-sided cortical neuronal heterotopias.

Results: We describe an infant with a severe BWS phenotype with manifestations including both cardinal and secondary findings including cardiomegaly, omphalocele, placental mesenchymal dysplasia, ear lobe creases, hepatomegaly, liver lesions, pancreatic cysts, and hypoglycemia with nesidioblastosis. Hemihypertrophy was evident with features involving the right side (right rib cartilaginous lesions, right tibia cartilaginous lesion, right nephromegaly, right adrenal cytomegaly, and right cortical heterotopias). In addition, several novel features including myocyte disarray, cortical neuronal heterotopias, and multifocal atypical chondromatous lesions were identified in this child with BWS confirmed by molecular findings suggestive of parental uniparental disomy.

Conclusion: Our patient presented with phenotypically severe BWS due to paternal uniparental disomy. The findings of corpus callosum agenesis, nodular heterotopias, and atypical cartilaginous lesions have not been previously described in a BWS patient to our knowledge. In addition, the finding of cardiomyocyte disarray is unexpected in a patient with hyperinsulinemia. Although these findings may be incidental, the possibility of novel secondary features of a severe phenotype BWS must be recognized.

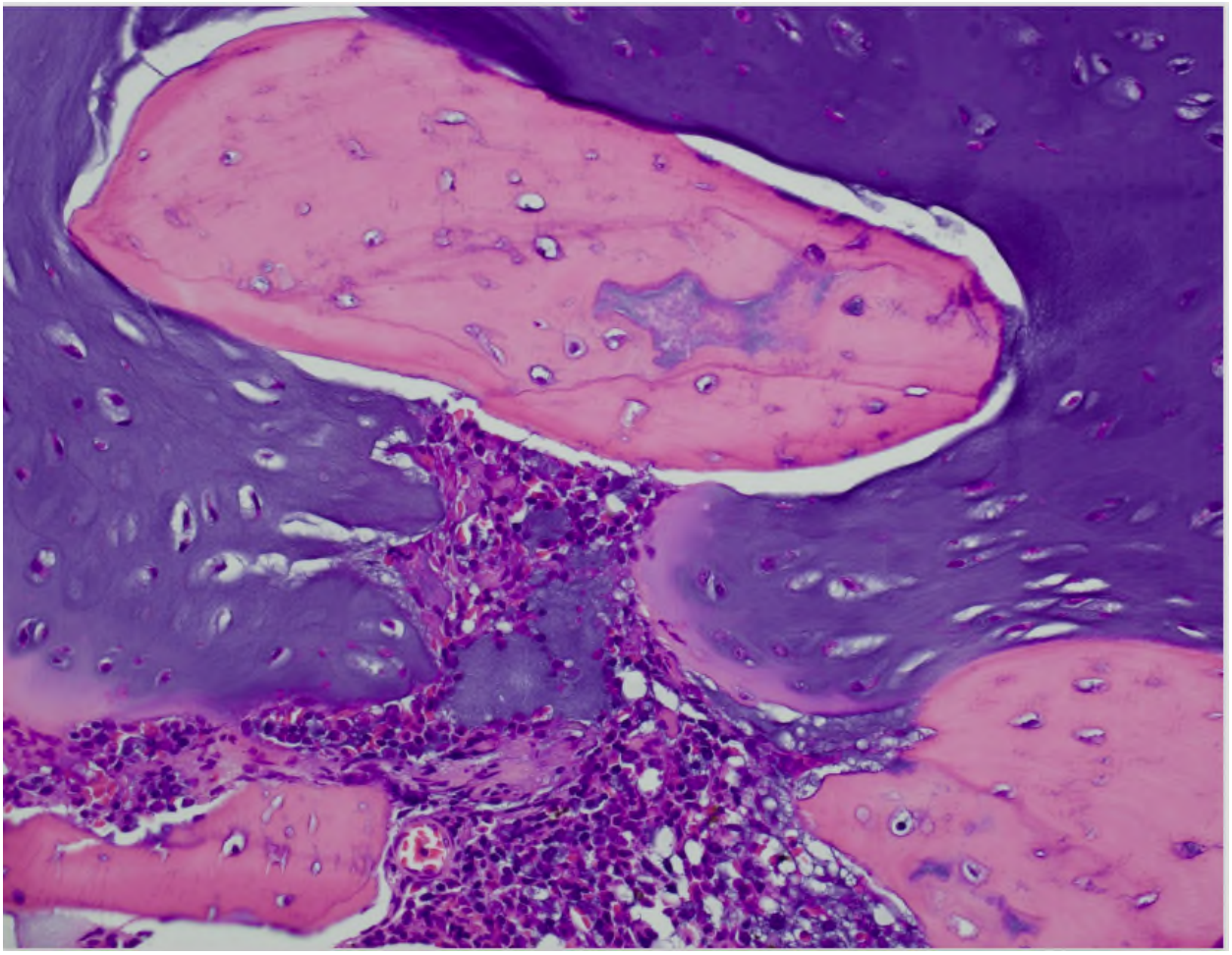

23

Follicular Derived Carcinoma, High Grade of the Thyroid in a Patient Harboring RB1 Germline Mutation

S Mangray [1], C Cottrell [2], J Aldrink [2], A Rubrecht [2], B Fung [2], K Nicol [2], S Chekuri [2], S Chen [2], V Prasad [2], E Yakirevich [3], M Conces [2]; [1] Nationwide Children's Hospital, [2] Nationwide Children's Hospital, [3] Rhode Island Hospital

Background: The category of follicular derived carcinoma, high-grade (FDCHG) of the thyroid that includes follicular thyroid carcinoma, high-grade (FTCHG) and papillary thyroid carcinoma, high-grade (PTCHG) was recently introduced into the updated 2022 WHO classification of Endocrine and Neuroendocrine Tumors. Only a rare example of papillary thyroid carcinoma (PTC) has been reported in a patient with RB1 germline mutation. The PTC in that case was attributed to neck radiation. In contrast, we describe a FTCHG variant of FDCHG in a patient harboring RB1 germline mutation.

Methods: The clinicopathologic and molecular findings are reviewed.

Results: The patient first presented to our institution as an infant when he was diagnosed with bilateral retinoblastomas at which time RB1 germline mutation was confirmed. He was treated with radiation therapy followed by enucleation of the left eye at 23 months of age after recurrence. He developed osteogenic sarcoma of the left radius at 9 years of age treated by resection post-chemotherapy, and acute lymphoblastic leukemia (ALL) at the age of 14 years. His ALL was treated with chemotherapy followed by bone marrow transplantation and CAR-T therapy for relapsed ALL. At 21 years of age the patient discovered a right neck swelling. An ultrasound of the neck demonstrated a right thyroid nodule with central cystic change and a TRads score of 4, but an FNA biopsy of the right thyroid nodule was evaluated as consistent with a benign follicular nodule (Bethesda II). He underwent a right lobectomy that demonstrated a 4.2 x 2.7 x 2.1 cm encapsulated fleshy mass with central cystic change. Histologically, micro-follicular, trabecular and solid architecture predominated with a central macro-follicular pattern. Neoplastic cells had dense nuclear chromatin and mitotic activity ranged from 6/10 HPFs to 10/10 HPFs (9 mitoses per 2 square millimeters) in hotspots and was confirmed by a phosphohistone H3 (PHH3) immunohistochemical (IHC) stain. Focal necrosis was present. Capsular and angioinvasion were present and given the mitotic rate greater than 5 mitoses per 2 square millimeters a diagnosis of FTCHG variant of FDCHG was rendered. A completion thyroidectomy demonstrated benign nodules. Somatic disease/germline comparator exome analysis of the carcinoma and the patient’s blood confirmed the RB1 germline mutation in addition to a somatic TSHR activating missense mutation and 13q13.2-q14.2 loss. The latter resulted in loss of the CYSLTR2, FOXO1, LCP1, LHFPL6, NBEA and RB1 genes. IHC performed on a section containing the carcinoma and adjacent non-neoplastic thyroid with the antibody to RB1 demonstrated loss of nuclear reactivity in neoplastic cells while positive staining was retained in the stromal and endothelial cells within the lesion and in non-neoplastic thyroid follicular cells correlating with the molecular findings. At three months follow-up the patient is free of tumor.

Conclusion: We report an example of FTCHG variant of FDCHG of the thyroid, arising in a

patient with RB1 germline mutation and previous multiple malignancies, associated with a double hit in the RB1 gene and activating missense mutation of the TSHR gene. As far as we are aware this form of carcinoma has not been previously reported in patients with RB1 germline mutation.

24

Papillary Renal Cell Carcinoma (RCC) in an Adolescent Patient with Prior Bone Marrow Transplant for Omenn Syndrome (OS)

E Barletta [1], S Kandukuri [2], T Lee [1]; [1] USC/LAC+USC Medical Center, [2] Keck School of Medicine of USC

Background: Pediatric renal tumors are uncommon and comprise around 7% of pediatric malignant tumors. Clinical and pathophysiological features of RCC in children and adults vary significantly. An example of these differences is etiology where smoking, obesity, and high blood pressure are known to increase the risk of RCC in adults, but in children genetic translocations play a main role. In pediatrics, the microphthalmia family (MiTF) translocation is the main type of RCC.

Methods: The partial nephrectomy specimen was grossed and fixed in formalin. Representative tissue sections were submitted for paraffin embedding and microscopy. Morphologic assessment was performed as well as immunohistochemical staining (IHC) for diagnosis on a formalin fixed paraffin embedded (FFPE) section of the tumor along with single nucleotide polymorphism (SNP) evaluation. Results were interpreted by a genitourinary specialty pathologist for final diagnosis.

Results: Tumor histology showed papillary architecture and wide fronds with focal areas of histiocytes within papillary cores (Figure 1). The tumor cells showed moderate amount of pink cytoplasm and WHO/ISUP grade 3-4 large nuclei with prominent enlarged nucleoli. No necrosis, rhabdoid, or sarcomatoid features were identified. Immunohistochemical staining pattern is summarized in Figure 2. The IHC results showed AMACR, CD10, OSCAR cytokeratin, and Keratin AE1/AE3 diffusely positive in tumor. Keratin 7 had patchy positivity and CD117, HMB-45, and Keratin 20 among other IHC stains were all negative in tumor cells (Table 1). Fluorescence in situ hybridization analysis (FISH) was negative for Transcription Factor E3 (TFE-3). SNP evaluation showed relative (2 copy) increase in copy number amplitude of chromosomes 2, 7, 12, 17, 20 besides other changes suggestive of germline instability. The final diagnosis of the resected specimen was reported as “Renal cell carcinoma, most consistent with papillary type”.

Conclusion: Pediatric renal neoplasms are uncommon and when detected, they are most often Wilms tumor/nephroblastoma or MiTF family RCC. Our patient with OS, a rare immunodeficiency syndrome diagnosed in infancy, had significant risk factors including a family history of cancer. Since OS is extremely rare and only recently curable with medical advancements, literature has never reported solid organ tumors in patients with OS. This is the first ever known case report of pediatric renal cell carcinoma, papillary type in a patient with OS. By providing the pathologic characteristics of this tumor in the setting of such a rare immunodeficiency syndrome, we aim to contribute meaningful information to better classify and clinically treat these tumors in the pediatric population.

Figure 1:

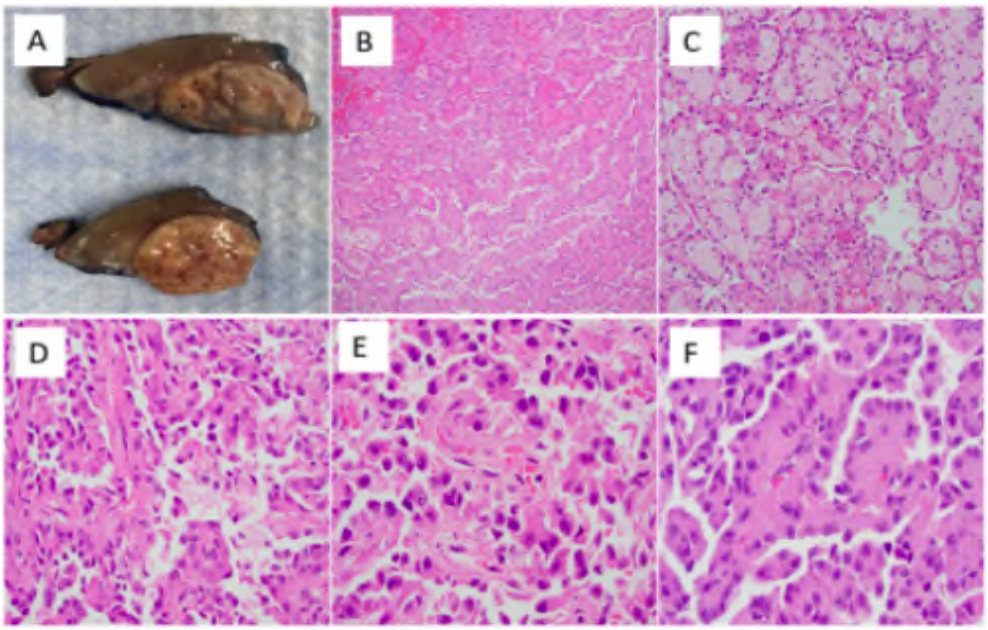

A. Gross photograph of tumor mass in a partial nephrectomy reveals a tan-yellow mass with focal grummous material.
B. Low power view of the renal cell carcinoma reveals papillary architecture.
C. High power view reveals macrophages within the fibrovascular cores of the papillae.
D - F. High power view of the tumor cells reveals moderate amount of eosinophilic cytoplasm with ISUP/WHO grade 3-4 nuclei.

Figure 2:

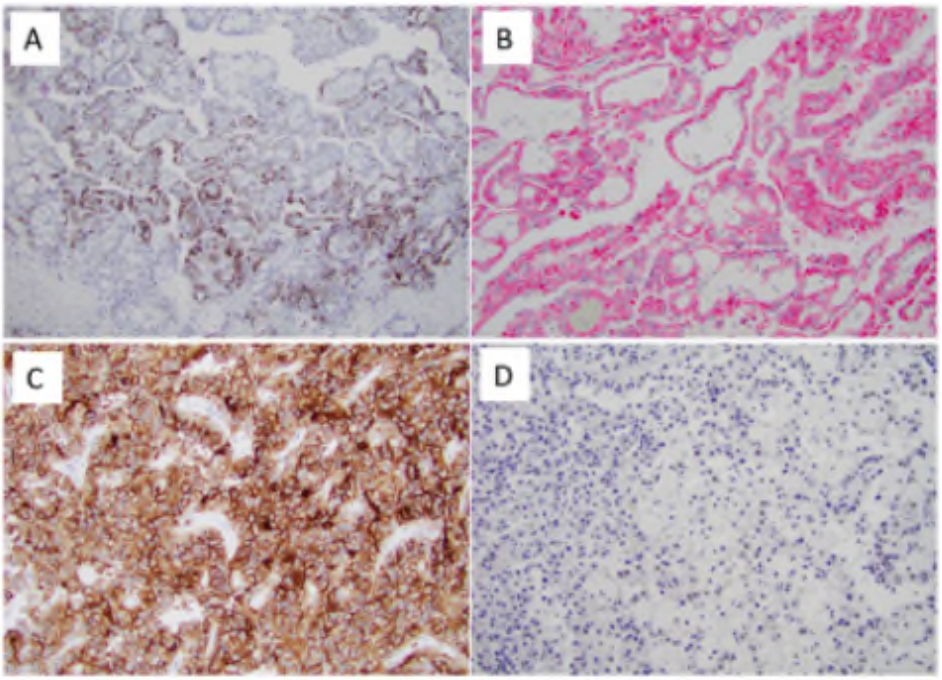

A. Immunohistochemical staining with Keratin 7 shows patchy, strong positivity.
B. Immunohistochemical staining with AMACR shows diffuse, strong positivity.
C. Immunohistochemical staining with with CD10 shows diffuse, strong positivity.
D. Immunohistochemical staining with TFE-3 is essentially negative in tumor cells.

Table 1:

IHC	RESULTS
Keratin 7	Patchy positive
AMACR (PS045)	Diffusely positive
CD10	Diffusely positive
Keratin AE1/AE3	Diffusely positive
OSCAR keratin	Diffusely positive
CD117	Negative
HMB-45	Negative
Melan A	Negative
Cathepsin- K	Negative
Keratin 20	Negative
GATA-3	Negative
Succinate dehydrogenase (SDH-B)	Retained
Fumarate hydratase (FH)	Retained
2 Succinocysteine (2SC)	Not expressed
Transcription Factor E3 (TFE-3)	Negative

25

MICRORETICULAR PERINEURIOMA: A NEW MORPHOLOGICAL SUBTYPE OF A RARE ENTITY

J D'Ardis [1], H Salah [2]; [1] CAP, USCAP, TSP, [2] Houston Methodist Hospital

Background: Perineurioma is a peripheral nerve sheath tumor of perineurial cells. Perineuriomas are grossly well-circumscribed, nodular, firm, and lobulated, with a tan-white cut surface. Many histological subtypes of perineuroma, including reticular, sclerosing, and plexiform, have been reported. Reticular perineuroma has been previously described by showing a reticular lace-like growth pattern consisting of anastomosing cords of spindle-shaped cells..

Methods: We present a case of an 11-year-old male who presented with a tan-white lesion on the finger that was present for two years and slowly enlarged.

Results: Microscopically, the lesion consisted of cells with ovoid nuclei and delicate cytoplasmic processes, showing a microreticular pattern. The lesional cells were markedly positive for EMA and claudin-1, highlighting the delicate cytoplasmic processes. Based on those features, the case was called a microreticular perineuroma. The patient underwent complete excision of the lesion with no recurrence nine months after follow-up.

Conclusion: Knowledge about this entity is important to avoid inappropriate management.

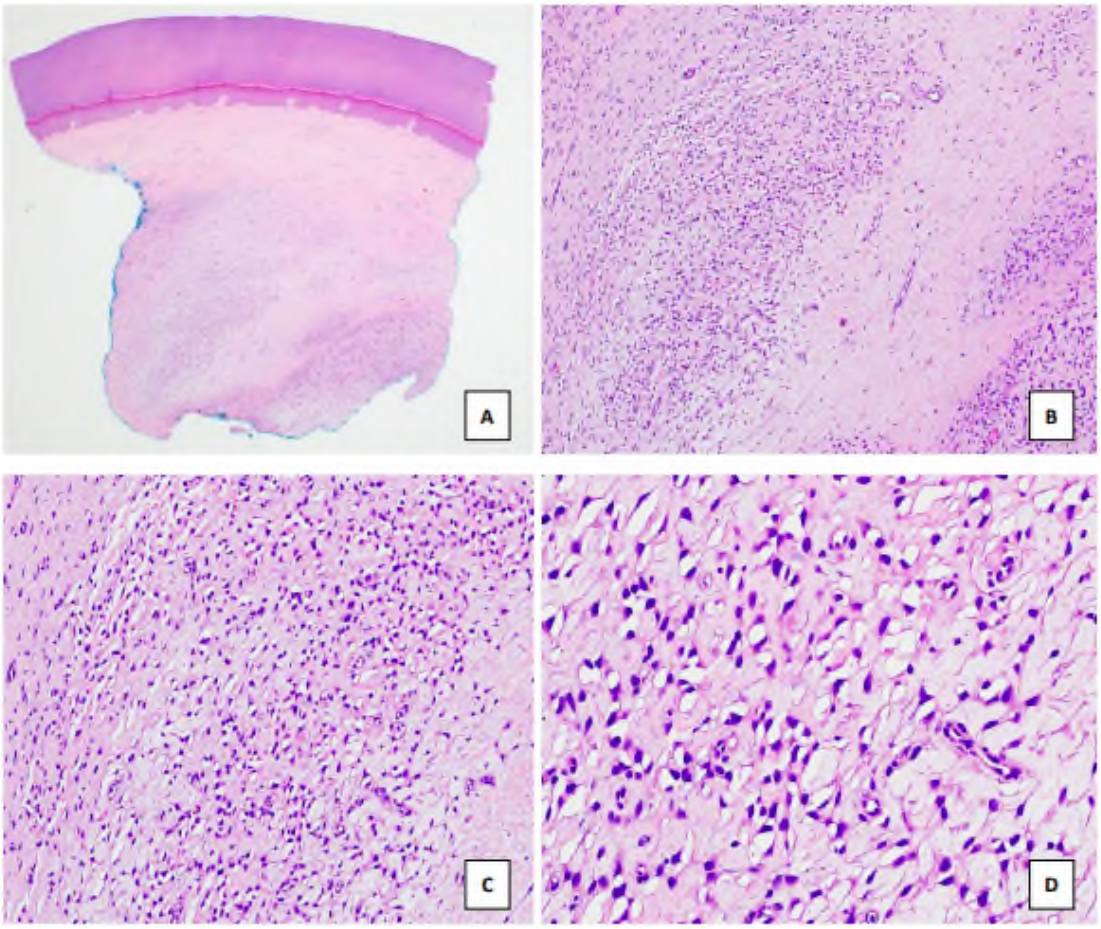

Figure 2: Microscopic features of the punch biopsy **(A)** showing a low-power view of a dermal-based spindle cell tumor (H&E, x2), **(B)** The lesion showing intervening areas of fibrosis, and chronic inflammation in the mid and deep dermis (H&E, x10), **(C & D)** The tumor consisting of cells with rounded ovoid nuclei and delicate elongated cytoplasmic processes arranged around clear and empty spaces in a microreticular pattern (H&E, x20)(H&E, x40).

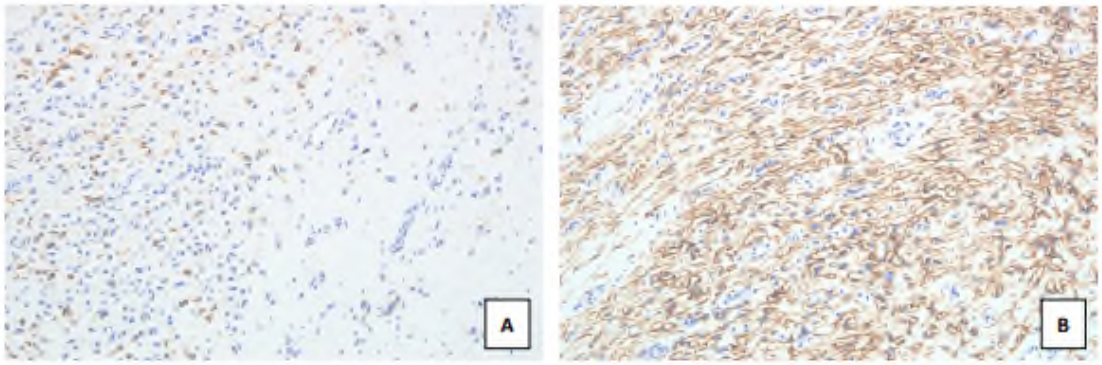

Figure 3: Immunohistochemical staining of tumor cells showing **(A)** patchy positive pan-cytokeratin (AE1/AE3) (x20), **(B)** strong and diffusely positive EMA (x20).

26

Epstein–Barr Virus associated (EBV+) Smooth Muscle Tumors in Children and Young Adults: A Clinicopathological Review

B Challa [1], S Koo [2], A Rubrecht [3], R Abraham [4], S Mangray [4], V Prasad [4], S Kahwash [4], A Shenoy [4]; [1] The Ohio State University Wexner Medical Center, [2] St. Jude Children's Research Hospital, [3] Nationwide Children's Hospital, [4] Nationwide Children's Hospital/The Ohio State University College of Medicine

Background: Epstein-Barr Virus associated Smooth Muscle Tumors (EBV-SMTs) are uncommon tumors with uncertain biologic potential that arise in the context of primary or secondary immunodeficiencies. We report here a cohort of EBV-SMTs in patients seen at two pediatric institutions.

Methods: A retrospective review of pathology records (01/2012- 12/2022) was undertaken to identify patients with EBV-SMTs at two children's hospitals. Clinicopathological characteristics, predisposing factors, relevant genetic findings and outcomes were recorded.

Results: A total of 16 tumors were identified from 12 patients (Age range: 5-23 years; Male: Female ratio 2:1). Six patients had multifocal tumors identified on imaging, while the six others had a single site of involvement. Affected sites included brain, soft tissue of head/neck, lungs, gastrointestinal tract, liver, spleen, pancreas, retroperitoneum, and vertebrae. Post-transplant lymphoproliferative disorder (PTLD) was diagnosed concurrently in two patients, while a diagnosis of PTLD preceded the diagnosis of EBV-SMT in one patient. Tumors from all patients demonstrated Epstein-Barr encoded RNA (EBER) by in-situ hybridization, and diffuse smooth muscle actin positivity at initial diagnosis. Desmin was focal/variably positive in three cases. Tumors developed post solid organ transplantation (heart = 4, liver = 1) in five patients (Post-transplant duration: 1- 10 years). Tumors in five patients were associated with non-iatrogenic immunodeficiency: two patients (siblings) with CARMIL2 deficiency (a germline combined immunodeficiency with immune dysregulation), two patients with vertical transmission of Human Immunodeficiency Virus and one patient with Common Variable Immunodeficiency. Clinical follow up was available for six patients (50%) (range: 4 – 14 months post-diagnosis). Three patients died with disease and three patients are alive with two having persistent disease.

Conclusion: EBV-SMTs can present in a multitude of sites throughout the body, including viscera, soft tissue and bones. Multifocality can contribute to considerable disease burden and morbidity. In the pediatric population, inborn errors of immunity (primary immunodeficiency) are an important association in addition to solid organ transplantation.

27

BK Polyomavirus-Associated Carcinoma: A Rarely Encountered Neoplasm in Childhood

J Steele [1], J Slack [2], S Vargas [2], A Church [2], N Collins [2], M Hirsch [3], A Perez-Atayde [2]; [1] Boston Children's Hospital, [2] Boston Children's Hospital, [3] Brigham and Women's Hospital

Background: BK polyomavirus is a well-known cause of hemorrhagic cystitis in immunosuppressed patients. In rare instances, the large tumor antigen can inhibit tumor suppressor proteins, leading to development of carcinoma. BK polyomavirus-associated carcinoma (BKPVC) is rare and disproportionately affects adults. Pediatric cases are extremely rare, and mostly occur in the setting of a renal transplant.

Methods: We reviewed two cases of BKPVC. The first was a 21-year-old male with history of cardiac re-transplantation who presented with intermittent gross hematuria and had 2 bladder wall masses on ultrasound. The second case was a 14-year-old male with history of lung re-transplantation complicated by post-transplant lymphoproliferative disorder (PTLD) who presented with gross hematuria and BK viruria. BUN/Cr increase, EBV viremia and new lymphadenopathy (LAD) raised concern for recurrent PTLD. Imaging showed hydronephrosis, 1% kidney function and LAD with pulmonary nodules. An obstructed ureter was found during stent placement. A nephrectomy was performed for suspected PTLD.

Results: Histologic examination of the first patient’s bladder mass biopsies revealed invasive high grade papillary urothelial carcinoma, with tumor cells arranged singly, in nests, and in single file. Markedly pleomorphic cytomorphology with irregular nuclear contours, nucleoli, and coarse chromatin was noted. SV40 and p53 immunohistochemical stains (IHC) were diffusely positive within tumor cells; Ki-67 ranged from 75-100%. Cytogenetics showed 46,XY,t(1;10). A radical cystoprostatectomy was performed, with no recurrence reported to date after >5 years follow-up. The second patient had tumor cells with abundant eosinophilic cytoplasm, large pleomorphic nuclei, prominent nucleoli, and anaplasia arranged in nests, tubular, glandular and pseudoalveolar structures, diffusely infiltrating the renal parenchyma. SV40 and p53 IHC were diffusely positive, as were PAX8, AE1/AE3, Cam 5.2, CK7 and weakly GATA3; INI-1 and AmCar were retained; ALK-1, CEA, 34Be12, 2SC and uroplakin were negative. Molecular analysis discovered alterations in ARID1A and CDH1, and amplification of POLB and CRKL. These findings suggested urothelial origin. The carcinoma involved perinephric fat, a regional lymph node, the adrenal gland. At last follow-up, ten weeks post nephrectomy, he is undergoing chemotherapy and PET scan showed stable LAD and pulmonary nodules.

Conclusion: The diagnosis of BKPVC in a pediatric transplant patient is exceedingly rare, with only three reports. Our two tumors – the only known instances of BKPVC at our institution in the last 80 years – occurred in patients without a renal transplant history, an even scarcer event. This report makes pathologists aware of this entity, and supports that intense immunosuppression markedly increases the risk of this malignancy.

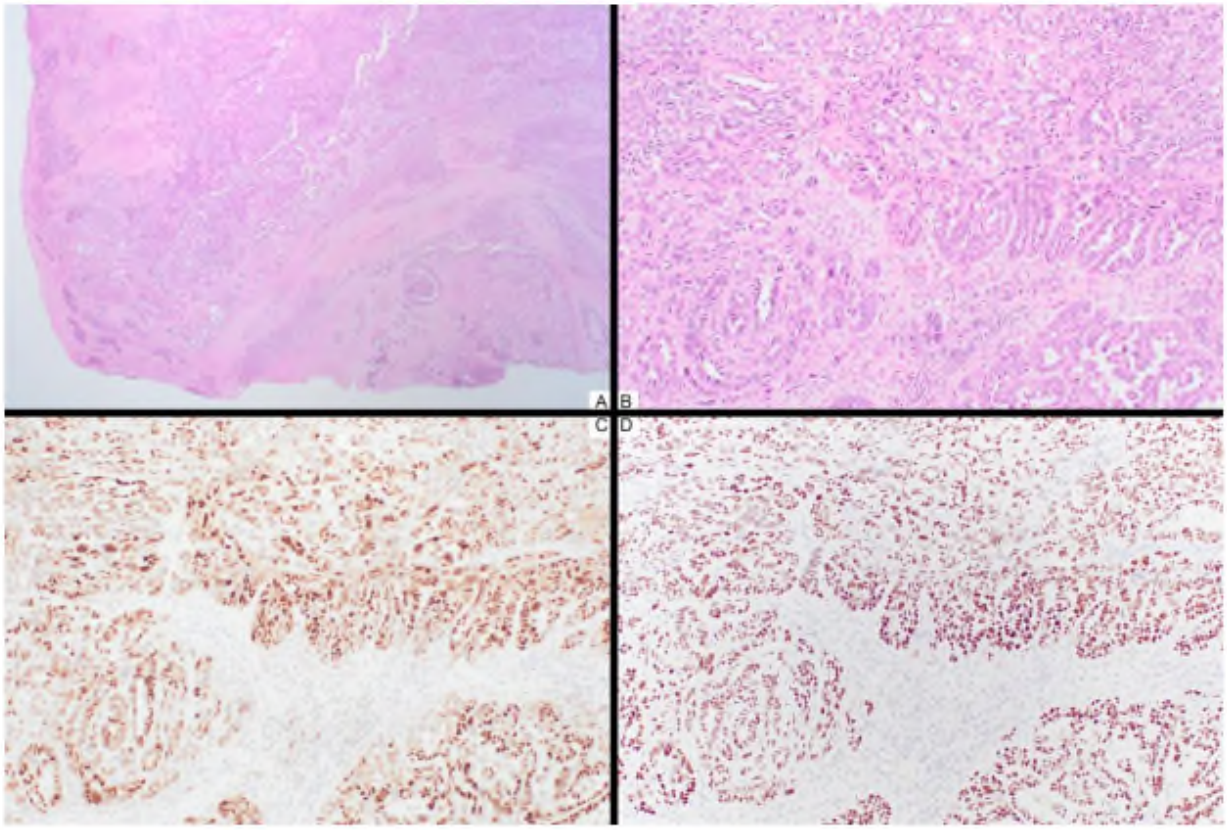

Figure 1. Post-transplant BK polyomavirus-associated high grade carcinoma of the kidney. (A) Low power (1.25x) H&E image of tumor showing infiltration through kidney. (B) Medium-power (10x) H&E image of tumor, showing tubular and glandular architecture, and anaplasia. (C) SV40 immunohistochemical stain is diffusely and strongly positive within tumor cells. (D) P53 immunohistochemical stain is diffusely and strongly positive within tumor cells.

28

Large Malignant Testicular/Paratesticular Tumors in Adolescence: Assessment of Gross Tumor Size in a Vulnerable Age Group

A Bakker [1], J Steele [2], S Vargas [2]; [1] Boston Children's Hospital, [2] Boston Children's Hospital

Background: Our institution noted several cases of very large testicular tumors in the adolescent age group. We hypothesized that reticence to discuss sexual health or lack of health literacy may result in increased tumor size, especially around the onset of puberty or in adolescence. In this study, we aimed to document gross tumor size for testicular and paratesticular tumors in the adolescent population and explore the relationship between tumor size to patient age.

Methods: We reviewed malignant testicular and paratesticular tumors (malignant germ cell tumors and rhabdomyosarcomas) from consultation and in-house materials reviewed at our institution over the last 30 years for patients aged 11 through 19. Patient age at the time of surgery, tumor histotype, and gross tumor measurements were recorded and patients were subdivided into three age group categories: 11-13, 14-16, and 17-19 years of age. Statistical analyses were performed using Statistical Package for the Social Sciences [SPSS] 28.0.1.0 (IBM Corp., NY, USA).

Results: 74 cases were identified. Patients ranged in age from 11.3 to 19.9 years (mean 16.8 years, median 16.9 years). The greatest tumor dimension ranged from 0.8 to 18.0 cm (mean 4.5 cm, median 3.5 cm). Ten tumors (13.5% of cases) were ≥ 10.0 cm. There was no statistically significant difference in the mean tumor size between age group categories. However, in the 11-13-year-old age group, 75% of tumors (3/4) were ≥10 cm. The proportion of tumors ≥10 cm was significantly higher in the 11-13-year-old age group than in either the 14-16-year-old ($p=0.002$) or 17-19-year-old ($p< 0.001$) age groups. There was no significant difference in the proportion of tumors ≥10 cm between the 14 -16 or 17-19-year-old age groups.

Conclusion: In this study of malignant testicular and paratesticular tumors in an adolescent cohort, the average tumor size (4.5 cm) was comparable to a recent study of testicular tumors in the general population (4.1 cm, median age 34, UK study from 2007-2012). Interestingly, in our study, 13.5% of tumors were equal to or larger than 10 cm. Although the reason for the high proportion of large tumors is unknown and likely multifactorial, this study suggests that adolescents are a vulnerable population, and that patient embarrassment or lack of sexual health literacy, particularly in the 11-13-year-old age group, may be contributing factors to delayed patient presentation.

29

Myxoid Neoplasm with COL1A1::PDGFB Gene Fusion: A Case Report

A Bakker [1], A Al-Ibraheemi [2]; [1] Boston Children's Hospital, [2] Boston Children's Hospital

Background: COL1A1::PDGFB fusions have been described in dermatofibrosarcoma protuberans (DFSP), giant cell fibroblastoma (GCFB), and occasionally in other neoplasms. Myxoid DFSP is a recognized variant of DFPS that typically demonstrates areas with typical DFSP histology.

Methods: A 6-year-old previously healthy male presented at approximately 3 years of age with a right-hand mass. He had three resections with subsequent recurrence in a Caribbean country. Pathological reports were not available for review; however, the family reported that there was a diagnosis of sarcoma. He presented to our institution with an ulcerated, exophytic mass of the right hand. MRI showed a homogenous, enhancing soft tissue mass (8.1 x 4.8 x 2.8 cm) centered along the dorsal right hand which appeared confined to the subcutaneous tissues (Figure A) (insert image).

Results: Excisional biopsy showed a relatively homogenous hypocellular neoplasm with abundant myxoid stroma (Figures B and C). Neoplastic cells appeared spindled to stellate with inconspicuous cytoplasm and bland nuclei. Immunohistochemistry demonstrated diffuse CD34 positivity (Figure D) and patchy smooth muscle actin positivity. S100, MUC4, desmin, and myogenin were negative; INI1 was retained. PanTRK showed weak/focal cytoplasmic staining but no definitive nuclear staining. An RNA-based next-generation based fusion panel (custom Archer FusionPlex kit (ArcherDX, Boulder, CO) on an Illumina MiSeq sequencer) showed a COL1A1::PDGFB fusion (chr17:48266264 to chr22:39631879). This fusion connects exon 41 of COL1A1 (NM_000088.3) to exon 2 of PDGFB (NM_002608.3) and is predicted to be in-frame. This fusion was confirmed by a DNA-based next-generation sequencing-based assay (Oncopanel illumina HiSeq2500 assay). The patient is currently receiving targeted treatment with imatinib, a tyrosine kinase inhibitor, with the aim of shrinking the tumor to maximize post-operative preservation of the function of his right hand. At the time of writing, the patient is completing cycle 4 of imatinib with no toxic effects; there is a significant decrease in the clinical size of the tumor from 7 x 4 cm to 3.5 x 3 cm.

Conclusion: We present a unique case of a myxoid neoplasm with an unexpected molecular finding of a COL1A1::PDGFB fusion. Although the immunohistochemical profile could be compatible with DFSP/GCFB and myxoid variants have been described, the histology is not entirely in keeping with a myxoid DFSP, and no areas with typical DFSP histology were identified. This case highlights the utility of identifying molecular alterations in soft tissue neoplasms, especially in cases with partial resections and/or when systemic therapy is being considered.

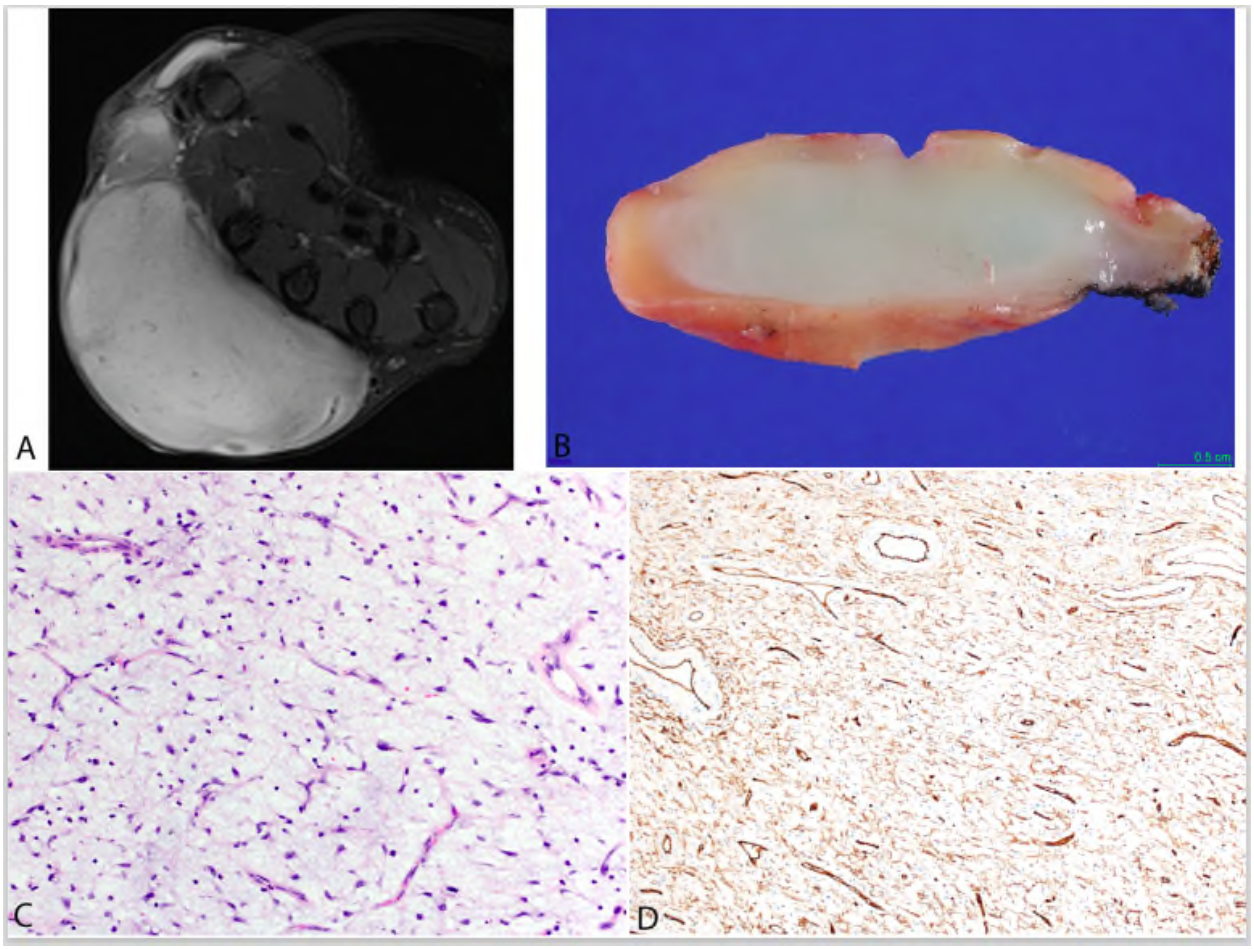
A
B
C
D

30

Immunohistochemical Expression of Lymphatic Endothelial Markers in Blue Rubber Bleb Nevus Syndrome

A Bakker [1], A Al-Ibraheemi [2], S Fishman [2], H Kozakewich [2], M Liang [2], J Slack [2]; [1] Boston Children's Hospital, [2] Boston Children's Hospital

Background: Blue rubber bleb nevus syndrome (BRBNS) is a rare vascular disorder characterized by multifocal cutaneous, visceral, and other soft tissue or solid organ venous malformations (VM). It is due to activating somatic TIE2 mutations and draws its name from the characteristic multiple, cutaneous, blue papules and nodules. Although BRBNS lesions are venous malformations, lesional endothelial cells in BRBNS almost always express one or more immunohistochemical markers of lymphatic differentiation, and as such, risk misdiagnosis as a lymphatic malformation. Herein, we describe the immunohistochemical expression of lymphatic endothelial markers in a cohort of BRBNS patients.

Methods: BRBNS cases seen at our institution during the prior 30 years were reviewed and a subset with a suitable amount of lesion present were selected for this study. H&E slides were reviewed and the involved anatomic compartments, presence/absence of intravascular thrombi, and presence/absence of perivascular smooth muscle were noted. Immunohistochemical expression of PROX1 (nuclear) and D2-40 (membranous/cytoplasmic) were evaluated semi-quantitatively with cases being assigned to one of four categories for each stain, based on the proportion of lesional endothelial staining as follows: (A) none; (B) between 0 and 10% = “focal”; (C) >10% to 50% = “patchy”; and (D) >50% = “diffuse”.

Results: 18 BRBNS specimens were selected from 15 patients (9 male, 6 female, age range = 18 months to 35 years, mean age = 12.5 years). Of these, 9 were cutaneous, 8 were gastrointestinal, and 1 was hepatic. Some PROX1 staining was seen in all cases, and the majority (88.9%) demonstrated patchy or diffuse positivity (greater than 10% nuclear staining). D2-40 staining was present in one-third (33%) of cutaneous lesions, most commonly confined to the most superficial channels, whereas all gastrointestinal and hepatic lesions were negative throughout. Patchy non-specific focal staining was occasionally seen within organizing thrombi. Both PROX1 and D2-40 tended to be negative in lesional vascular channels with greater than one layer of perivascular myocytes.

Conclusion: Although BRBNS lesions are venous malformations, all demonstrated immunohistochemical positivity for one or more lymphatic endothelial markers which may lead to misdiagnosis as a lymphatic or lymphatico-venous malformation.

31

Novel CDH13::STX8 fusion in cellular neurothekeoma with atypical features: a case report.

P Zamiara [1], C Guardado Salazar [2], R Schmidt [2], N Shillingford [2], S Zhou [2], L Wang [2], B Pawel [2], M Warren [2]; [1] Children's Hospital Los Angeles, [2] Children's Hospital Los Angeles

Background: Cellular neurothekeoma is a rare superficial soft tissue tumor of uncertain histogenesis. The typical clinical scenario is that of a painless cutaneous nodule of the head and neck or upper extremity of a teenage or young adult female with characteristic nodular architecture, plump spindled cells, and appreciable mitotic activity. In a large series of this entity, up to 25% of cases showed frankly pleomorphic cells. A recurring molecular alteration has not yet been elucidated, however point mutations in PI3K, ALK, SMO, and ERBB3 have recently been reported. CDH13, found on chromosome 16q, encodes cadherin-13, a noncanonical member of the cadherin superfamily of cell surface proteins. It is downregulated in multiple carcinoma and leukemia cell lines, often through epigenetic modification (hypermethylation). STX8, found on chromosome 17q, encodes syntaxin-8, a protein involved in intracellular protein trafficking. It has not yet been linked to cancer biology.

Methods: Microscopic examination with H&E and immunohistochemical stains was performed. Ancillary techniques included targeted next generation sequencing (NGS) panel, chromosomal microarray, and RNAseq analysis. The CDH18::STX8 fusion was further confirmed by Sanger sequencing.

Results: A 2-year-old girl presented to outpatient clinic with a 1.5 cm painless nodule on the dorsal right hand. Ultrasound revealed a 1.3 cm hypoechoic nodule with no appreciable vascularity. Histologic sections following excision showed a relatively circumscribed lesion with vague lobular architecture and tongues of lesional tissue extending beyond the fibrous periphery. The large, bizarre pleomorphic tumor cells had vesicular nuclei, prominent nucleoli, and frequent mitoses (including occasional atypical forms). Chromosomal microarray revealed subclones with partial gains of losses of multiple chromosomes (including tumor suppressors such as TP53, NF1, and NF2) that were not characteristic of any particular entity, and a targeted NGS panel was negative for clinically significant variants. Additional testing with RNA sequencing was sought and revealed an in-frame CDH13::STX8 fusion of unknown clinical significance. The CDH13 gene accounted for the 5’ end of the fusion product and lacked the membrane anchor domain, suggestive of potentially disrupted protein function. Immunostain panel, including diffuse positivity for NKI-C3, was most suggestive of neurothekeoma. A diagnosis of cellular neurothekeoma with striking cytologic atypia was rendered.

Conclusion: We report a novel CDH13::STX8 fusion in cellular neurothekeoma with striking cytologic atypia. The CDH13 fusion partner is predicted to have altered function due to absence of its membrane anchoring domain.

32

Novel SRF::SOHLH1 fusion in a myofibroma/myopericytoma spectrum tumor: a case report.

P Zamiara [1], C Guardado Salazar [2], R Schmidt [2], N Shillingford [2], M Warren [2], S Zhou [2], L Wang [2], B Pawel [2]; [1] Children's Hospital Los Angeles, [2] Children's Hospital Los Angeles

Background: The perivascular/myoid family of tumors includes glomus tumor, myofibroma, myopericytoma, and angioleiomyoma. These entities share morphologic and immunohistologic features, but molecular genetic investigations revealed different characteristic molecular alterations in member tumors. A cellular variant of myofibroma/myopericytoma was found to harbor SRF::RELA fusion, and more recently, additional fusion partners (CITED1, CITED2, NFKBIE, and NCOA2) have been identified through RNA sequencing of pediatric tumors within this family of neoplasms. SOHLH1, found on chromosome 9, encodes a transcription factor that is expressed during spermatogenesis and oogenesis. Mutations in this gene are associated with nonobstructive azoospermia; it has not thus far been associated with neoplasia.

Methods: Microscopic examination with H&E and immunohistochemical stains was performed. Ancillary techniques included targeted next generation sequencing (NGS) panel, chromosomal microarray, and RNAseq analysis. The SRF:SOHLH1 fusion was further confirmed by Sanger sequencing.

Results: A 14-year-old male presented to medical attention with a slow-growing right lower leg mass. Diagnostic imaging revealed a 10.2 cm calcified mass in the soft tissue, with no bony changes of the fibula or tibia. CT-guided needle biopsy was performed, showing tumor composed of round to plump spindle cells featuring amphophilic to cleared cytoplasm, arranged haphazardly and in small clusters, and associated with ample background matrix. There were 2 mitoses per 10 high-power fields. Immunostains did not indicate a clear line of differentiation. Chromosomal microarray revealed partial gains of losses of multiple chromosomes that were not characteristic of any particular entity, and a targeted NGS panel was negative for clinically significant variants, including gene fusions. Additional testing with RNAseq was sought and revealed SRF::SOHLH1 fusion. Based on molecular results, additional immunostains were performed and tumor cells were positive for SMA, MSA, and calponin, consistent with myofibroma/myopericytoma spectrum tumor. Resection with negative margins was subsequently achieved. A concurrent lung nodule initially concerning for metastasis proved to harbor Coccidioides on wedge biopsy.

Conclusion: We report a novel SRF::SOHLH1 fusion in pediatric cellular myofibroma/myopericytoma family tumor.

33

Renal-hepatic-pancreatic dysplasia-1 with symmetric cardiac hypertrophy in the setting of biallelic inactivation of NPHP3: a case report

P Zamiara [1], C Guardado Salazar [2], R Schmidt [2], S Zhou [2], N Shillingford [2], L Wang [2], B Pawel [2], M Warren [2]; [1] Children's Hospital Los Angeles, [2] Children's Hospital Los Angeles

Background: Renal-hepatic-pancreatic dysplasia-1 (RHPD1), originally given the eponymous designation Ivemark II syndrome, is a rare syndrome caused by biallelic inactivation of NPHP3, which is located on chromosome 3q and encodes the protein nephrocystin 3, a component of the ciliary complex. Clinical characteristics are variable, but diagnosis requires cystic renal dysplasia, pancreatic fibrosis, and hepatic ductal plate malformation. Cardiac involvement in RHPD1 usually takes the form of situs abnormalities. RHPD1 is a highly lethal disorder, with most patients succumbing within the neonatal period or within the first year of life.

Methods: Unrestricted autopsy was performed. Prior to death, peripheral blood was collected for whole exome sequencing (WES). Diagnostic modalities to complement gross examination included H&E histology, special stains, microbial cultures, and electron microscopy.

Results: The decedent was a 4-week-old female born at 36 +1/7 weeks gestational age. The prenatal course was complicated by oligohydramnios and pulmonary hypoplasia. Imaging revealed liver and pancreatic cysts and a normal brain. Her postnatal course was complicated by persistent pulmonary hypertension requiring mechanical ventilation. Echocardiogram revealed left ventricular hypertrophy. Her laboratory testing showed hyperbilirubinemia (total/conjugated bilirubin 28.1 and 23.5 mg/dL) with concern for biliary atresia, but MRCP was inconclusive. In the second week of life, she developed kidney failure with fluid overload and electrolyte derangements. She developed C. albicans urinary tract infection and fungemia. On the day of death, she experienced pulmonary hemorrhage and was coded for profound hypotension and bradycardia. Despite resuscitative efforts, she passed away. At autopsy, gross examination revealed bilateral hydroureteronephrosis, cortical cysts in the left kidney, multiple microabscesses in the right kidney, cholestatic hepatic parenchyma with 0.7 cm subcapsular cyst, and enlarged, firm pancreas with two 2.6 cm cysts. On microscopic evaluation, both kidneys displayed cystic renal dysplasia, with microabscesses containing pseudohyphae consistent with C. albicans apparent in the right kidney. Early hepatic ductal plate malformation and a simple cyst were eminent in the liver, and widespread fibrosis and two pseudocysts within the pancreas. In the lungs, the radial alveolar count was as low as 2, indicative of pulmonary hypoplasia. The heart showed left ventricular free wall and septum thicknesses of 1.0 cm each, with myocyte hypertrophy. WES demonstrated compound heterozygosity for inactivating mutations of NPHP3: c.2104C>T, p.Arg702* and c.434_437delAAAG, p.Glu145Valfs*3.

Conclusion: We report a case of RHPD1, a rare ciliopathy with only 52 previous cases reported in the literature. The autopsy revealed characteristic features of RHPD1. The cause of death was multiorgan failure due to RHPD1 sequelae and severe pulmonary hemorrhage likely caused by coagulopathy due to uremia and liver failure. Our case uniquely showed symmetric cardiac hypertrophy without apparent alternative explanation. WES played an essential role in diagnosis.

34

Bilateral Glomerulocystic Kidney Disease with Extensive Nephrogenic Rests in a Setting of HNF1B Mutation

J Havens [1], B Hill [2], A Treece [2]; [1] The University of Alabama at Birmingham, [2] Children's of Alabama

Background: Glomerulocystic renal disease has numerous etiologies, including HNF1B mutations. Morphologic renal findings in a setting of HNF1B mutations may also include cystic renal dysplasia, solitary functioning kidney, horseshoe, and oligomeganephronia. The finding of numerous nephrogenic rests (NRs) has been reported in very rare cases of GCKD, but none have been genetically characterized. NRs are foci of persistent metanephric blastema that have potential to transform into Wilms tumor (WT). We report a case of bilateral GCKD with numerous interspersed NRs of uncertain clinical significance in a setting of germline HNF1B mutation.

Methods: The clinical history, gross and histologic examination, and literature are reviewed.

Results: A 2-year-old male presented for renal transplant due to bilateral polycystic kidney disease (PKD) with progressive renal failure. He was first diagnosed with PKD and anhydramnios on routine prenatal ultrasound studies, and his prenatal PKD panel was reportedly normal. At birth, appropriate APGARs were recorded following resuscitation (8, 8). Serum creatinine increased for the first few days of life until stabilization at 4.5-4.8; metabolic acidosis and hyperkalemia improved with enteral base supplementation. His labs remained relatively stable with an elevated serum creatinine and mildly elevated BUN. Dialysis was started around 4 months of age. Further genetic workup demonstrated an HNF1B mutation consistent with renal cysts and diabetes syndrome (RCAD). A renal transplant with explant of the native kidneys was performed at 26 months of age. Bilateral kidneys were received (57 g left, 48 g right) with total replacement of renal parenchyma by innumerable, smooth-walled, cysts containing serous fluid and ranging in size from 0.1-0.7 cm. Microscopy showed cysts lined by single layers of bland cuboidal cells, with many containing glomerular tufts. Numerous nephrogenic rests were identified throughout the intervening stroma of both kidneys. Hyperplastic areas were not present.

Conclusion: GCKD may be seen in a setting of HNF1B mutation; however, the additional finding of extensive, admixed NRs has only very rarely been reported. Germline HNF1B mutations are associated with maturity-onset diabetes, chromophobe renal cell carcinoma, and RCAD with widely variable renal disease. One reported patient with identical histology also had hemihypertrophy, which may be associated with NRs and alterations on 11p15, and another had no other underlying conditions. Molecular testing was not performed in either case. The neoplastic potential of NRs in this setting is unknown. We report this case to highlight a novel combination of morphologic and genetic findings in GCKD.

35

EWSR1::NFATC2-rearranged vascular anomaly arising in early childhood with morphologic atypia

B Siegele [1], S Wicks [2], M Haag [3], C Galambos [2]; [1] Children's Hospital Colorado, [2] Children's Hospital Colorado, [3] Colorado Genetics Laboratory

Background: EWSR1::NFATC2-rearranged tumors constitute an emerging spectrum of disease entities with wide-ranging pathologic features. On the benign end, solitary bone cysts in the young and vascular malformations/hemangiomas of the bone in elderly patients have been reported to harbor EWSR1::NFATC2 rearrangements and display benign behavior. By contrast, EWSR1::NFATC2 fusion-positive round cell sarcomas are a recently described subtype of "Ewing family" tumors with highly aggressive behavior and poor response to chemotherapeutic regimens. Very recently, a cohort of five adult patients with epithelioid vascular lesions harboring EWSR1::NFATC2 rearrangements was described with cytologic atypia, including a distinct morphology comprised of alternating vasoformative and solid growth and mild to moderate nuclear pleomorphism. We report a EWSR1::NFATC-rearranged epithelioid vascular tumor originating in infancy and presenting with unique immunophenotypic and morphologic features.

Methods: An 11-year-old female presented for care at our institution with an extensive history of vertebral bony pathology.

Results: At 2 years of age, the patient had presented with an L4 vertebral fracture with pathology showing a fibrovascular lesion with hemosiderin deposition, inciting a working diagnosis of chronic recurrent multifocal osteomyelitis. At 6, 8, and 10 years of age, the patient received sequential biopsies of a progressively expansile L4 vertebral process mass, resulting in the diagnosis of a benign vascular malformation. At the most recent presentation, imaging revealed a progressive 4.4 x 4.8 x 7.4 cm mass expansile into the retroperitoneum. Grossly, the mass was red-brown, lobulated, and firm, with cut surfaces demonstrating spiculated bony tissue with marked hemorrhage. Histologically, the tumor was composed of large thin- and thick-walled vascular structures with rare focal areas of intraluminal endothelial cell proliferation and nests of proliferative epithelioid endothelial cells with mitotic activity and rare atypical mitoses. Immunohistochemical staining revealed intraluminal spindle cells to be CD31+. CD34-, and Prox1+ consistent with lymphatic-type endothelial cells. Additional markers including synaptophysin, chromogranin, CD56, panCK, EMA, DUX4, BCL-2, CD99, NKX2.2, P53, myogenin, Phox2b, Glut-1, HMB-45, HHV-8, S-100, CAMTA1, and TFE3 were negative. BAF47/INI1 was retained. Ki-67 was focally increased in regions of hemorrhage with associated epithelioid cells. Routine cytogenetics studies showed a normal female karyotype (46,XX), while next generation RNA sequencing revealed a EWSR1::NFATC2 fusion, later confirmed by fluorescence in situ hybridization break apart probes for EWSR1.

Conclusion: The histologic, immunohistochemical, and molecular findings are overall consistent with a vascular anomaly with EWSR1-NFAT2C rearrangement, scattered proliferative endothelial cell clusters with epithelioid cell morphology, and rare atypical mitotic figures. The combination of the patient's very early age at initial presentation (2 years old) and epithelioid

endothelial and intravascular endothelial proliferations represent a unique pediatric presentation of an EWSR1::NFATC-rearranged epithelioid vascular tumor.

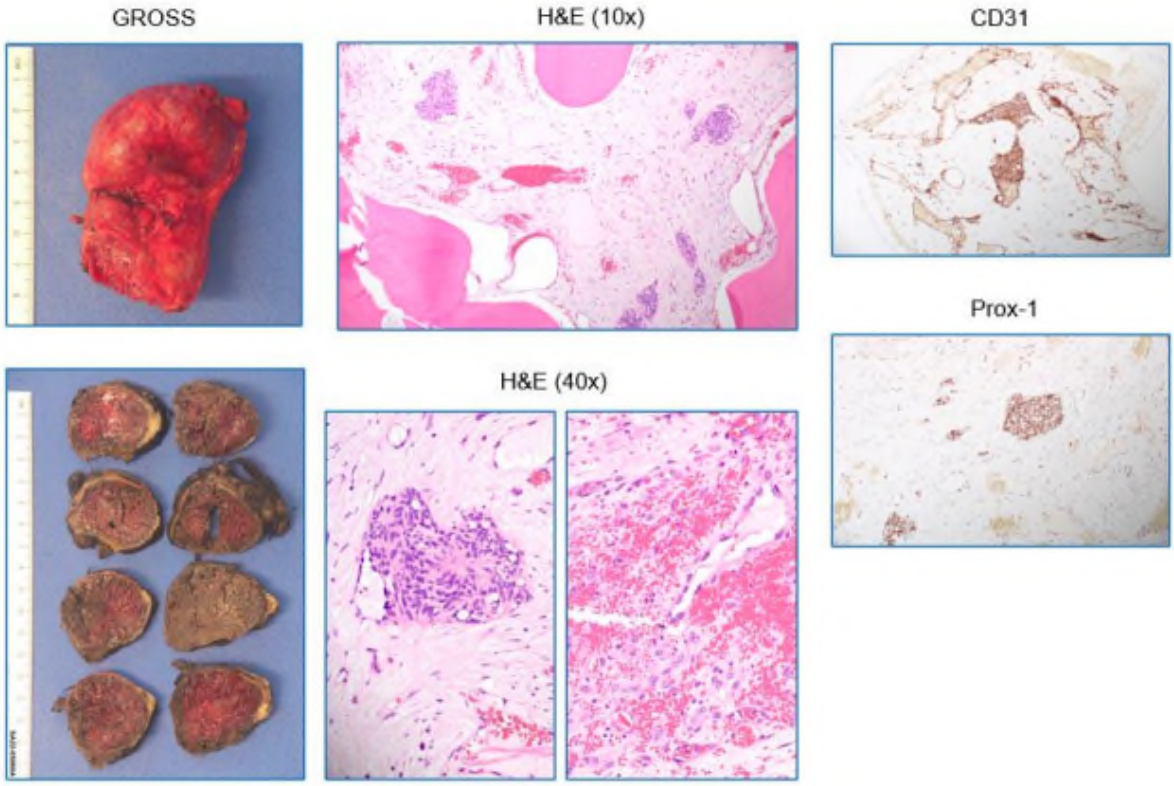

37

Lower Mesodermal Defects (LMD): An Institutional Experience of a Rare Congenital Malformation Spectrum

K Weaver [1], A Breaux [2], L Berklite [2], A Bernieh [2], O Lopez-Nunez [2], J Stanek [2]; [1] Cincinnati Children's Hospital Medical Center, [2] Cincinnati Children's Hospital Medical Center

Background: LMD (Cloacal dysgenesis/CD, urorectal septum malformation sequence/URSMS) refers to a spectrum of rare genitourinary (GU) and anorectal congenital anomalies, some of which are fatal in the perinatal period. The broad spectrum of clinical presentations of these malformations has limited the development of consistent classification systems. We present a series of 5 autopsy cases, including 4 cases of complete URSMS and 1 case of CD highlighting unusual features.

Methods: All autopsy cases of LMD were identified from the files of a single institution between 2009-2022 and available surgical pathology material and reports were reviewed.

Results: A total of 5 autopsy cases with a final diagnosis of LMD were identified. The findings in all patients are summarized in Table 1 (insert image).

Conclusion: As illustrated by our series, there are likely no two identical cases of LMD, resulting in overlapping diagnostic features between variously named entities in this spectrum of malformations as well as challenges in creating consistent terminology, but all share agenesis/atresia of the urethra and absence of meaningful genetic abnormalities. The association of some cases with maternal diabetes mellitus may implicate environmental factors in the pathogenesis with the severity of the malformation depending on timing of the insult. Most important clinically, despite varying symptomatology, is the low likelihood of recurrence in subsequent pregnancies if known environmental factors can be identified/controlled.

Table 1. Clinical and Autopsy Findings in 5 Cases of LMD

Case	Age	Sex	Maternal PMH	Genetics	Genitalia	Urinary tract	Hindgut	Additional Anomalies
1	29 1/7 wks	F	G2P0101 35 years, type 1 diabetes, chronic HTN, preeclampsia, preterm delivery	cfDNA with no aneuploidy, microarray with likely unconsequential interstitial duplication of Xp	**Ext:** No vaginal opening **Int**: Bicornuate uterus with a dilated cornu, UR bilateral ovaries and fallopian tubes, blind-ended vagina	UR kidneys, dilated bladder, patent ureters, No urethral meatus, vesicovaginal fistula	UR	Ascites, Pulmonary hypoplasia, Disruption at the cervicothoracic junction and multiple bone abnormalities
2	34 4/7 wks	M	G4P1012 31 years, placenta previa	cfDNA low risk for aneuploidy	**Ext:** Penoscrotal transposition **Int**: UR bilateral testes	R renal agenesis, L MCDK, Dilated bladder, no patent ureteral openings or urethra, portion of fused prostatic tissue; No urethral meatus	Blind-ending, fused with bladder, absent anal opening	Pulmonary hypoplasia, facial dysmorphism, L equinovarus deformity, 2 vessel umbilical cord
3	39 1/7 wks	M	G1P1 18 years, low PAPP A, carrier for *NPHS2* mutation	cfDNA with low risk for aneuploidy	**Ext:** Absent phallus, anterior clefting and tufting of the scrotal tissue, absent scrotal and perineal median raphe **Int:** UR descended bilateral testes	Bilateral MCDK, patent ureters, hypoplastic bladder, no urethra or prostate	UR	

4	21 wks	M	G2P001, abnormal quad screen	UK	**Ext:** UR phallus **Int:** Bilateral undescended inguinal testes	Bilateral hydronephrosis, hydroureters, enlarged, thickened bladder, no urethral meatus	Blind-ending/ fused with bladder, Absent anal opening	Agenesis R umbilical artery, Potters facies, pulmonary hypoplasia, bilateral talipes calcaneovalgus, ascites, chest deformity, features of prune belly syndrome
5	28 wks	M	UK	normal 46XY karyotype	**Ext:** Edematous phallus, **Int:** UR bilateral testes	Bilateral MCDK, enlarged, thickened bladder, no urethral opening	Blind-ending/fused with bladder, Absent anal opening	Flexion contractures, laryngeal atresia, ascites

UR- unremarkable; HTN- hypertension; Ext- external; Int- internal; MCDK- multicystic dysplastic kidney; UK- unknown

38

Focal Nodular Hyperplasia in Children and Young Adults: Our Experience

L Berklite [1], A Breaux [2], R Sheridan [2], S Ranganathan [2]; [1] Cincinnati Children's Hospital Medical Center, [2] Cincinnati Children's Hospital Medical Center

Background: Focal nodular hyperplasia (FNH) is a benign hepatocellular proliferation that typically presents as an incidental solitary mass with a female predominance, and infrequently occurs in children. FNH has been reported to occur with higher frequency in pediatric patients with a history of remote malignancy, hematopoietic stem cell transplant, and biliary atresia as well as in association with hepatic vascular anomalies or underlying cardiovascular conditions. The aim of this study was to retrospectively review the FNH cases diagnosed at our institution and characterize the prevalence, clinical features, and types of predisposing conditions in our patient population.

Methods: A retrospective review of all pathologically diagnosed FNH at our institution from 1998-2023 was performed after IRB approval. Relevant clinical and imaging data was collected from the electronic medical record including age, sex, underlying conditions/disease, presenting symptoms, location, and multifocality.

Results: A total of 49 cases of FNH in 44 patients were identified. Patients were aged 3 months to 39 years with a 1:1.5 male to female ratio. Among the 44 patients, 15 (34%) had a history of remote malignancy including medulloblastoma (n=2), choroid plexus carcinoma (n=1), neuroblastoma (n=3), ALL (n=2), Wilms tumor (n=1), sacral chordoma (n=1), melanoma (n=1), rhabdomyosarcoma (n=1), and liver neoplasms. 20 (45%) had a history of underlying cardiovascular disease or vascular anomalies including Fontan procedure for congenital cardiac disease (n=11), Abernathy malformation (n=1), cavernous transformation of the portal vein (n=1), cardiac transplantation (n=2), and infantile hemangiomas (n=1). Syndromic associations included WAGR syndrome, nephronopthhisis-medullary cystic disease, Lennox-Gaustat syndrome and Hurler’s syndrome. One patient had an underlying diagnosis of PFIC2. 4 patients had a history of hematopoietic stem cell transplant. 29(65%) patients had multiple liver lesions on imaging felt to be additional FNH lesions with 11 confirmed by biopsy as multifocal and 11 (25%) had concurrent liver neoplasia including inflammatory adenomas, beta catenin-mutated adenomas, hepatoblastoma, cholangiocarcinoma, well-differentiated hepatocellular carcinoma (HCC), and fibrolamellar HCC. 27 (61%) patients had background liver disease confirmed pathologically.

Conclusion: In our cohort, FNH were more frequently multifocal and seen in the context of underlying vascular anomalies, congenital cardiac disease, or a remote history of malignancy. The finding of concurrent adenomas and rarely hepatic malignancy in patients with FNH highlights the importance of continuing monitoring of these lesions and the utility of biopsy in young patients with underlying conditions.

39

Transnasal Endoscopy (TNE) Esophageal Biopsies are Sufficient for Comprehensive Pathology Evaluation

O Lopez-Nunez [1], A Bernieh [2], K Kliewer [2], P Kemtur [2], S Bolton [2], V Mukkada [2], M Rothenberg [2], M Collins [2]; [1] Cincinnati Children's Hospital Medical Center, [2] Cincinnati Children's Hospital Medical Center

Background: TNE does not require general anesthesia and therefore provides an attractive alternative to conventional endoscopy (CE) for monitoring chronic diseases such as eosinophilic esophagitis (EoE). We tested the adequacy of esophageal biopsies obtained by TNE compared to CE using the EoE histology scoring system (HSS).

Methods: Our institutional database was searched for upper endoscopies performed by TNE from 7/21-7/22. Proximal and distal esophageal biopsies obtained by the same endoscopist using CE were matched to those of patients in the TNE group. EoEHSS features (eosinophil inflammation, basal zone hyperplasia, eosinophil abscesses, eosinophil surface layering, dilated intercellular spaces, surface epithelial alteration, dyskeratotic epithelial cells, lamina propria fibrosis) were scored for severity (grade) and extent (stage) in biopsy whole slide images. Mann-Whitney test was used to determine median (interquartile range) values, and Fisher exact test for categorical variables; $P \leq 0.05$ was considered significant.

Results: Patients in the TNE group (N=17) did not differ from those in the CE group (N=17) in median age (14.3 (13.6, 17.2) vs 15.8 (12.0, 17.3) years, respectively, P=0.82) or height (168.4 (148, 175.8) vs 168.7 (149.4,174.9 cm, respectively, P=0.83). Most patients were male (N=32/34). All had a diagnosis of EoE, (active at the time of evaluation in 9/17 TNE, 10/17 CE, P=1). All 8 EoEHSS features were evaluated in each group; the only missing feature was lamina propria fibrosis (missing in 19/34 TNE vs 11/34 CE, P=0.09). The median peak eosinophil count differed (15 (1, 66) TNE vs 3 (0, 29) CE, P=0.03), but median total grade (0.17 (0.10, 0.29) TNE vs 0.22 (0.14, 0.46) CE, P=0.12) or stage (0.14 (0.10, 0.24) TNE vs 0.20 (0.10, 0.43) CE, P=0.15) scores did not differ between the groups.

Conclusion: TNE yields esophageal biopsies that are comparable to those obtained by CE, and appear suitable for clinical evaluation and clinical trials.

40

Intrahepatic cholangiolitis in Cystic Fibrosis (ICCF): an under-appreciated cause of persistent cholestasis in infancy.

K Bove [1], A Bernieh [2], G Tiao [2], V Garcia [2], L Lazar [3], M Sathe [3], J Sanchez [4], R Gonzalez [5], I Gonzalez-Gomez [5]; [1] Cincinnati Children's Hospital Medical Center, [2] Cincinnati Children's Hospital Medical Center, [3] University of Texas Southwestern Medical Center, [4] The University of Texas at Austin, [5] Johns Hopkins All Children's Hospital

Background: Liver biopsy findings in infants with CF and persistent cholestasis are seldom reported except in rare instances when extrahepatic biliary abnormalities may mimic biliary atresia (Bove et al, AJSP 2021). In four such infants, we described a distinctive intrahepatic cholangiopathy (ICCF).

Methods: We report clinical details, intraoperative cholangiograms and liver biopsy findings in 3 additional infants homozygous for CFTR mutations and a fourth with a heterozygous CF mutation and summarize our experience in 8 infants with CFTR mutations and persistent cholestasis who were subjected to clinical investigation.

Results: Cholangiograms demonstrated patent extrahepatic ducts; one infant with CF had uniform dilatation interpreted as a choledochal cyst. Liver histology in three CF homozygotes had evidence for severe cholangiocyte injury with cholangiolitis principally affecting small ducts near the portal area margins. The CFTR heterozygote had a severe generalized ductular reaction with paucity but minimal features of cholangitis. Cholestasis slowly subsided in all four infants. ICCF is characterized by severe local cholangiocyte injury, focal acute necrotizing cholangiolitis, local bile leakage leading to prominent local aggregates of portal ceroid and variable, occasionally severe, reactive ductular proliferation concentrated at the periportal margins (Figure).

Conclusion: ICCF as previously described is confirmed. ICCF is the most consistent histologic feature in liver biopsies from infants with cystic fibrosis being investigated for unexplained persistent cholestasis. Extrahepatic biliary tract abnormalities may coexist but evidence for obstruction is inconsistent in infants with CF. ICCF is an early manifestation of CF not related to meconium ileus or the specific genotype of CFTR. We hypothesize that ICCF may be a prototype for pathogenesis of cystic fibrosis liver disease later in life.

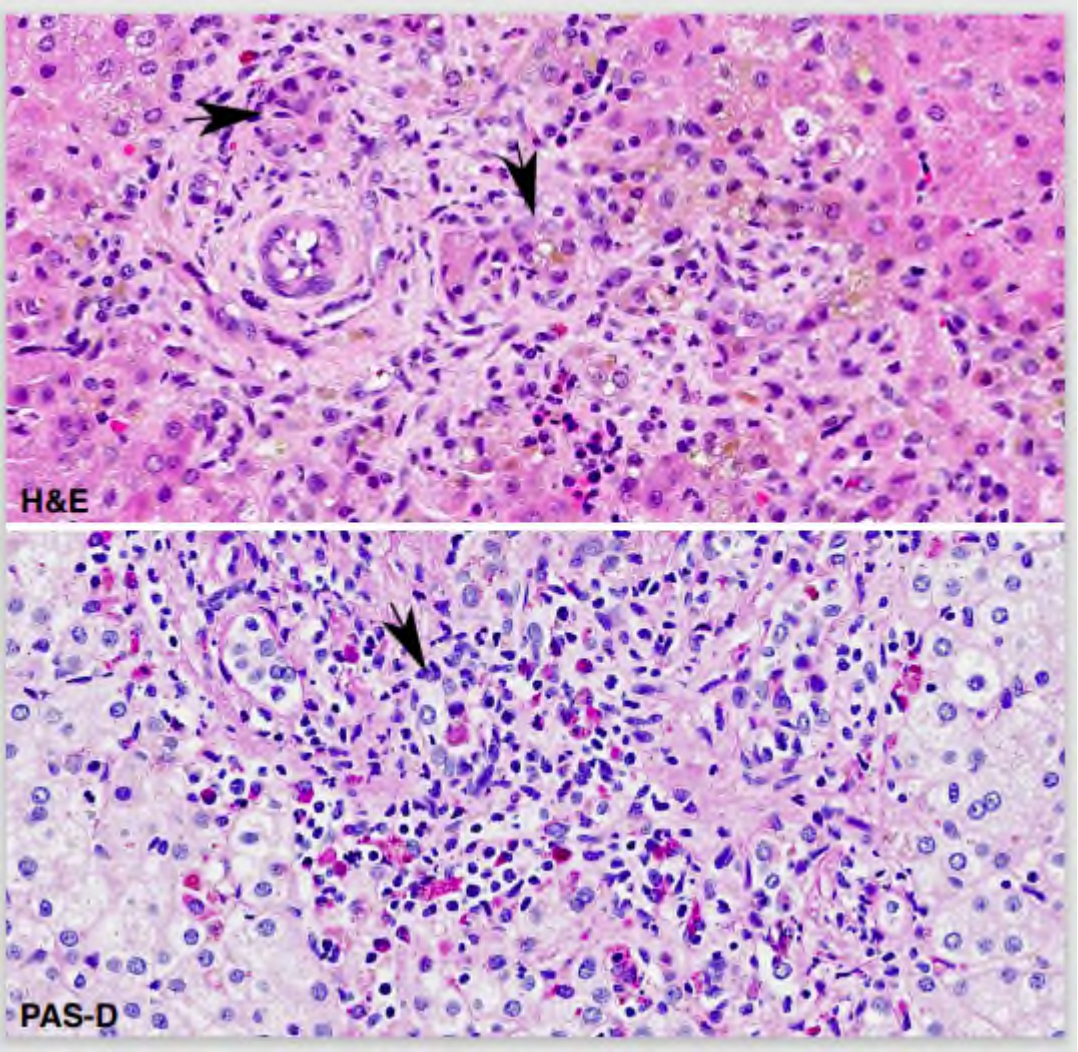
H&E
PAS-D

41

Granulomas in Pediatric Liver Biopsies: single center experience

M Shaheen I Gonzalez; Indiana University School of Medicine

Background: Granulomas in liver biopsies are rare and seen in < 5% of liver biopsies and are associated with multiple conditions, the most common one being primary biliary cholangitis. However, most of the series are either primarily based on adults or a mixed adult-pediatrics cohort of cases. The largest single center report with an exclusively pediatric cohort is >20 years old hence an updated cohort is much needed considering the multiple changes throughout those years.

Methods: From 2000 to 2021 a retrospective search was made for liver biopsies with granulomas in our department database. Cases were reviewed for different histologic features and the clinical information was retrieved from the electronic medical records.

Results: A total of 17 liver biopsies with granulomas were identified which presented in 10 boys (59%) and a median age of 13 years (1 – 19) (Table-1). 5 cases presented in allografts livers which were transplanted due to OTC deficiency (2 cases), biliary atresia (2 cases) and Budd-Chiari syndrome (1 case). 4 patients had a history of neoplasms (Hodgkin lymphoma, Wilms tumor, astrocytoma and colon adenocarcinoma [one each]). Other significant comorbidities included autoimmune hepatitis, Crohn disease and SCID status post SCT (one each). The most common indication for liver biopsies was the presence of a nodule/mass (8 cases). 11 patients were taking multiple medications at the time of biopsy (Table 1). The most common location of the granulomas was pan-acinar (11 cases) followed by subcapsular (4 cases), portal (1 case) and periportal (1 case). In 10 cases necrosis was seen within the granuloma. 8 cases had no inflammation associated with the granulomas, 6 cases had rare lymphocytes, 2 a mixed inflammation and 1 rare neutrophils. 12 granulomas had focal giant cells and 1 case had multiple giant cells. Only one granuloma was associated with a vessel, a portal vein. None of the granulomas were associated with fat droplets or bile ducts. 2 cases had a positive GMS stain, consistent with histoplasma (one in an allograft liver). Cultures were performed in 5 cases which were positive in 2, one for Pseudomonas putida (allograft liver) and one for Candida species. The cases with a positive GMS stain and positive cultures showed central necrosis within the granulomas.

Conclusion: Our experience with 17 liver biopsies with granulomas is heterogenous and reinforces the association of necrosis with infectious etiologies. Of the allografts' biopsies, 2 neither showed necrosis nor were associated with an infectious etiology. Cases with non-necrotizing granulomas were associated with multiple medications suggesting a drug-induced liver injury as a possible etiology.

Table 1. Clinicopathologic characteristics (N: 17)

Gender, n (%)	
Male	10 (58.8%)
Female	7 (41.2%)
Age, median (range) [years]	13 (1 – 19)
Medical history, n (%)	
Liver transplant	5 (29.4%)
Neoplasm	4 (23.5%)
Non-significant	3 (17.6%)
Autoimmune hepatitis	1 (5.9%)
Crohn disease	1 (5.9%)
Bipolar disorder	1 (5.9%)
SCID status post SCT	1 (5.9%)
Sickle cell disease	1 (5.9%)
Indications for liver transplant, n (%) (n: 5)	
OTC deficiency	2 (40.0%)
Biliary atresia[1]	2 (40.0%)
Budd-Chiari syndrome	1 (20.0%)
Neoplasm history, n (%) (n: 4)	
Hodgkin lymphoma	1 (25.0%)
Nephroblastoma/Wilms tumor	1 (25.0%)
Astrocytoma	1 (25.0%)
Colon adenocarcinoma	1 (25.0%)
Immunocompromised, n (%)	
Yes	9 (52.9%)
No	8 (47.1%)
Indication for liver biopsy, n (%)	
Liver nodule/mass	8 (47.1%)
Cholestatic hepatitis	3 (17.6%)
Rule out autoimmune hepatitis	2 (11.8%)
Rule out acute cellular rejection	1 (5.9%)
Elevated liver enzymes	1 (5.9%)
Allograft biopsy, time 0 (reperfusion biopsy)	1 (5.9%)
Not available	1 (5.9%)
Medications at time of biopsy, n (%)[2]	
None	6 (35.3%)
SSRI	2 (11.8%)
Tacrolimus	2 (11.8%)
Cyclosporine	1 (5.9%)
Methotrexate	1 (5.9%)
Antibiotics	2 (11.8%)
Antifungal	1 (5.9%)
Ganciclovir	2 (11.8%)
Acyclovir	1 (5.9%)
ACE inhibitor	2 (11.8%)
Beta-blocker	1 (5.9%)
Calcium channel blocker	1 (5.9%)
Anticonvulsant	3 (17.6%)
Adderall	1 (5.9%)
Antihistamine	2 (11.8%)

ALT, median (range) [Units/L] (available in 12)	103.5 (12 – 818)
AST, median (range) [Units/L] (available in 12)	65 (25 – 1,222)
GGT, median (range) [Units/L] (available in 9)	115 (18 – 183)
ALP, median (range) [Units/L] (available in 11)	274 (76 – 363)
T. Bil, median (range) [mg/dL] (available in 10)	1.1 (0.1 – 37)
C. Bil, median (range) [mg/dL] (available in 10)	0.3 (0 – 26.1)
Culture performed, n (%)	
No	11 (64.7%)
Negative	3 (17.6%)
Positive, *Pseudomona putida*	1 (5.9%)
Positive, *Candida* species	1 (5.9%)
Patient status, n (%)	
Alive	14 (82.4%)
Deceased	3 (17.6%)
Follow-up, median (range) [months]	33 (0 – 260)

[1]one patient additionally with A1AT deficiency and the other with Baraister-Winter syndrome
[2]Percentage do not add to 100 due to combination of medications
Abbreviations: SCID – severe combined immunodeficiency; STC – stem cell transplant; OTC – ornithine transcarbamylase; ACE – angiotensin-converting enzyme; AST – aspartate transaminase; ALT – alanine transaminase; GGT – gamma-glutamyl transferase; alkaline phosphatase; T. Bil – total bilirubin; C. Bil – conjugated bilirubin; SSRI – selective serotonin reuptake inhibitors.
References ranges: ALT: 5 – 45 Units/L; AST: 20 – 64 Units/L; GGT: 14 - 23 Units/L; ALP: 70 – 345 Units/L; T. Bil: 0.6 – 1.4 mg/dL; C. Bil: 0.0 – 0.3 mg/dL

42

Neonatal Cholestasis in Patients with Congenital Hyperinsulinism

I Gonzalez [1], A Baccarella [2], A Bennett [2], K Kennedy [2], T Bhatti [2], P Russo [2]; [1] Indiana University School of Medicine, [2] Children's Hospital of Philadelphia

Background: Congenital hyperinsulinism (CHI) is a form of severe hypoglycemia in newborns and infants which can lead to irreversible brain damage. A subset of these patients develops conjugated hyperbilirubinemia which warrants timely evaluation and exclusion of important conditions such as biliary atresia. Rare reports have associated this presentation with bile acid synthetic defects and the use of octreotide, but the vast majority are idiopathic. We present our experience with patients with CHI and neonatal cholestasis, and report for the first time a histologic characterization of liver biopsies from these patients.

Methods: A retrospective search for liver biopsies of patients with CHI was made in our department from 2000-22. Only cases with available biopsies slides and with confirmed diagnosis of CHI were included in the study. In all cases the following stains were performed PAS, PASD, trichrome and reticulin as well as these immunostains CK7, BSEP, MYO5B and MDR3. All cases were reviewed by two pathologists. The clinical information was retrieved from the electronic medical records.

Results: A total of 7 patients were included in the study with a median age and gestational age of 2 months (1–8) and 36 weeks (26–38), respectively (Table-1). Three (43%) and 2 (29%) patients had an underlying ABCC8 variant and Beckwith-Wiedemann syndrome, respectively. All the patients received diazoxide for management of hypoglycemia and treated with ursodiol for cholestasis which improved in 5 patients. Most cases showed periportal fibrosis (4, 57%) and all cases showed some degree of bile duct proliferation, with 3 being generalized and marked; ductular reaction was absent in 5 cases. Only 2 cases had portal inflammation which was mild. All cases had cholestasis (focal in 3 cases and diffuse in 4) and hepatocyte swelling, and 4 cases showed focal pseudoacinar transformation. Hepatocyte giant cell (HGC) transformation was present in all cases and 2 cases show HGC necrosis. Five and 2 cases showed nonsignificant and mild (5–33%) macrovesicular steatosis, respectively. Portal and lobular extramedullary hematopoiesis was seen in 5 and 3 cases, respectively. None of the cases showed bile duct paucity, acute cholangitis, bile plugging, portal edema, lobular inflammation or microvesicular steatosis. In 3 cases a focal increase in hepatocellular glycogen was seen on PAS stain. Focal hepatocyte aberrant expression by CK7 was seen in 3 cases. All the cases had a normal expression pattern of BSEP, MYOB5 and MDR3 by immunohistochemistry.

Conclusion: CHI in our experience is associated with a neonatal hepatitis pattern and importantly shows in all cases a bile duct proliferation but without significant ductular reaction or bile plugs. Awareness of the different histologic findings is crucial when evaluating these cases and most importantly to avoid a misdiagnosis of an obstructive process.

Table 1. Clinical characteristics (N: 7)

Gender, n (%)	
Male	5 (71.4%)
Female	2 (28.6%)
Age, median (range) [months]	2 (1 – 8)
Age, median (range) [days]	63 (47 – 267)
Gestational age, median (range) [weeks]	36 (28 – 38)
Maternal/pregnancy history, n (%)	
Nonsignificant	3 (42.9%)
gHTN	2 (28.6%)
gDM and polyhydramnios	1 (14.3%)
Twin-Twin transfusion syndrome	1 (14.3%)
Underlying genetic alteration of HI	
ABCC8	2 (28.6%)
ABCC8 and *GLUD1*	1 (14.3%)
Beckwith-Wiedemann syndrome^	2 (28.6%)
No variants identified	1 (14.3%)
Unknown	1 (143%)
ALT, median (range) [Units/L]	84 (17 – 142)
AST, median (range) [Units/L]	215 (104 – 671)
GGT, median (range) [Units/L]	176 (60 – 395)
ALP, median (range) [Units/L]	402 (92 – 656)
T. Bil, median (range) [mg/dL]	6.5 (1.1 – 18.1)
C. Bil, median (range) [mg/dL]	2.0 (0.0 – 10.7)
INR, median (range)	1.2 (0.9 – 1.5)
Liver imaging findings, n (%)	
Normal	4 (57.1%)
Hepatomegaly	1 (14.3%)
Diminutive gallbladder without visible common bile duct	1 (14.3%)
Multiple hypoechoic liver masses	1 (14.3%)
TPN prior to liver biopsy, n (%)	
Yes	4 (57.1%)
No	3 (42.9%)
Treatment for HI, n (%)	
Diazoxide	3 (42.9%)
Diazoxide and partial pancreatectomy	3 (42.9%)
Diazoxide and glucagon	1 (14.3%)
Improvement of cholestasis, n (%)	
Yes	5 (71.4%)
No	2 (28.6%)
Follow-up, median (range) [months]	1.2 (0.2 – 131)

^One patient with 11p duplication and 3p deletion, and second patient with genome-wide uniparental isodisomy

Abbreviations: gHTN – gestational hypertension; gDM – gestational diabetes mellitus; HI – hyperinsulinism; AST – aspartate transaminase; ALT – alanine transaminase; GGT – gamma-glutamyl transferase; alkaline phosphatase; T. Bil – total bilirubin; C. Bil – conjugated bilirubin; INR – international normalized ratio; TPN – total parenteral nutrition.

References ranges: ALT: 5 – 45 Units/L; AST: 20 – 64 Units/L; GGT: 17 – 126 [1 – 7 mo], 10 – 42 [7 – 11 mo] Units/L; ALP: 70 – 345 Units/L; T. Bil: 0.6 – 1.4 mg/dL; C. Bil: 0.0 – 0.3 mg/dL

43

Severe Obstructive Biliopathy Mimicking Biliary Atresia in an Infant with Ciliated Hepatic Foregut Cyst

A Hebert C Hughes, J Liang, H Wang, H Correa; Vanderbilt University Medical Center

Background: Ciliated hepatic foregut cysts (CHFCs) are rare with only seven reported pediatric cases in the literature and with just two diagnosed prenatally. CHFCs are most commonly identified in segment 4 of the liver and arise from the embryonic foregut. There are no other primary hepatic cysts with ciliated epithelium which distinguishes CHFCs from other hepatic cysts. CHFCs are known to communicate with the biliary tree, but there are no reports of CHFCs causing large bile duct obstruction.

Methods: We present a case of an 8-week-old female with an unbalanced translocation between chromosomes 3 and 9, heterozygosity for a variant of uncertain significance (VOUS) in the TALDO1 gene, multiple congenital abnormalities, hyperbilirubinemia, and a cystic hepatic lesion. The infant underwent a liver biopsy which was suggestive of large duct obstruction. Prior to undergoing surgical intervention, the infant arrested and ultimately passed away. A limited abdomen-only autopsy was performed.

Results: On internal examination of the abdomen, a multiloculated, translucent, thin-walled, fluid-filled cyst was found at the porto-hepatic junction. Microscopic examination of the cyst showed ciliated columnar and pseudostratified epithelium, consistent with a CHFC. The size (5.5 x 5.3 x 1.8 cm) and the location of the cyst resulted in a large duct obstruction causing hyperbilirubinemia, jaundice, scleral icterus, and clay-colored stools. On microscopy, the liver showed typical features consistent with obstructive biliopathy, including bile plugging, bile duct proliferation, cholestasis, and bridging fibrosis.

Conclusion: It is unknown whether the CHFC was due to the decedent’s unbalanced chromosomal translocation or her heterozygosity for a VOUS in the TALDO1 gene. Due to the limited nature of the autopsy, a cause of death could not be determined. In conclusion, CHFC is a rare diagnostic entity that should be considered in the differential diagnosis of cystic hepatic along with cystic biliary atresia and choledochal cysts causing large bile duct obstruction.

44

Neonatal Perinatal Autoimmune Hepatitis in the Setting of Anti-RNP Antibodies

L Kroll-Wheeler [1], K Bove [2], M Arnold [3]; [1] Children's Hospital Colorado, [2] Cincinnati Children's, [3] Children's Hospital Colorado

Background: Neonatal lupus erythematosus (NLE) is an uncommon disease that results from transplacental passage of maternal autoantibodies, the most common of which are anti-Ro/SSA and anti-La/SSB, though other autoantibodies have been implicated. NLE commonly manifests as skin lesions or congenital heart block but can involve the liver. Rarely, hepatobiliary disease is the sole manifestation and can mimic gestational alloimmune liver disease (GALD). We present on a case of severe liver disease in an infant born to a mother with systemic lupus erythematosus (SLE) with histopathological features of GALD progressing to cirrhosis with the phenotype of autoimmune hepatitis in the explant.

Methods: An infant was delivered at 37 weeks gestational age for growth restriction to a 34-year-old G1P1 mother with SLE. The mother was diagnosed at 16 years old with symptoms including pericarditis, severe joint pain, fever, alopecia, and malar rash, without liver involvement. Her disease course had been stable before and during pregnancy while on azathioprine and hydroxychloroquine. At age one month, the infant presented with jaundice and thrombocytopenia. Liver biopsy showed cirrhosis with a micronesting pattern, increased iron deposition, and minimal inflammation. After rapid progression to liver failure at five months of age, liver transplant was performed. Histological examination revealed micronodular cirrhosis with a universally prominent active chronic inflammatory infiltrate along the margins of residual nodules. Hepatocytes within the smallest nests showed variable differentiation into cholangiocyte-like cells with florid proliferation and occasional inspissated bile without iron deposition.

Results: The overall features were most consistent with active progressive autoimmune hepatitis with cirrhosis, a diagnosis at odds with the young age of the patient. We propose that the infant’s liver disease is related to transfer of maternal antibodies associated with SLE to the fetus. Serologic testing of the infant at the time of presentation revealed positive anti-ANA (1:320) and anti-ribonucleoprotein (anti-RNP) antibodies; post-transplantation testing was negative for both markers. The mother was positive for anti-ANA (>1:1280) and anti-RNP antibodies, along with low-positives for anti-dsDNA and anti-LC1 antibodies. Both the mother and the infant were negative for anti-SSA and anti-SSB antibodies. While rare cases of NLE associated with anti-RNP have been reported, liver disease has not been a previously described feature.

Conclusion: This case represents a unique hepatobiliary manifestation of presumed NLE involving anti-RNP antibodies, resulting in a liver disorder that initially had histological features of GALD and during rapid progression acquired a phenotype of end-stage autoimmune hepatitis.

45

Clinicopathologic Features of MEDNIK Syndrome in a Term Infant: Histologic and Ultrastructural Changes in the Gastrointestinal Tract

J Lu [1], S Namjoshi [1], A Niehaus [1], S Tahata [1], C Lee [1], L Wang [1], E McDonnell [1], M Seely [1], M Martin [2], F Hazard [1]; [1] Stanford HealthCare, [2] UCLA Health

Background: Inherited syndromes of congenital enteropathy are rare, with many genetic causes described. Mutations of the AP1S1 gene results in one such syndrome characterized by intellectual disability, enteropathy, deafness, peripheral neuropathy, ichthyosis, and keratoderma (MEDNIK). To our knowledge, the clinicopathologic features of the enteropathy associated with MEDNIK syndrome have not been fully explored. We report the case of an 11-day-old full term infant with MEDNIK syndrome.

Methods: Using standard methods, histopathologic examination of the gastrointestinal tract was performed, with an emphasis on the duodenum. PAS histochemical staining was performed. CD10 (Novocastra) and MOC31 (Agilent Dako) immunohistochemical stains were performed. Ultrastructural examination using electron microscopy was also performed. Finally, trio exome sequencing was performed on blood.

Results: Histologic sections of tissue from the duodenum demonstrated mild villous blunting and patchy enterocytes with prominent intracytoplasmic vacuoles. There were no epithelial tufts. Sections of the rectum showed similar findings. On both the duodenum and rectum, CD10 immunostaining highlighted a disrupted brush border and scattered enterocyte intracytoplasmic inclusions. MOC31 showed no abnormalities. PAS staining highlighted intracytoplasmic vacuoles. Electron microscopy of tissue from the duodenum showed enterocytes with shortened and disrupted apical microvilli. There were no microvillous inclusions. Mitochondria were morphologically normal with no inclusions or abnormalities of the cristae. Tight junctions and desmosomes of the lateral cell walls were normal in structure and not increased in number. There were no atypical infiltrates or abnormal cytoplasmic contents.

Conclusion: We describe the clinicopathologic features of the gastrointestinal tract in an infant with MEDNIK syndrome. While there is some histopathologic overlap with microvillous inclusion disease, the ultrastructural features and gene alterations are distinctive. More reports describing these features are needed to fully characterize the clinical course, histopathologic changes and efficacy of treatment regimens.

46

A Challenging Case of Unusual Presentation of "Cecal Mass" in a Morbidly Obese Adolescent Girl

S Garg, B Kittredge, J Bae; Phoenix Children's Hospital, Phoenix, Arizona

Background: Diverticulosis with fecalith has conventionally been noted in adulthood and most cases are identified pre-operatively or during surgery; we report a case of large submucosal cecal fecalith (6.3 x 4.5 x 3.6 cm) in a morbidly obese adolescent girl. This mass had clinical and radiological impression of a malignant neoplasm but the hemicolectomy specimen on pathology exam was correctly interpreted as, "Ruptured diverticulitis with fecalith".

Methods: Patient had a broad clinical, serological, and radiological work-up. Fine needle aspirate of the cecal mass, U/S guided fine needle biopsy and ultimately right hemicolectomy were undertaken. Complete gross and histopathology exam were performed. Routine H&E staining and comprehensive immunohistochemistry panel were obtained.

Results: A previously healthy, 14-year-old girl presented with constipation and a 1-week history of severe lower abdominal pain, which was escalated during bowel movements. On physical exam, there was tenderness in the right and left lower quadrant. CBC, CMP, and UA were unremarkable without signs of infection. CT Abd/Pelvis w/ contrast showed a 6 cm well circumscribed bilobed hyperdense mass of right colon consistent with tumor, with a differential of carcinoid vs gastrointestinal stromal tumor. Given the location and size of this mass, a formal right hemicolectomy was performed, by the surgeon, to have adequate margins for potential malignancy. FNA of the mass showed "Necrotic tissue, favoring spindle cell neoplasm" and a biopsy for further characterization was recommended. Fine needle biopsy specimen revealed non-viable necrotic and calcified material. Gross examination of hemicolectomy specimen revealed a 6.3 X 4.5 x 3.6 cm yellowish brown fecalith- like mass that was impacted within a cecal diverticular outpouching. Histopathology was diagnostic for cecal diverticulitis with associated fecalith. No neoplastic process was identified. A pericolonic abscess secondary to rupture of diverticular wall was noted. Immunoprofile of mass was negative for viable tissue or neoplasm.

Conclusion: In the literature there have been occasional reports of pediatric cecal fecalith measuring up to 4 cm, with most having distinctive features on imaging studies; here we are reporting a first case in which a true cecal diverticulum with large fecalith (measuring 6.3 cm) was found in an adolescent age girl and unlike any previous case, this mass masqueraded as a malignant tumor till the time pathologic diagnosis of, "fecalith" was performed on the hemicolectomy specimen. Therefore, clinical staff, radiologists and pediatric surgeons need to keep this entity in mind in the differential diagnosis of a cecal mass. Early clarification of the etiology will enable strategic planning of the best treatment option.

47

Expanding the Molecular Genetic Landscape of Pediatric Intestinal Ganglioneuromatosis

L Samson [1], E Medina-Ceballos [2], S Witchel [2], D Vargas De Stefano [2], A Gomez [2], Q Wang [2], E Zambrano [2], C Salgado [2], M Reyes-Mugica [2]; [1] UPMC Children's Hospital of Pittsburgh, [2] UPMC Children's Hospital of Pittsburgh

Background: Intestinal ganglioneuromas are rare benign neoplasms originating from any of the bowel nerve plexus. They are formed by proliferating ganglion cells, satellite cells, and nerves. The term intestinal ganglioneuromatosis (IGNMs) refers to multiple or syndrome-associated ganglioneuromas, and it should not be confused with tumors within the “neuroblastoma-ganglioneuroma spectrum”. Typically examples of IGNMs are associated with neurofibromatosis type 1 (NF1), multiple endocrine neoplasia 2B (MEN2B), and more recently, PTEN-associated hamartomatous syndrome. Apart from those associations, there is scant literature addressing their molecular alterations.

Methods: The pathological features of IGNMs diagnosed at our institution between 2008 and 2022 were reviewed and correlated with their clinical features. Molecular analysis (Oncomine® next-generation sequencing-NGS) was performed on available material to assess for possible mutations.

Results: Eleven cases of intestinal ganglioneuromatosis were identified, nine of which had adequate material for molecular analysis. NGS showed NF1 mutations in four patients (4/9, 44%), RET mutations in three (3/9, 33%), and PTEN mutations in two (2/9, 22%). One patient showed mutations in both NF1 and RET genes. SETD2 and ARID1A mutations were seen in two patients, one of them showing an additional PTEN mutation, as previously mentioned. ARID1A and SETD2 mutations represent novel alterations, not previously described in intestinal ganglioneuromatosis.

Conclusion: Eleven cases of pediatric intestinal ganglioneuromatosis and their molecular genetic alterations are presented. Mutations in NF1 and RET genes were the most common. Two cases showed PTEN mutations, and two additional cases showed mutations in SETD2 and ARID1A genes. These findings highlight the importance of timely diagnosis of intestinal ganglioneuromatosis as a feature of multiple neoplasia-predisposing syndromes such as NF1, MEN2B, and PTEN-associated hamartomatous syndrome. Our observations expand the molecular landscape of intestinal ganglioneuromatosis, adding two mutations to those previously described.

48

Coexisting Ovarian Clear cell Carcinoma and Seromucinous Borderline Tumor at a Young Age

L Samson [1], E Elishaev [2], D Vargas De Stefano [3], C Salgado [3], A Gomez [3], E Zambrano [3], M Reyes-Mugica [3], Q Wang [3]; [1] UPMC Children's Hospital of Pittsburgh, [2] UPMC Magee Women's Hospital, [3] UPMC Children's Hospital of Pittsburgh

Background: Coexisting clear cell carcinoma and seromucinous borderline tumor in the same ovary is rare.

Methods: In this study, we report the case of a 17-year-old female patient with a microscopic mural nodule of clear cell carcinoma arising in a large seromucinous borderline tumor of the ovary.

Results: The patient presented with a history of abdominal pain of two-week duration. A left-sided 13 cm cystic ovarian mass was identified radiologically, and serological analysis showed a moderately elevated CA-125. She underwent left side oophorectomy. Grossly, a unilocular cystic mass with patchy papillary excrescences involving the inner surface was seen. Microscopic examination revealed a seromucinous borderline tumor with a 2 mm solid focus of clear cell carcinoma. Both tumors demonstrated loss of PTEN and intact ARID1A expression by immunohistochemistry.

Conclusion: To the best of our knowledge, this is the first report of a coexisting clear cell carcinoma and seromucinous borderline tumor in a pediatric setting.

49

Aberrant Neural Crest Cell Migration Leads to Melanocytes in the Umbilical Cord

L Samson [1], E Medina-Ceballos [2], S Worrell [3], O Faye-Peterson [4], R Bendon [3], C Salgado [2], M Reyes-Mugica [2]; [1] UPMC Children's Hospital of Pittsburgh, [2] UPMC Children's Hospital of Pittsburgh, [3] UPMC Magee Women's Hospital, [4] UAB Hospital

Background: Systematic evaluation of the umbilical cord is an integral part of perinatal/placental examination. Among the important parameters of this exam is assessment of visible lesions such as knots and discoloration. The latter can be due to funisitis (white), meconium stain (green-brown), vascular congestion (red-blue), or maternal hyperbilirubinemia (yellow). We present four cases of umbilical cord lesions characterized by foci of brown-black discoloration caused by melanin pigment deposition, and provide evidence for a possible error in neural crest cell migration.

Methods: Placental pathology cases from our institution mentioning melanocytes or melanin pigment were reviewed, and the histological slides pulled for analysis. Immunohistochemistry for SOX10, and histochemical staining for melanin (Fontana-Masson) were performed retrospectively on the umbilical cord sections.

Results: Four cases of umbilical cord with grossly visible brown-black punctate discoloration were reviewed. Microscopic examination showed increased melanin pigment deposition in the cellular amnion layer, along with scattered SOX10 positive melanocytes. There was no history of melanocytic lesions in either mothers or fetuses/neonates. No malformations associated to neural crest anomalies were documented.

Conclusion: Four cases of grossly visible pigmented lesions of the umbilical cord owing to melanin deposition associated to amniotic melanocytes are presented. Since there is no documented presence of neural crest cells (NCCs) migrating through the umbilical cord, an aberrant migration of neural crest cells, with subsequent differentiation into melanocytes is the most likely etiological hypothesis. To the best of our knowledge, this is the first documentation of melanocytes and melanin pigment in the umbilical cord. Specific details about the abnormal migration and differentiation of these NCCs deserve additional study to further determined the possible mechanisms and consequences of this exceptional observation.

50

Fetal Sex-Dependent Risk of Developmental Delay in Twins Diagnosed with Chorangiosis
P Tran T Morgan; ohsu

Background: Chorangiosis is a histologic diagnosis describing a relative increase in chorionic villous angiogenesis. If it is defined as “diffuse” (multifocal in multiple sections), it is diagnosed in approximately 5-10% of singleton placentas submitted to pathology at our institution. We have previously reported a potential association between chorangiosis and an increased risk for developmental delay (DD) in singleton males, but not females. This fetal sex-effect may be related to an increased fetal:placental ratio in males. Therefore, one would suspect that chorangiosis may be more common in monochorionic twins compared with dichorionic twins versus singletons and developmental delay may be more common in monochorionic twin males.

Methods: Retrospective clinicopathologic study of all twin placentas received by pathology at our institution from 2015 and 2020. Medical records were reviewed for maternal age, gravida, absence of complications other than preterm birth, gestational age, placental weight, twin zygosity, fetal sex, birth weight, and pediatrician documented developmental milestones. 207 twin deliveries met inclusion criteria. Of these, 66/207 twin placentas (32%) had a documented diagnosis of chorangiosis by an experienced placental pathologist (tkm). Diagnoses required involvement of at least 10 contiguous villi in at least ten 10x objective fields in at least two separate placental sections. A diagnosis of developmental delay within five years of delivery was documented in 105 of the twin pairs [177/414 individuals (43%)]. ANOVA and odds ratios were used to test for an association between fetal sex and developmental delay with a p-value < 0.05 considered significant.

Results: Twins were born prematurely (32-36 weeks, mean 33 +/- 0.8) and there was no difference in gestational age between fetal sex groups. Maternal age, gravida, and fetal:placental weight ratios were also similar between groups with the exception of female monozygous twins who had a lower birthweight ($P< 0.01$). Female, but not male, twins revealed a relationship between chorangiosis and risk for DD [table]. [insert Table pdf]

Conclusion: Twins are often born premature (< 38 weeks’), which in part may account for their known increased prevalence of developmental delay compared with singletons. Unlike singleton males with chorangiosis, this twin study suggests males with chorangiosis may not be at an increased risk for developmental delay. Surprisingly, females with chorangiosis had an increased risk in dichorionic twins and reduced risk in monochorionic twins (only group with reduced birth weight compared with the other three groups).

Zygosity	Fetal Sex	Yes Chorangiosis Positive for DD	Yes Chorangiosis Negative for DD	No Chorangiosis Positive for DD	No Chorangiosis Negative for DD	Risk of DD +/- Chorangiosis OR [95% CI]; p-value
Di-chorionic	Female N=139	22/139 (16%)	20 (14%)	30 (22%)	67 (48%)	2.5 [1.7-5.2]; P=0.01
	Male N=135	17/135 (13%)	26(19%)	34(25%)	58 (43%)	1.1 [0.5-2.3]; P=0.46
Mono-chorionic	Female N=78	14/78 (18%)	18 (23%)	32 (41%)	14 (18%)	0.34 [0.13-0.87]; P=0.02
	Male N=62	8/62 (13%)	6 (10%)	20 (32%)	28 (45%)	1.87 [0.56-6.20]; P=0.24

51

Impact of Low or High Sodium Maternal Diet on Transgenic Mouse Model of Fetal Growth Restriction

P Kutson T Morgan; ohsu

Background: The objective of this study was to approximate the impact of high salt versus low salt diet on pregnancy using a genetic mouse model simulating African women compared with Northern European women. We employed a published angiotensinogen (AGT) gene-titration transgenic (TG) mouse construct with 2- versus 3-copies of the murine AGT gene. This model mimics the common human A(-6) AGT promoter variant associated with fetal growth restriction (FGR). Notably, the A(-6) variant similar to the 3-copy AGT mouse is the original primate form of the gene mutated into G(-6) [2-copy model] in Northern Europeans. We hypothesized that 3-copy mice would be infertile when fed a high salt diet; whereas, FGR may be rescued by maternal low salt diet [similar to original African diet].

Methods: Transgenic (AGTdup) dams were generated de novo for each breeding experiment against WT males to compare with their 2-copy (WT) female siblings. Adult females were trained on low, normal, high salt diets per published criteria and then mated with WT males. Pregnancy outcomes included the number of viable litters, litter size, birth weights, newborn growth and long-term survival.

Results: Progeny from WT dams on a normal sodium diet served as the reference with 8/8 litters delivering on average 8 pups with a birth weight of 1.42+/-0.04 grams. As reported previously, TG dams on normal sodium diet yielded FGR pups 1.26+/-0.02. WT dams on a low salt diet had FGR (1.25+/-0.05), but normal birth weights on high salt diets. TG dams on a low salt diet yielded 1/8 litters (2 pups with FGR), while HS diet in TG dams failed to yield viable progeny. Interestingly, the progeny from HS WT dams lived up to 2 years and died of renal failure with significant glomerular sclerosis.

Conclusion: Both murine AGT genotypes did not tolerate low salt diets, but 2-copy (WT) mice had viable litters. High salt diet was tolerated by WT mice, but there may be long-term renal programming affects leading to eventual renal failure.

52

Latent Class Analysis Identifies 5 Distinct Patterns of Placental Pathology in Preeclampsia

L Ernst [1], A Freedman [2], G Miller [3], S Suresh [1]; [1] NorthShore University HealthSystem, [2] NorthShore University HealtSystem, [3] Northwestern University

Background: The purpose of our analysis was to use latent class analysis (LCA) to identify subtypes of preeclampsia based on placental pathology.

Methods: We obtained electronic medical records for all singleton livebirths between January 2009 and March 2018 at a single institution. Pregnancy and birth outcomes were abstracted and preeclampsia was identified based on ICD codes and diagnosis fields. Presence of individual placental lesions were abstracted from the placental pathology report. Individual lesions encompassed four major categories: acute inflammation (AI), chronic inflammation (CI), fetal vascular malperfusion (FVM) and maternal vascular malperfusion (MVM). Latent class analysis was used to investigate subtypes of preeclampsia based on individual placental lesions. Placental lesions were included in the LCA model if they were present in >1% of placentas in the sample. LCA models with 2-6 classes were considered and the optimal model was identified based on model fit statistics and class interpretability. Clinical outcomes were compared across classes.

Results: Of the 109,773 singleton live births during the study period, 1,373 (1.1%) had a documented diagnosis of preeclampsia, 728 of which (53%) also had a complete placental pathology report. In the LCA, 23 binary placental lesions were included. The 5-class model was selected based on fit and interpretability. Class 1, the most common class (26.0%), was characterized by high prevalence of villous and vascular MVM lesions (Table 1). Class 2 was characterized by lesions consistent with CI and FVM and was present in 9.4% of the sample. Like Class 1, Class 3 (23.0%) was also characterized by MVM lesions, particularly villous lesions of increased syncytial knots and distal villous hypoplasia with lower prevalence of vascular lesions than Class 1. Class 4 (19.2%) was characterized by both maternal and fetal AI lesions. Class 5 (22.4%) did not have any unifying placental characteristics, though delayed villous maturation and chorangiosis were most common in this class (7.3% and 5.9%, respectively). Preterm birth varied across the classes ($p< 0.01$), with the highest prevalence of preterm birth observed among the classes characterized by MVM (Class 1: 87.6%; Class 3: 63.0%) and the lowest prevalence among the class characterized by AI (Class 4: 23.5%). Small for gestational age infant also varied by class ($p=0.03$), with the highest prevalence observed in Class 1 (23.8%; high grade MVM) and Class 2 (23.3%; CI and FVM) and the lowest prevalence in Class 5 (11.5%; other).

Conclusion: We identified 5 classes of placental pathology in preeclampsia. The latent classes were largely grouped by the defined patterns of placental injury, with 2 classes characterized by MVM, 1 by CI and FVM, 1 by AI, and 1 without unifying placental characteristics.

Table 1. Prevalence of placental pathology by latent class (n=728). Darker shading corresponds to increased prevalence.

	Class 1	Class 2	Class 3	Class 4	Class 5
Class name	High grade MVM	CI and FVM	Low grade MVM	AI	Other
Prevalence	26.0%	9.4%	23.0%	19.2%	22.4%
Acute inflammation (AI)					
Maternal	22.9%	32.7%	15.6%	100.0%	19.3%
Fetal	11.3%	26.1%	7.5%	100.0%	10.7%
Chronic inflammation (CI)					
Chronic villitis	13.6%	100.0%	8.5%	23.9%	11.7%
Chronic deciduitis	29.3%	68.8%	11.5%	15.5%	16.3%
Chronic chorionitis	5.5%	42.7%	1.9%	2.0%	3.3%
Fetal vascular malperfusion (FVM)					
Any thrombus	16.3%	23.6%	12.5%	12.0%	7.6%
Avascular villi/villous stromal-vascular karyorrhexis	31.1%	76.5%	21.4%	27.8%	16.1%
Any umbilical cord abnormality	31.4%	40.5%	36.8%	29.4%	29.5%
Maternal vascular malperfusion (MVM)					
Fibrinoid necrosis/acute atherosis	55.7%	7.9%	4.4%	4.1%	6.9%
Muscularized basal plate arterioles	51.3%	25.4%	9.5%	14.4%	7.7%
Mural hypertrophy of membrane arterioles	41.5%	10.1%	6.4%	4.6%	8.9%
Basal decidual vascular thrombus	16.8%	0.0%	0.2%	2.1%	2.4%
Infarct, single	36.8%	15.2%	19.7%	24.6%	16.4%
Infarct, multiple	35.9%	13.5%	5.6%	8.0%	6.2%
Increased syncytial knots	100.0%	36.6%	99.0%	41.0%	0.0%
Villous agglutination	36.3%	6.2%	12.4%	10.5%	4.8%
Perivillous fibrin deposition	33.3%	20.7%	12.9%	16.3%	5.8%
Distal villous hypoplasia	94.8%	20.7%	61.3%	16.6%	0.0%
Retroplacental blood/hematoma	16.8%	0.0%	2.2%	2.6%	1.8%
Small for gestational age placenta	57.6%	44.1%	32.5%	25.2%	17.3%
Other significant pathology					
Delayed villous maturation	0.6%	0.0%	0.6%	0.0%	7.3%
Chorangiosis	3.0%	1.2%	2.0%	3.3%	5.9%

53

Quality Improvement in the Placental Pathology Process: An Interdisciplinary Approach

K Machina [1], P Kling [2], M Fritsch [2], C Bockoven [2]; [1] Univeristy of Wisconsin Madison, [2] University of Wisconsin Madison

Background: The placenta functions to provide fetal nutrients, adapt its nutrient supply to match extraction, and mount key inflammatory responses. Placental pathology exams can offer insights and explain long- and short-term adverse events for both birther and fetus. The combination of recent indication developments (i.e. COVID-19) and varying education around pathology reports is resulting in increased pathology workload, result turnaround times, and timing of family consults. For placental pathology to guide clinical decision-making, order indications must be informative to decrease pathologist workloads reviewing electronic record, and timely reports must be returned. The objective of the study is to identify gaps in the workflow of placental pathology processing to facilitate informative orders, improve interdepartmental communication, and educate for better clinical counseling.

Methods: Quality improvement (QI) fishbone diagrams outlined problems and solutions for timely pathology report turnarounds. 3 mixed-methods surveys were sent to UW pathology and general obstetrics (Ob) residents, maternal-fetal medicine (MFM) and neonatal intensive care (NICU) fellows, and attending Ob and MFM providers to identify knowledge gaps, preferred educational tools, and free text thoughts about interdepartmental communication around placental pathology. Rates were compared by Chi2, Likert scale data were compared by Mann-Whitney.

Results: Survey response rates from pathology trainees, combined Ob, MFM, and NICU trainees, and the Ob attendings were 23.8%, 27.2%, and 50%, respectively. Sufficiency of placental education for Ob and MFM trainees and attendings was rated 1.95/10 (n=21) and 5.5/10 (n=8), respectively. Delivery attending Ob/MFM providers rated their confidence family counseling as 4.86/10 (n=14), with MFM providers' expressed rating higher (7/10, n=5) than Ob (3.67/10, n=9). Overall, interdepartmental communication surrounding placentas was rated an average of 1.9/10 (n=30). 4 Ob residents reported receiving no training on the topic. 3 Ob providers expressed that reports often provided no clinically relevant data.

Conclusion: Utilizing survey responses, 4 interventions were chosen to improve education and communication, including the use of a ".placentalpath" SmartPhrase, a teaching tool, updated indication guidelines, and regular joint interdisciplinary perinatal case conferences on relevant topics. Future directions include implementing, following, and assessing the effectiveness of these instruments.

55

Single Umbilical Artery Umbilical Cord Is Associated with High-Grade Distal Fetal Vascular Malperfusion

J Stanek; Cincinnati Children's Hospital

Background: Umbilical cord abnormalities, particularly hypercoiled umbilical cord, and particularly those associated with clinical signs of cord compromise are associated with lesions of fetal vascular malperfusion (FVM). Single umbilical artery (SUA) was reported to be associated with adverse pregnancy outcome, fetal genetic and nongenetic anomalies, other umbilical cord abnormalities, and with high grade FVM in fetal growth restriction, but not in unselected placental population which is the objective of this retrospective analysis.

Methods: Clinical and placental phenotypes of 55 consecutive placentas with SUA (Group 1) were statistically compared to 655 placentas with 3-vessel umbilical cord (Group 2) from 2nd half of pregnancy (analysis of variance or chi-square where appropriate). Placentas were examined according to the Amsterdam criteria expanded by the separately described lesions and patterns, with use of CD 34 immunostaining and clustered villous mineralization.

Results: Average gestational age was same in both groups, assuring comparability thereof, but Group 2 was by no means a “Control Group” as although fetal congenital anomalies were more common in Group 1, they were also very common in Group 2 42 (76%) and 409 (61.5%) (difference statistically not significant), which reflects the population of cases treated in the Children’s Hospital.(insert image). Premature rupture of membranes, neonatal deaths, abnormal 3rd stage of labor, variable decelerations (Fig. A), thin umbilical cord (Fig. B), edematous umbilical cord (Fig. C), velamentous cord insertion (Fig. D), and high grade distal FVM based on H&E examination (stromal vascular karyorrhexis, avascular villi) and/or endothelial fragmentation by CD34 and/or villous mineralization were statistically significantly more common in Group 1, while preeclampsia, hypercoiled cord and decidual clusters of multinucleate trophoblasts were more common in Group 2. Notably, when H&E and CD34 immunostaining were evaluated separately, high grade distal FVM was also more common in Group 1 than in Group 2, but without statistical significance. There were no statistically significant differences in low grade distal FVM or large vessel FVM or its components (fetal vascular ectasia, stem vessel obliteration, vascular thrombi, or intramural fibrin deposition).

Conclusion: SUA is a specific cord anomaly predisposing to high-grade distal villous FVM, remote, advanced, and recent, but only if hematoxylin & eosin, CD34 immunostain and villous mineralization are analyzed together. Pathogenesis of FVM associated with SUA is at least in part different than that of stasis induced FVM, likely related to fetal anomalies associated with SUA. SUA is not associated with large vessel/proximal/global FVM, features of fetal hypoxia, shallow placental implantation or maternal vascular malperfusion.

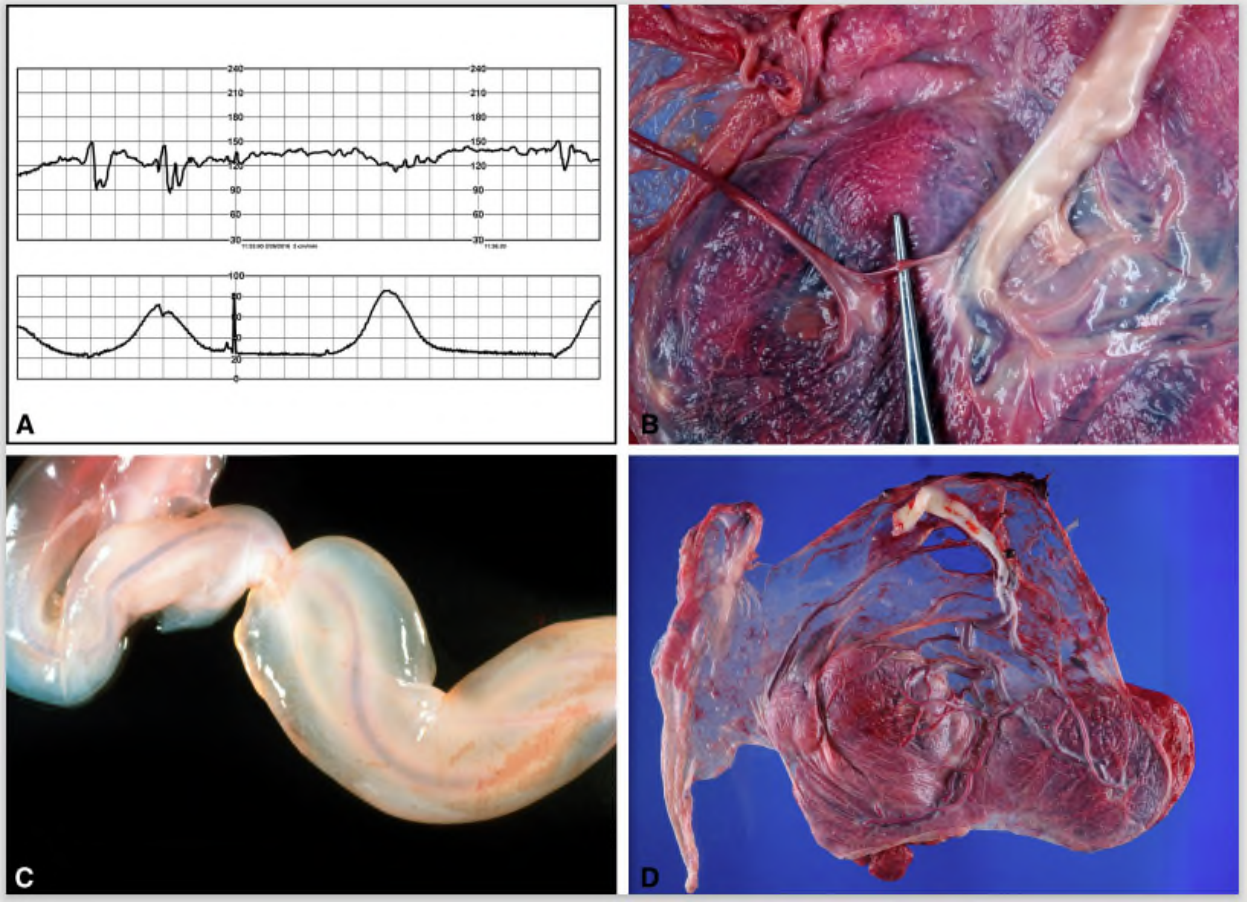
A
B
C
D

56

Patterns of Placental Injury in Various Types of Fetal Congenital Heart Disease
J Stanek; Cincinnati Children's Hospital

Background: Fetal blood circulation may be modified in congenital heart disease (CHD) which could differ in placental blood supply in pregnancy. This retrospective statistical study has been designed to analyze placental morphology in various types of CHD with various patterns fetal blood circulation and various placental blood brain and placental blood supply.

Methods: 184 placentas from deliveries in the 2nd half of pregnancy from years 2006-2022, complicated by CHD, were analyzed. If an autopsy was performed, the final diagnosis of CHD and its type was established by autopsy. In the remailing cases, the diagnosis was established by a combination of antepartum and neonatal diagnostics. 3 types of CHD based on presumed proportion of placental (rich in oxygen and nutrients) and systemic blood distribution in fetal circulation were analyzed: Group 1:89 cases with low placental blood content (hypoplastic left heart syndrome, transposition of great arteries, coarctation of aorta), Group 2: 71 placentas with intermediate placental and systemic blood content due to increased intracardiac blood mixing (tetralogy of Fallot, septal defects, truncus arteriosus, double inlet/outlet ventricle), and Group 3: 24 placentas with high placental blood content (tricuspid or pulmonary atresia, Ebstein anomaly). Frequencies of 27 independent clinical and 47 placental phenotypes among those 3 groups were statistically compared (analysis of variance, chi-square).

Results: Macerated stillbirths, neonatal mortality, abnormal amniotic fluid volume (oligohydramnios or polyhydramnios), other (non cardiac) congenital anomalies, distal lesions of fetal vascular malperfusion (FVM) (fig.A), placental edema and amnion nodosum were most common in Groups 2 and 3. The most advanced gestational age at delivery, and large vessel (global) FVM (fetal vascular ectasia (Fig. B), stem vessel obliteration (Fig. C), and intramural fibrin deposition (Fig. D)) were most common in Group 1, although the placental findings were not statistically significant after Bonferroni correction), (insert image)

Conclusion: Although placental histological lesions in CHD are regarded nonspecific and less frequent than in other major types of high-risk pregnancy, in this material, CHD with intracardiac increased blood mixing or with right heart defects is associated with average preterm gestational age at delivery and placental lesions of distal villous FVM (Fig. A), villous edema and amnion nodosum. The left heart obstructive lesions, potentially likely to be associated with brain maldevelopment, showed statistically not significant increase in lesions of global FVM in aggregate and individually: fetal vascular ectasia (Fig. B), stem vessel obliteration (Fig. C), and intramural fibrin deposition (Fig. D), such as are otherwise typically seen in umbilical cord compromise, particularly in term pregnancy.

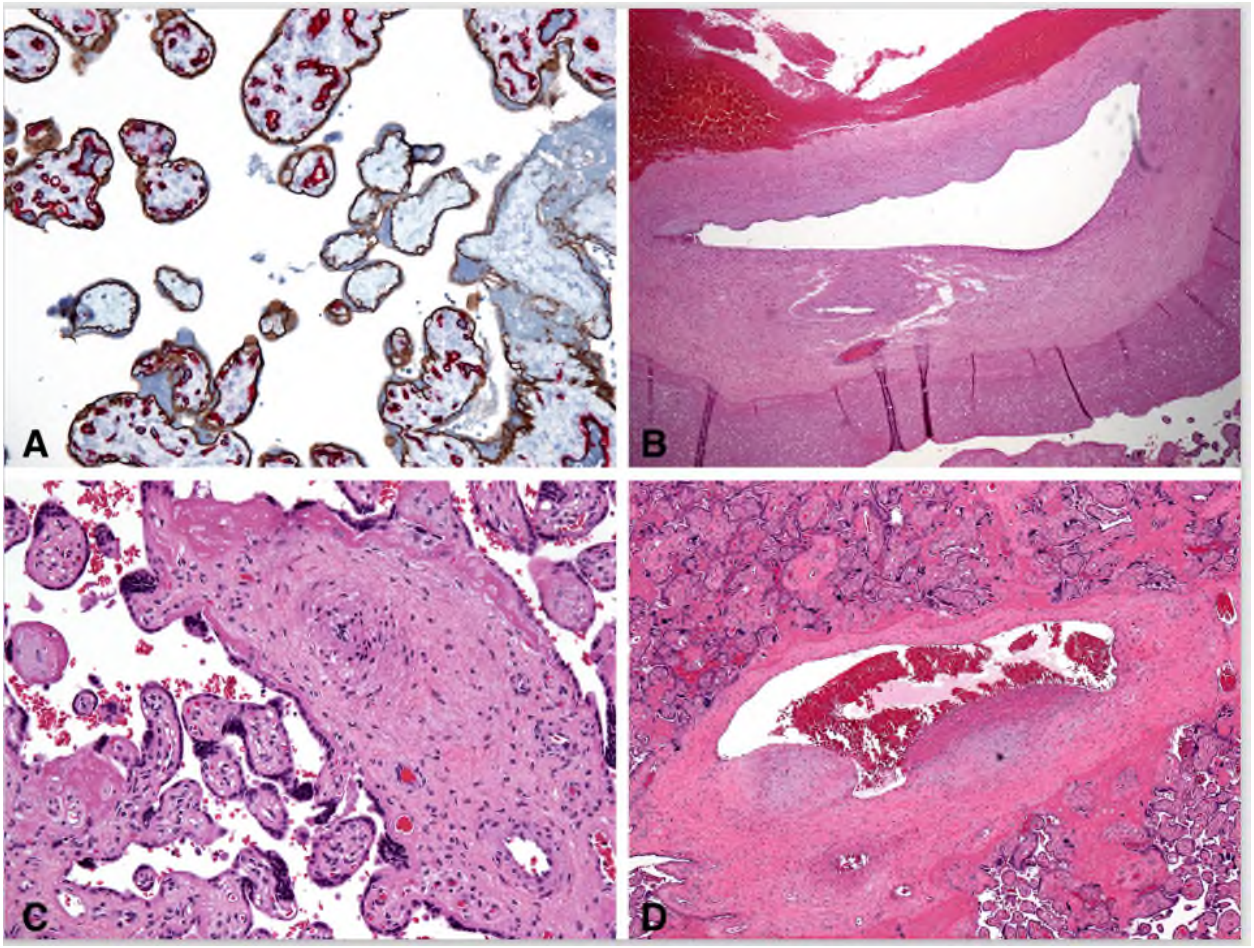
A
B
C
D

57

A Case of Infant Mortality from Pneumonia Secondary to 8p Inversion Duplication Deletion Syndrome

E McLeod [1], A Saunders [2], A Jones [3], W Wendy [4]; [1] Walter Reed National Military Medical Center, [2] Howard University College of Medicine, [3] Madigan Army Medical Center, [4] Armed Forces medical Examiner System

Background: 8p inversion duplication deletion syndrome (8p invdupdel) is an uncommon chromosomal anomaly that is seen in approximately 1/20,000 births. It is thought to be caused by abnormal pairing of chromosomes during meiosis I, leading to unequal crossover. Manifestations include hypotonia, facial abnormalities, agenesis of the corpus colosseum, and intellectual and developmental delays. We present a case of a 3-month-old female born at 28+1 weeks gestation via cesarean section after early delivery due to HELLP syndrome. The pregnancy was complicated by intrauterine growth restriction and agenesis of the corpus collosum diagnosed on ultrasound, prompting amniocentesis, and revealing the diagnosis of 8p invdupdel. At birth, the patient was transferred to the NICU due to patent ductus arteriosus (PDA), bronchopulmonary dysplasia, and central hypoventilation. A PDA coil was placed successfully at about 11 weeks of age. The patient was stable before deteriorating 10 days later. She developed pulmonary hypertension, likely caused by pneumonia. She ultimately died due to suspected aspiration and ventilator associated pneumonia. PCR revealed the infection was caused by Pseudomonas and Klebsiella.

Methods: At the request of the family, hospital autopsy and medical records review were performed via standardized pediatric autopsy procedures.

Results: At autopsy, findings consistent with 8p invdupdel were noted. Her ears were low set, below the palpebral fissure, and the nasal bridge was broad with anteverted nares. Her forehead was prominent, and her neck was shorter than average. There was congenital absence of the gallbladder and complete agenesis of the corpus callosum. Evaluation of the cardiovascular system revealed the coiling device in place, a patent foramen ovale, and a single ventricular septal defect. Both lungs were diffusely consolidated with copious, purulent fluid in the right mainstem bronchus, consistent with the diagnosis of pneumonia. The right upper lobe was also found to have multiple intraparenchymal nodules and pleural plaques. On microscopic examination, mixed inflammation, bronchial and vessel destruction, necrosis, and copious bacilli organisms were present. All other organ systems were unremarkable.

Conclusion: While 8p invdupdel is not a fatal disease, certain features likely contributed to disease progression in this patient. Hypotonia increases susceptibility to developing pneumonia as muscle hypotonia can lead to hypoventilation and atelectasis, as well as impaired swallowing and subsequent aspiration. A case study was published in 2022 of an infant with Prader Willi Syndrome that died from infection after aspiration of tube feedings secondary to hypotonia from his condition. Ultimately, the combination of prematurity, chromosomal anomaly, and

complications of medical therapy related to this all contributed to the patient's demise.

58

A Case of a Placental Nodular Fasciitis-Like Lesion of Maternal Origin

M Covinsky [1], K Eldin [2], S Zhang [1]; [1] McGovern Medical School University of Texas Health Science Center at Houston, [2] Salem Hospital

Background: Nodular Fasciitis is a self limited mesenchymal neoplasm usually seen in soft tissue. It is most commonly contains a USP6 gene rearrangement. There have been two previously reported cases of nodular fasciitis of the placenta. We report a case of a nodule arising in the maternal surface of the free membranes of one of a pair of monochorionic diamnionic male twins. It was comprised of a bland loose myxoid spindle cell proliferation with delicate vasculature and scattered inflammatory cells.

Methods: Immunohistochemical stains for Ki-67, cyclin D1, estrogen receptor (ER), progesterone receptor (PR), Alk-1, smooth muscle actin (SMA), desmin, caldesmon, pan-keratin, CD10, CD34, S100, and beta-catenin were performed in our laboratory. Unstained slides and one H&E slide were sent to Mayo Clinic Laboratories for USP6 and X and Y centromere FISH testing.

Results: Immunohistochemical stains demonstrated a low Ki-67 prolferation index (less than 10%), diffuse cyclin D1 nuclear staining and PR nuclear staining. ALk-1, SMA, Desmin, Caldesmon, Pan-keratin, CD10, CD34, and estrogen receptor were negative in tumor cells. S100 demonstrated rare cytoplasmic reactivity. Beta-catenin demonstrated cytoplasmic staining only. FISH studies demonstrated no rearrangement of the USP6 gene. FISH testing for X and Y chromosomes indicated that all the spindled cells were XX consistent with maternal origin. The chorionic villi located on the same slide demonstrated an XY pattern.

Conclusion: The overall findings are most consistent with a non-USP6 rearranged nodular fasciitis. These results indicated that tumors associated with the placenta can be of maternal origin.

59

Investigation of the Current Algorithm for Evaluating Ciliary Biopsy Specimens: An Institutional Review

A Breaux [1], L Berklite [2], S Ranganathan [2]; [1] Cincinnati Children's Hospital Medical Center, Cincinnati, OH, USA, [2] Cincinnati Children's Hospital Medical Center

Background: Primary ciliary dyskinesia (PCD) is a rare, recessive, genetically heterogeneous defect of motile cilia with lifelong complications for those afflicted with this disorder. Consequent pathologies include chronic sinusitis, bronchiectasis, situs inversus, and fertility issues. Available testing modalities to screen and evaluate patients with a high-suspicion clinical phenotype include motility studies and electron microscopy (EM), yet challenges in diagnosing PCD still exist. At our institution, we utilize a clinical screening form to help triage cases and determine which of those should go on from motility testing to EM examination. This form has been in use since 2008, without further review or revision. We sought to examine cases from a two-year period to evaluate the utility of this form in triaging high risk patients and identify ways to optimize our algorithm for evaluating cases of suspected PCD in our patient population.

Methods: We reviewed the results of the triage form, motility report, and ultrastructure report from cases obtained in 2018 and 2019. The high speed videomicroscopy (motility) and ultrastructure (EM) with normal, abnormal, and insufficient results were reviewed to determine the distribution of results. The number of cases with high and low suspicion for PCD based on the clinical screening form and those with EM requested regardless of motility result were also recorded, as was the number of cases that also had genetic testing performed.

Results: 138 total cases were reviewed. The total number of motilities performed was 135, the total number of EMs performed was 108. There were 75 normal motility studies and 49 abnormal studies. 11 motility studies were insufficient for evaluation. The total number of EMs performed was 108 with 67 normal EMs, 4 abnormal EMs, and 37 insufficient EMs. 72 cases were noted as "low suspicion" on the screening form. 51 were noted as "high suspicion". 13 cases did not have EM studies requested if motility was normal. 114 cases requested EM regardless of motility results. 20/51 of the cases designated "high suspicion" had abnormal motility results. Only 1 case designated "high suspicion" on the form had abnormal EM results, and this case had normal motility results. 37 cases also had genetic testing performed. 20 cases had abnormal genetic results and 7/20 of those had abnormal motility results. 2/20 had abnormal EM results.

Conclusion: The results suggest further investigation into our screening and case triage method is necessary. Most cases had EM requested despite normal motility results. Additionally, EM requests were made regardless of clinical suspicion and only 4 total cases had abnormal EM results. We believe improved triaging of these cases could help reduce unnecessary costs and help better identify patients who are high risk. Consideration of incorporating genetic results in

our form might also be helpful.

60

Pediatric inpatient genetic stewardship

R Craver; LSU Departments of Pathology and Pediatrics

Background: Sendout genetic test costs on inpatients are billed to the hospital. Turnaround times for results are several weeks, often extending past the inpatient hospitalization. We instituted a concurrent review of all sendout genetic test requests on pediatric hospitalized patients. In consultation with the ordering physician, we assessed if the patient would be hospitalized when the results would be available, and if those results could alter therapy. In the absence of extenuating circumstances, outpatient testing was encouraged. If testing was still required, we identified alternative less expensive laboratories performing comparable tests, and if sponsored tests were available. We determined the subsequent cost savings, the percentage of diagnostic tests, identified only disease carriers, had only VUSs, and were negative. We assessed the change of ordering practices based on this program.

Methods: Over a period of 18 months (June 2021 through November 2022), we kept a concurrent record of genetic test requests and their disposition- deferred, sent to the original laboratory, sent to a less expensive laboratory, and if sponsored tests were identified by the review. Original laboratory costs and cost savings (if any) were tabulated. Retrospectively, the percentage of tests 1) diagnostic of a disease, 2) indicative of a carrier status only, 3) containing only VUSs, and 4) determined as no variants identified (negative) were determined. Data divided into 1st and 2nd 9-month periods were compared.

Results: Totals are given, followed by the 1st and 2nd periods. There were 121 test requests (68,53). Tests were deferred in 25(20.7%) (18, 26.5%, 7, 13.2%) for a savings of $29,467.50 ($20,875.50, $8592.50). Alternate laboratories were identified for 8 (6,2) for a saving of $10,711.40 ($4741.40, $5970.00). There were 37 (18, 19) sponsored tests, 16(13,3) identified by review, for a savings of $12,750 ($10,500, $2250). Total savings was $52,928.90 ($36,116.40, $16,812.50). The total cost before review would have been $125,090.50 ($75,398.00, $49,692.50), the savings represented 42.3% (47.9%, 38.3%). Of the 96 tests sent, 18 (18.8%) identified an explanatory genetic abnormality, 1 (1%) had a combined pathogenic and VUS of the same gene, 12 (12.5%) identified non-diagnostic carrier status, 34 (35.4%) had VUSs only, 23 (24.0%) were negative, 3(3.1%) failed, and 5 (5.2%) had no results.

Conclusion: ~ 40% of the sendout genetic testing costs were reduced with prior test review. Familiarity with the review reduced the requests for genetic tests on inpatients which were ultimately deferred for outpatient testing. Alternative laboratories and sponsored tests contributed to cost savings. Efficiency of diagnostic inpatient genetic testing was ~ 20%.

61

Successful Validation of a Dual-Modality (Live and Scan View) Telepathology System for Remote Frozen and Rush Diagnosis in a Multidisciplinary Pediatric Practice.

P Rungsiprakarn [1], A Edwards [2], C Neel [2], K Spencer [2], M Rigney [3], M Santi [2], A Viaene [2], M Paessler [2], E Margolskee [2], M Queenan [2], L Finn [2], P Kreiger [2]; [1] Children's Hospital of Philadelphia, [2] Children's Hospital of Phila, [3] Children's Hospital of Philadelphia

Background: Telepathology systems enable remote rapid pathologic diagnosis using remote control of glass slides under a specialized light microscope (live-view), rapid whole slide imaging of glass slides with review of scanned images (scan-view), or both. Telepathology systems must be validated to ensure equivalency to standard light microscopy (SLM) before use in clinical practice. This study sought to validate a telepathology system for both remote live-view and scan-view intraoperative and rush diagnosis within a multidisciplinary pediatric practice.

Methods: Cases were identified retrospectively to include intraoperative consultations, rush histology and cytology, routine cases of similar type to rush cases, and cases reported in the literature as challenging using telepathology. Separate study sets were compiled for neuropathology, hematopathology, and pediatric pathology to represent specimens typical of each service. Each study set included rush histology (n=60) and rush cytology (n=20), a subset with immunohistochemistry (IHC, n=20) or special stains (SS, n=20), as well as intraoperative consultations (n=20) with frozen sections (FS) and touch preps (TP). Live-view and scan-view interpretations using the Motic Easy Scan Pro were each compared to SLM with minimum 2 weeks washout between reads for each participating pathologist (n=6). Compared diagnoses were categorized into two groups: agreement/acceptable variance versus unacceptable variance/unsatisfactory. Average intraobserver diagnostic agreement between methods (live-view vs SLM; scan-view vs SLM) for each case type was quantified by Cohen's kappa.

Results: Almost perfect or substantial intraobserver agreement was seen between diagnoses using live-view and SLM for rush histology (k=0.96), FS/TP (k=0.96), IHC (k=0.98), SS (k=0.82), and rush cytology (k=0.8) and between scan-view and SLM for rush histology (k=0.94), FS/TP (k=0.93), SS (k=0.85), and IHC (k=0.8). However, only moderate agreement was seen for cytology diagnoses (k=0.52) rendered using scan-view vs. SLM. This was largely due to the inability of the instrument to auto-focus on cytology slides with low cellularity, mostly neuro- and heme-path cases (k=0.2); cellular pediatric pathology cytology slides showed substantial intraobserver agreement (k=0.83).

Conclusion: This validation study shows that telepathology can be used clinically in a multidisciplinary pediatric practice for either live-view of glass slides or scan-view of whole slide images to render remote rapid frozen section or rush diagnoses with the only limitation being scans of low cellularity cytology slides.

62

Utility of Fresh versus Frozen Tissue in a New High Resolution Microarray Platform

P Katzman M Iqbal, M Maali, J Santiago; University of Rochester Medical Center

Background: The Microarray Laboratory in our institution replaced the O44K microarray comparative genomic hybridization (MaCGH) Agilent platform (4 x 44K, lower resolution platform, LRP) with the Agilent 4 x 180K CGH +SNP MaCGH higher resolution platform (HRP) for clinical genetic testing due to poor resolution, limited utilization, and need to batch the LRP. While the LRP provided only copy number gain or loss information, the HRP gives information on both copy number gain or loss and uniparental disomy. FFPE specimens, which were used for the LRP do not yield reliable results on the HRP; therefore, only fresh tissue and cell cultures are processed using the HRP. Due to logistics in the surgical pathology gross room, the requirement for fresh tissue for the MaGCH HRP was limiting our service's ability to obtain genetic information on products of conception. Many times, fresh tissue send for karyotyping from either fetal or placental tissue yielded a "no growth" result. Both frozen tissue and tissue saved in a nucleic acid preservative, such as RNAlaterTM or DNAgard®, has been found to yield adequate genetic results (Wolfe LM, et al. Banking placental tissue: an optimized collection procedure for genome-wide analysis of nucleic acids. Placenta 2014;35:645-54).

Methods: Our lab compared MaCGH results on the HRP using paired product of conception specimens with requested or indicated cytogenetics (such in ruling out a hydatidiform mole). Equal portions of tissue (at least 1 mm2) was submitted in buffered media (RPMI and refrigerated) and snap frozen in liquid nitrogen, in addition to tissue submitted for karyotyping and for histology. The snap frozen tissue was wrapped in foil and placed in a labelled cassette before placement of liquid nitrogen. The frozen tissue was sent to the microarray lab after having been frozen for at least 1 hour. DNA was extracted from both samples of the pair per lab protocol. Briefly, DNA was labelled and MaCGH was performed on SurePrint G3 ISCA CGH+SNP Microarray Kit, 4x180K v2.0 platform (Agilent Technologies, Santa Clara, CA), featuring approximately 110,715 custom oligonucleotides + 59,647 SNPs (60 mers) and covering 1282 ISCA regions, resulting in a 25.3 Kb resolution. Patient data was scanned (Agilent Model #G2505C) at 3µm resolution and visualized (Cytogenomics Software) with log2 threshold ratios of -0.25 for losses and 0.25 for gains.

Results: 10 sample pairs were collected. Based on QA/QC metrics (using absorbance acceptability ranges of 1.8-2.0 and 1.8-2.3 for 260/280 and 260/230 ratios, respectively), 2 of 20 frozen samples failed based on QA/QC metrics and 1 of 10 RPMI samples failed DNA extraction. (DNA extraction ranged from 2940 ng to 19,700 ng.) There was concordance between frozen and refrigerated RPMI samples in the remaining 8 sample pairs, which included 5 aneuploidies, when compared to karyotyping done in 7 of the 8 cases.

Conclusion: Although fresh tissue and tissue preserved in nucleic acid preservatives yields optimal DNA extraction, frozen tissue can also be used for DNA extraction on a 180K CGH

+SNP MaCGH platform.

63

Establishing Quantitative Normal Mucosal Eosinophil Counts in Pediatric Gastrointestinal Biopsies at a Single Institution in the Southern United States

M Stark [1], R Beyl [2], K Glisson [3], C LeBlanc [3], N Zeky [3]; [1] Children's Hospital New Orleans, [2] Pennington Biomedical Research Center, [3] LSUHSC

Background: Eosinophils are commonly found in normal mucosal biopsies throughout the gastrointestinal tract; interpretation of their significance is hampered by lack of established reference ranges (RR) in the pediatric population. Aside from the well-defined histopathology of Eosinophilic Esophagitis (EoE), the remainder of the gastrointestinal (GI) tract shows considerable variability in normal ranges of eosinophil counts. Previous studies have shown RR for mucosal eosinophil counts differ by geographic distribution. This study aims to establish quantitative RR for mucosal eosinophils in discreet pediatric age ranges in distinct GI tract anatomic sites in Louisiana.

Methods: This study is a retrospective chart review of randomly selected surgical and endoscopic procedures from two selected years, 2018 and 2021, at Children's Hospital of New Orleans. Archived tissue samples were evaluated by the pediatric pathology department to determine eosinophils per 400 x high power field. Patient demographics, past medical history, medications at the time of endoscopy obtained. Counts of eosinophils/hpf performed by single pathologist, and average counts grouped by age, gender and past medical history.

Results: Our study included 378 total patients with 189 female patients (50%), with a mean age of 11.3 years at the time of the procedure (age range 0-18 years). Evaluation of tissue samples included 373 biopsies from the esophagus, 385 from the stomach, 378 from the duodenum, 92 from the ileum, 60 from the cecum, 112 from the right colon, 118 from the left colon (including transverse and descending colon), and 128 from the rectosigmoid colon. Eosinophil counts in each section of the GI tract were averaged by age including 0 to < 6 years, 6 to < 11 years, 11 to < 16 years and 16-18 years. Results from each section of the GI tract respective to these groups were as follows. Esophagus: 9.4 eos/hpf ± 25.4; 9.3 eos/hpf ± 24.4; 5.9 eos/hpf ± 17.8; 4.7 eos/hpf ± 17.1. Stomach: 11.6 eos/hpf ± 17; 12.1 eos/hpf ± 8.7; 13 eos/hpf ± 16.1; 13 eos/hpf ± 13.8. Duodenum: 22 eos/hpf ± 11.8; 28.9 eos/hpf ± 23.9; 23.6 eos/hpf ± 14.2; 24.2 eos/hpf ± 18.5. Ileum: 41.2 eos/hpf ± 16.3; 49 eos/hpf ± 23.8; 42.2 eos/hpf ± 39.3; 48 eos/hpf ± 38. Right colon: 40 eos/hpf ± 12.2; 61.2 eos/hpf ± 29.5; 60 eos/hpf ± 32.3; 50.1 eos/hpf ± 37.2. Left colon: 33.2 eos/hpf ± 15.2; 42.8 eos/hpf ± 31.8; 35.8 eos/hpf ± 22.1; 42.9 eos/hpf ± 34.3. Rectosigmoid colon: 24.3 eos/hpf ± 34.9; 26.3 eos/hpf ± 22.8; 19.8 eos/hpf ± 20.5; 16.8 eos/hpf ± 18.6.

Conclusion: This study establishes RR for mucosal eosinophil counts for our population of pediatric patients in Louisiana. Differences in eosinophil counts not only vary by location within the GI tract but also by age group and gender. The data will be further stratified to determine if medications at the time of endoscopy and underlying medical history influence the eosinophil count. The RR for mucosal eosinophil counts allow interpretation with regard to normal

background eosinophils.

64

Chromosome 4, Partial Trisomy 4p associated with multiple small, partially fused lung lobes

C Renner [1], J Gulliver [2], E Brooks [2]; [1] University of Wisconsin School of Medicine and Public Health, [2] University of Wisconsin Hospital and Clinics

Background: Chromosome 4, Trisomy 4p is a rare chromosomal disorder with a wide range of associated symptoms and physical findings dependent upon length and location of the duplication. Commonly, affected infants will have characteristic craniofacial abnormalities (microcephaly, dental irregularities, short neck, small/flat forehead, flat/depressed nasal bridge), feeding and breathing difficulties, abnormalities of the hands and feet (arachnodactyly, camptodactyly, rocker-bottom feet), reproductive abnormalities, as well as severe intellectual disabilities. We present the case of a 28-year-old female with Trisomy 4p whose medical history was otherwise significant for autism, moderate persistent asthma, obstructive sleep apnea requiring CPAP, scoliosis, reconstructive hip surgery, complete partial seizures, GERD, hypertension, and recurrent aspiration pneumonias with prior collapsed lung with extensive pulmonary hemorrhage in the setting of extracorporeal membrane oxygenation (ECMO) for aspiration pneumonia with sepsis.

Methods: Complete autopsy and microscopic examination were performed. Postmortem bilateral lung tissue bacterial and fungal cultures were performed. GMS staining was also performed.

Results: Autopsy revealed a superiorly displaced diaphragm, compressing the heart and lungs upward into a small thoracic cavity. The heart was small, weighing 230 g (expected 362 g +/- 77 g) but without congenital cardiac abnormalities. Notably, the lungs had multiple small, partially fused lung lobes bilaterally, and had blood in the larger airways and alveolar airspaces. Histology of the lung revealed predominantly lymphocytic interstitial inflammation, and a few foci of alveoli filled with pink, foamy, amorphous material, without evidence of fungal elements from GMS stain. There was no growth on bacterial and fungal cultures. Other abnormalities included kidney size asymmetry (right: 200 g, left: 130 g) with renal hypoplasia and reduced number of pyramids, microcephaly, dentition irregularities, short neck, optic nerve hypoplasia, arachnodactyly, rocker-bottom feet, scoliosis status post T3-L2 fusion, status post right total hip arthroplasty for complex degenerative joint disease (leg length discrepancy), tanner stage II breast development, and polycystic ovaries (cysts filled with serous fluid).

Conclusion: Trisomy 4p has been previously linked with recurrent respiratory infections, commonly secondary to aspiration, as a significant contributor of morbidity and mortality in the patient population. Cause of death in this case was extensive pulmonary hemorrhage arising in the setting of ECMO, which has been linked with a well-established risk factor for coagulopathy, in the context of aspiration pneumonia and sepsis. Trisomy 4p was thought to have significant contributory factors; the wide array of abnormalities described above are likely attributable to

Trisomy 4p. This case serves to further illuminate the significant range of possible abnormalities observed in trisomy 4p. To the best of our knowledge, the physical lung abnormalities such as those described in this case have not been previously reported and may represent a novel finding in Trisomy 4p.

65

In Lungs from Fetuses with Congenital Diaphragmatic Hernia, Beta-catenin mRNA Expression is Not Different from Control Lungs, but Tissue Sections Show Different Distributions of Beta-catenin Protein

A Lee [1], C Park [2], C Cheung [3], Y Li [3], B Poon [3], E Skarsgard [4], P Lavoie [5], M Mudri [4], M Prusinkiewicz [6]; [1] Children's and Women's Health Centre of British Columbia; University of British Columbia, [2] University of British Columbia, [3] BC Children's Hospital Research Institute, [4] Children's and Women's Health Centre of British Columbia; University of British Columbia, [5] BC Children's Hospital Research Institute; Children's and Women's Health Centre of British Columbia; University of British Columbia, [6] BC Children's Hospital Research Institute; University of British Columbia

Background: Congenital diaphragmatic hernia (CDH) is a developmental abnormality due to a defect in the diaphragm, with abdominal organs herniating through the defect. CDH is associated with lung hypoplasia. The dual-hit hypothesis of lung hypoplasia in CDH states that altered lung developmental gene expression plus mechanical factors contribute to its pathogenesis. Animal model studies of CDH with lung hypoplasia show alterations of the Wnt/Beta-catenin signaling pathway. We hypothesized that Wnt/Beta-catenin signaling pathway alterations also arise in human cases of CDH.

Methods: Archived formalin-fixed paraffin embedded autopsy lung tissues were selected from "Cases": fetuses obtained by pregnancy termination (TOP) for autopsy-confirmed CDH, or "Controls": fetuses obtained by TOP for autopsy-confirmed isolated brain anomaly or neural tube defect. Beta-catenin immunohistochemistry (IHC) was performed on formalin-fixed paraffin embedded lung tissue sections. Bilateral lung sections were stained for each Case (n = 5). One randomly selected lung was stained for each Control (n = 7). Stained slides were scanned and a high magnification image was collected. On each image, non-epithelial (interstitial) cells with nuclear, cytoplasmic, and/or membranous Beta-catenin positivity, and negative interstitial cells, were counted. mRNA quantification by qPCR was performed in a larger number of Cases (n = 20) and Controls (n = 9) including the samples subjected to IHC. mRNA was extracted with a commercial kit, then reverse transcribed to generate a stable gene expression library. Gene expression was assessed by qPCR using Beta-catenin primers.

Results: Characterization of Beta-catenin Protein in Lung Tissue Sections: For Cases (n=5; 18-28 weeks of gestation) and Controls (n=7, 18-36 weeks of gestation), Beta-catenin protein was consistently expressed in epithelial cells across the examined gestational ages. The percentage of interstitial cells expressing Beta-catenin increased with gestational age (Cases: $r2 = 0.8853$, $p = 0.0171$; Controls: $r2 = 0.6716$, $p = 0.0895$). On average and across the examined gestational ages, the percentage of interstitial cells expressing Beta-catenin was lower in Cases (range: 1.9%-44.1%; average 22.4%) than in Controls (range: 56.3%-70.6%; average 61.9%) ($p = 0.0008$). Figure 1 shows a representative Case and Control, both 18 weeks of gestation. Quantification of Beta-catenin mRNA: For 11/20 (55%) Cases and 4/9 (44%) Controls, the Beta-catenin mRNA was non-detectable. For 9/20 (45%) Cases and 5/9 (56%) Controls that had detectable B-catenin mRNA, the B-catenin mRNA levels in Cases (RQ: 2.17; RQmin = 0.74,

RQmax = 6.38, n=6) and Controls (RQ: 1.00; RQmin = 0.38, RQmax = 2.64, n=3) were not significantly different (p = 0.331). There were slight positive correlations with Beta-catenin mRNA and gestational age, but neither were significant (Cases r2 = 0.3194, p = 0.2425; Controls r2=0.040, p = 0.8717).

Conclusion: Our findings may suggest that human CDH is associated with Wnt/B-catenin pathway alterations, as found in animal models. Our study found alterations at the protein level, with a lower percentage of Beta-catenin protein expressed in interstitial lung cells from fetuses with CDH compared to non-CDH control lungs.

Figure 1. Smaller proportion of interstitial (non-epithelial) cells expressing Beta-catenin in CDH lung tissue compared non-CDH (control) lung tissue